UNDERSTANDING PROLINE METABOLISM IN HYPOXIC CANCER CELLS

By

LISA VETTORE

A thesis submitted to the University of Birmingham for the degree of

DOCTOR OF PHILOSOPHY

Institute of Metabolism and Systems Research

College of Medical and Dental Sciences

University of Birmingham

September 2022

UNIVERSITY OF BIRMINGHAM

IMSR

INSTITUTE OF METABOLISM AND SYSTEMS RESEARCH

ABSTRACT

To survive, cancer cells adapt their metabolism to sustain increased biomass production and bioenergetic demand as well as modulation of redox homeostasis. In addition, tumour proliferation often demands oxygen to the extent that the vasculature cannot supply, leading to tumor hypoxia. This condition selects for the most aggressive cancer clones, promoting increased metastasis, drug resistance and invasion. How cancer cells adapt their metabolism to survive at low oxygen tensions, and if this metabolic reprogramming contains targetable vulnerabilities is not completely understood.

The aim of this thesis was to uncover metabolic vulnerabilities based on previous findings from our lab, highlighting proline biosynthesis as a dysregulated pathway in hypoxic cancer cells. This study demonstrates that the cytoplasmic proline-producing enzyme PYCRL regenerates NAD^+ and promotes cell proliferation and survival in glioblastoma cancer stem cells. In addition, results suggest that other NAD^+ regenerating pathways, such as lipid desaturation, are engaged to compensate for PYCRL loss. Additional results show that proline import through SLC38A2 is essential for growth in redox oxidized cancer cells. Overall, we propose PYCRL in cancer stem cells and SLC38A2 in hypoxic IDH-mutant cells as potential drug targets for the treatment of cancer patients.

DEDICATION

To my parents and my grandparents

Acknowledgments

I thank my supervisor Prof. Daniel Tennant for all the mentorship and advice during the years of my PhD. He would always find some time for scientific discussions and challenged me to become a better scientist. I wish to thank past members of the Tennant lab Jennie Roberts and Katarina Kluckova and all the current members, in particular Adam Boufersaoui and Cristina Escribano-Gonzalez for all their support, friendship, and scientific discussions. I would also like to thank my second supervisor Dr. Christian Ludwig for having found some time to teach me NMR and for his advice for the next steps of my career.

I additionally wish to thank my collaborators, Prof. Matthew Vander Heiden and all the Vander Heiden group, in particular, Keene Abbott, Evan Lien, Alicia Darnell and Jeff Davies for having found some time to teach me new things and challenged my ideas.
I thank Sophie Honeder, visiting PhD student in the Vander Heiden group for all the time we have spent sharing ideas, discovering, and learning new things together. I acknowledge members of Dr. Melissa Skala's group, Rupsa Datta and Danielle Desa for having hosted me and introduced me into the world of two-photon microscopy.
I thank Dr. Sonu Subudhi, part of Prof. Rakesh Jain lab, for all his help with my project and the wonderful advice for my future career. I also thank Cancer Research UK for having funded my PhD.

Lastly, I immensely thank my family for all their support and love and for always cheering me up in the difficult moments of my PhD.

Chapter 1 provides an overview of the field of cancer metabolism and includes the published reviews “New aspects of amino acid metabolism” (Appendix 1), and “proline metabolism and redox; maintaining a balance in health and disease” (Appendix 2) as well as the research articles published in co-authorship “Succinate dehydrogenase deficiency in a chromaffin cell model retains metabolic fitness through the maintenance of mitochondrial NADH oxidoreductase function”, “Loss of SDHD promotes dysregulated iron homeostasis, oxidative stress, and sensitivity to ascorbate” and “Proline synthesis through PYCR1 is required to support cancer cell proliferation and survival in oxygen-limiting conditions”. **Chapter 2** was conducted in collaboration with Dr. Adam Boufersaoui (Tennant lab) who analysed the LC-MS samples for this chapter and Alicia Darnell from the Vander Heiden group who provided the double PYCR1 and 2 KO cells. The GC-MS lipid samples in **Chapter 3** were analysed by Dr Adam Boufersaoui in the Tennant lab. The staining of the primary brain tissue sections in **Chapter 4** was conducted by Ana Teodosio (IHC and imaging support officer). Chapter 2 on the cytoplasmic proline transporter PYCRL and chapter 4 on the proline importer SLC38A2 are in preparation for submission to a research journal.

TABLE OF CONTENTS

ABBREVIATIONS

α-KG: α-ketoglutarate

ACO2: Aconitase 2

ACLY: ATP citrate lyase

ACSS1/2: Acetyl-CoA synthetase 1/2

AICAR: 5-Aminoimidazole-4-carboxamide ribonucleotide

AMP: Adenosine monophosphate

AOA: Aminoxyacetic acid

ASL: Argininosuccinate lyase

ASS1: Argininosuccinate synthase 1

ATP: Adenosine triphosphate

BCA: Bicinchoninic acid

BBB: Blood-brain barrier

BSA: Bovine serum albumin

BODIPY: Boron-dipyrromethene

BSO: Buthionine sulfoximine

BTB: Brain-tumour barrier

CA9: Carbonic anidrase 9

CAF: Cancer-associated fibroblast

CD36: cluster of differentiation 36

CNS: Central nervous system

CoQ9/10: Coenzyme Q 9/10

CSF: Cerebrospinal fluid

CTP: Cytidine triphosphate

DKO: double-knockout

DOX: Doxycycline

dTMP: thymidine monophosphate

EGF: Epidermal growth factor receptor

ER: Endoplasmic reticulum

ETC: electron transport chain

FA: Fatty acids

FAD^+: Flavin adenine dinucleotide

$FADH_2$: Reduced flavin adenine dinucleotide

FAO: Fatty acid oxidation

FADS1-3: Fatty acid desaturase 1-3

FATP: Fatty acid transport protein

Fe-S: Iron-sulfur

FGF-2: Fibroblast growth factor-2

FH: Fumarate hydratase

FIH: Asparaginyl hydroxylase

G6P: Glucose 6-phosphate

GBM: Glioblastoma multiforme

GC-MS: Gas chromatography-mass spectrometry

GDH: Glutamate dehydrogenase

GLS: Glutaminase

Glycerol-3-P: Glycerol-3-phosphate

GOT1/2: Aspartate aminotransferase 1/2

GSA: Glutamate–5–semialdehyde

GSSG: Oxidised glutathione

GSH: Glutathione

GTP: Guanosine triphosphate

HIF: Hypoxia-inducible factor

HOG: Human oligodendroglioma

HMG-CoA: 3-hydroxy-3-methyl-glutaryl-coenzyme A

IDH: Isocitrate dehydrogenase

IDH-mut: IDH-mutant

IDH-wt: IDH-wildtype

IMP: Inosine monophosphate

IOX2: HIF prolyl hydroxylase inhibitor

Ki67: Marker of proliferation Ki67

KD: Knockdown

LC-MS: Liquid chromatography-mass spectrometry

LDHA: Lactate dehydrogenase A

LY-109761: TGF-β inhibitor

ME1: Malic enzyme 1

MeAIB: α-(Methylamino)isobutyric acid

MID: Mass isotopologue distribution

MDH1/2: Malate dehydrogenase 1/2

mTOR: mammalian target of rapamycin

MTHFD2: Methylenetetrahydrofolate dehydrogenase 2

m/z: mass to charge

NAD: Nicotinamide adenine dinucleotide

NADK2: NAD kinase 2

NADP: Nicotinamide adenine dinucleotide phosphate

NADPH: Reduced nicotinamide adenine dinucleotide phosphate

NADH: Reduced nicotinamide adenine dinucleotide

NF: Normal fibroblast

NNT: Nicotinamide nucleotide transhydrogenase

NT: non-targeting

OAT: Ornithine aminotransferase

ODC1: Ornithine decarboxylase

OGDH: Alpha-ketoglutarate dehydrogenase

OXPHOS: oxidative phosphorylation

p53: Tumour protein p53

P5C: Pyrroline-5-carboxylate

P5CS: Pyrroline-5-carboxylate synthase

PBS: Phosphate-buffered saline

PE: phosphoethanolamine

PDAC: Pancreatic ductal adenocarcinoma

PDGFRA: Platelet derived growth factor receptor alpha

PHGDH: Phosphoglycerate dehydrogenase

PPP: Pentose phosphate pathway

PRODH/POX: Proline dehydrogenase/Proline oxidase

PTEN: Phosphatase and tensin homolog

PYCR1/2: Pyrroline-5-carboxylate reductase 1/2

PYCRL: Pyrroline-5-carboxylate reductase-like

R5P: Ribose 5-phosphate

ROS: reactive oxygen species

SCD: Stearoyl-CoA desaturase

SDH: succinate dehydrogenase

S.E.M.: standard error of the mean

SHMT: Serine hydroxymethyltransferase

shRNA: short hairpin RNA

siRNA: small interfering RNA

SLC38A1: System A transporters 1

SLC38A2: System A transporters 2

SLC36A1/4: Solute carrier family 36 member 1/4

SLC6A20: Solute carrier family 6 member 20

SLC7A5: Solute carrier family 7 member 5

SLC1A4: Solute carrier family 1 member 4

SLC6A7: Solute carrier family 6 member 7

SLC25A51: Solute carrier family 25 member 51

SLC25A39: Solute carrier family 25 member 39

SLC25A40: Solute carrier family 25 member 40

SMAD: Mothers against decapentaplegic

SOD2: Superoxide dismutase 2

SRB: Sulforhodamine B

TCA: Tricarboxylic acid

TERT: Telomerase reverse transcriptase

TKI: Tyrosine kinase inhibitors

TNBC: Triple negative breast cancer

TOF: Time-of-flight

UQCR11: Ubiquinol-Cytochrome C Reductase, Complex III Subunit XI

VEGF: Vascular endothelial growth factor

WHO: World Health Organization

xCT: Cysteine/glutamate antiporter

LIST OF FIGURES

CHAPTER 1:
REVIEW OF THE LITERATURE

1.1 The metabolic map of cancer

1.1.1 Fundamentals of cancer metabolism

Cancer is the unlimited growth of a mass from a single cell, as a consequence of DNA mutations that allow the bypass of normal genetic mechanisms, controlling proliferation and cell death[1]. From an historical point of view, people have been fighting cancer for 4000 years, trying to disentangle the knot of malignant growth from the normal one[1]. Even now, cancer is the second cause of death worldwide (1 in 6 deaths), after cardiac diseases, with numbers continuing to increase[2]. Over the past decades, scientists have been trying to delineate the metabolic hallmarks of cancer cells. It is now clear that malignant cells adapt their metabolism to fulfill three vital characteristics: preservation of redox homeostasis, increased energy generation and enhanced biomass production[3,4]**.** Altered metabolism is observed at all stages of tumour development, from primary lesion formation to metastatic colonisation, where cancer cells reprogram their metabolism to adapt and survive across different environments[4]. Overall, metabolic alteration in cancer is the output of tumour-intrinsic properties, such as DNA mutations; external constraints, for example oxygen and nutrient availability in a certain tissue; tumour-stroma interactions and systemic homeostasis[5]. In consequence, the metabolic network is often constrained by the complex nature of the tumour mass and can be used as therapeutic target for treating cancer patients.

1.1.2 Revisiting the Warburg effect

In 1920s our understanding of the deregulated metabolism of cancer cells was focused on aerobic glycolysis, a mechanism through which abnormal cells, even in the presence of oxygen, increase the glucose uptake and secrete a high fraction of lactate

for the production of adenosine triphosphate (ATP)[6]. This altered metabolic phenotype, known as the Warburg Effect, was considered at the time a consequence of irreversible defects in respiration[6]. Today, however, it is clear that the phenomenon of aerobic glycolysis as well as altered metabolism are a hallmark of cancer and are the result of inactivation of tumour suppressors and/or activation of oncogenes[4].

Although oxidative phosphorylation produces up to 38 moles ATP/mole glucose, aerobic glycolysis which generates 2 moles ATP/mole glucose is the preferential way that drives tumorigenicity. Evidence suggests that glycolytic intermediates are essential for biomass production and in this way offset the apparent disadvantage of favouring this metabolic pathway[7]. As an example, dihydroxyacetone phosphate is the glycolytic intermediate necessary for the synthesis of glycerol-3-phosphate[7]. The latter is a fundamental precursor of phospholipids and triacylglycerols, molecular bricks for membrane formation. Furthermore, through glycolysis, glucose can provide sufficient carbons to sustain *de novo* biosynthesis of purine nucleotides; building blocks for ATP, GTP, and their deoxy-forms as energy carriers as well as DNA and RNA biosynthesis[7]. During glycolysis, the glucose imported by plasma membrane transporters, named GLUTs, is phosphorylated by hexokinase to produce glucose 6-phosphate (G6P). After isomerisation and further phosphorylation, the glucose backbone is divided into two 3-carbon molecules while generating ATP[8]. The glycolytic process terminates with the production of two molecules of pyruvate from one molecule of glucose[8]. Alternatively, the glucose can be shunted into the pentose phosphate pathway (PPP), prompting the generation of ribose-5-phophate (R5P), a fundamental precursor for pyrimidine biosynthesis as well as reduced nicotinamide adenine dinucleotide phosphate

(NADPH) - an essential cofactor involved in protection from oxidative stress[8]. Downstream glycolysis, the fate of pyruvate can undertake three different routes, depending on cell requirements – being secreted as lactate, enter the tricarboxylic acid (TCA) cycle or being converted into alanine.

Today, Otto Warburg's hypothesis that cancers, even in presence of oxygen, exhibit high glycolytic rates culminating in lactate production, due to irreparable defects in mitochondrial respiration, has been revisited[9]. Even by the 1950's it was demonstrated that neoplastic cells display enzymatic activities of TCA cycle similarly to normal cells. Even recent studies provide evidence that mitochondrial metabolism is crucial for promoting cell proliferation[10]. Indeed, normal mitochondrial function is required to underpin rapid anabolic growth that is often observed in tumours, due to its central metabolic core – the TCA cycle being fundamental in the synthesis of the precursors to cellular macromolecules such as amino acids, nucleotides and lipids[11]. More recent evidence suggests that this mitochondrial activity is so important in cancer cells that they import directly metabolic precursors to 'feed' the TCA cycle. For instance, a subpopulation of cancer cells, favours the import of lactate produced by neighbour glycolytic cells, and catabolises the molecule via citric acid cycle (TCA) for biomass and ATP production. As a result, one of the multiple advantages is that citrate, one of the TCA cycle intermediates, can be shuttled to the cytosol for lipid (acetyl-CoA) and nucleotide (oxaloacetate) biosynthesis[10].

The TCA cycle activity in the mitochondrial matrix is also essential for producing reducing equivalents NADH and $FADH_2$ which transfer their electrons to the electron

transport chain (ETC)[10].The delivery of electrons to ETC is coupled by pumping of protons into the intermembrane space by complexes I,III, IV[10]. This mechanism generates the proton motive force, composed by a minor chemical component (ΔpH) and a major electrical moiety of membrane potential ($\Delta\psi$) which are dissipated by the ATP synthase (complex V) for ATP production (Figure 1.1)[10]. In the absence of oxygen as the terminal electron acceptor, it has been more recently shown that the electron transport chain can continue to function with fumarate as an alternative electron acceptor, allowing complex I (but not III and IV) to pump protons, maintaining the proton-motive force and oxidative phosphorylation of ATP[12]. In this context, brain, kidney and liver tissues have the best capability to reduce fumarate *in vivo*[12].

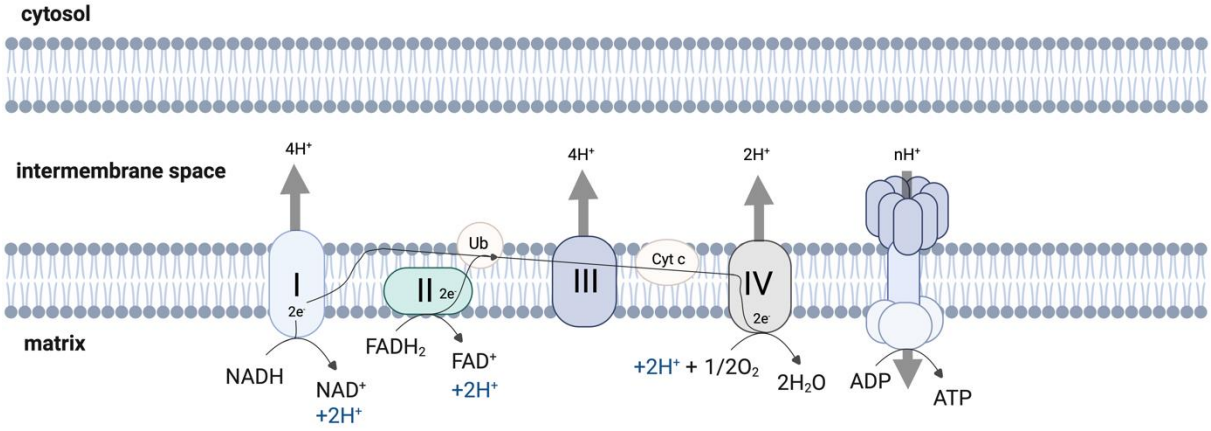

Figure 1.1 An overview of the electron transport chain

Schematic overview of the electron transport chain which pump electrons in the intermembrane space to generate the proton force to produce ATP. During this process NAD^+ and FAD^+ are recycled, respectively by complex I and II. In addition, oxygen is consumed by complex IV to produce two molecules of H_2O. Abbreviations: I, complex I; II, complex II; III, complex III; IV, complex IV; Ub, ubiquinone; Cyt c, cytochrome c.

The discoveries since 2000 that mutations in the TCA cycle enzymes succinate dehydrogenase (SDH), fumarate hydratase (FH) and isocitrate dehydrogenase (IDH), led to accumulation of specific metabolites that are involved in tumourigenesis, raised a novel paradigm[13]. Herein, recent studies have further characterized the role of these metabolites, leading them to be termed as “oncometabolites”, due to their action as oncogenic signaling molecules and their role in connecting mitochondrial dysfunction to metabolic reprogramming[13]. For instance, fumarate and succinate accumulation were shown to inhibit the activity of alpha-ketoglutarate-dependent dioxygenases, which amongst other activities hydroxylate hypoxia-inducible factor 1-alpha (HIF-1α) and target it for proteasomal degradation[13]. Nevertheless, the accumulation of oncometabolites is not a sign of complete mitochondrial dysfunction as shown in a chromaffin cell model that could retain normal complex I activity despite bearing a SDH-inactivating mutation[14]. Overall, fumarate, succinate and the *de novo* byproduct of IDH-mutant enzymes, 2-hydroxyglutarate, are powerful modifiers of the epigenome, via blockage of other members of the α-KG-dependent dioxygenase superfamily, which include histone and DNA demethylases[13]. The modification of genetic landscape due to chronic accumulation of oncometabolites, elicits oncogenic signaling cascades that expand the concept of genetic mutation as exclusive driver of cell transformation[15]. Another layer of evidence suggests that the cellular context matters – there is evidence for several oncogenes and tumour suppressor genes that the tissue in which the mutational event occurs can determine the phenotype that results. For example, SDHB-mutant cancer cells exhibit HIF-1α stabilization in hypoxia, known as pseudohypoxia, and increased metastatic potential, but not cancers with a mutation in the subunit D of complex II[16].

1.1.3 Amino acid metabolism in cancer

Much like in non-malignant cells, fuels besides glucose are required for the metabolic functions of tumours: preservation of redox homeostasis, energy generation and biomass production[11]. In this section we cover metabolites that are often altered in cancer cells.

A major nutrient is glutamine, which is catabolized by glutaminase (GLS) that promotes the conversion from glutamine to glutamate. Glutamine can be used as an alternative source from glucose to fuel TCA cycle turning, sustaining NADH production by oxidative phosphorylation[17]. Alternatively, glutamine is able to contribute to NADPH production by sustaining the conversion of malate into pyruvate via malic enzyme activity and IDH1-dependent reductive carboxylation[17]. Glutamate contributes to the formation of glutathione (GSH), a reactive oxygen species (ROS) scavenger composed by glutamate, cysteine, and glycine. GSH eliminates hydrogen peroxide-mediated damage via mechanisms including glutathione peroxidase activity[18]. Subsequently, the oxidised form of glutathione GSSG can be reduced back to GSH by the cofactor NADPH[18]. The rate-limiting amino acid for glutathione biosynthesis is cysteine, particularly in the step catalyzed by glutamate-cysteine ligase (GCL) which leads to the formation of a peculiar gamma-peptidic bond between cysteine and glutamate[18].

Cysteine is a non-essential amino acid, as it can be endogenously synthesized from methionine in the transsulfuration pathway or can be imported by the xCT transporter

and by the alanine/serine/cysteine transporter (ASCT) system[18]. Alternatively, cysteine can be produced from cystine by cystine reductase, in an NADH-consuming reaction[18].

In the cytosol, alanine indirectly modulates redox homeostasis via alanine transaminase (ALT), an enzyme which promotes the reversible conversion of alanine and α-ketoglutarate into glutamate and pyruvate[19]. The latter can be shuttled into the mitochondrial matrix by the mitochondrial pyruvate carrier (MPC) to contribute to the TCA cycle or can be converted into lactate by lactate dehydrogenase (LDH), enhancing the $NADH/NAD^+$ ratio[19]. Whereas one of the fates of glutamate is contributing to NADH and α-ketoglutarate regeneration coupled to ammonia production by the action of glutamate dehydrogenase (GDH)[19].

The growing list of tumour fuels include serine which can be either assimilated from the microenvironment or generated from 3-phospholycerate (3PG), a glycolytic intermediate[13]. The major moiety of serine is converted into glycine via cytosolic or mitochondrial serine hydroxymethyl transferase (SHMTs)[13]. During this process, the one-carbon unit donated by serine contributes to the one-carbon pool used for purine or thymidine monophosphate (dTMP) biosynthesis[13].

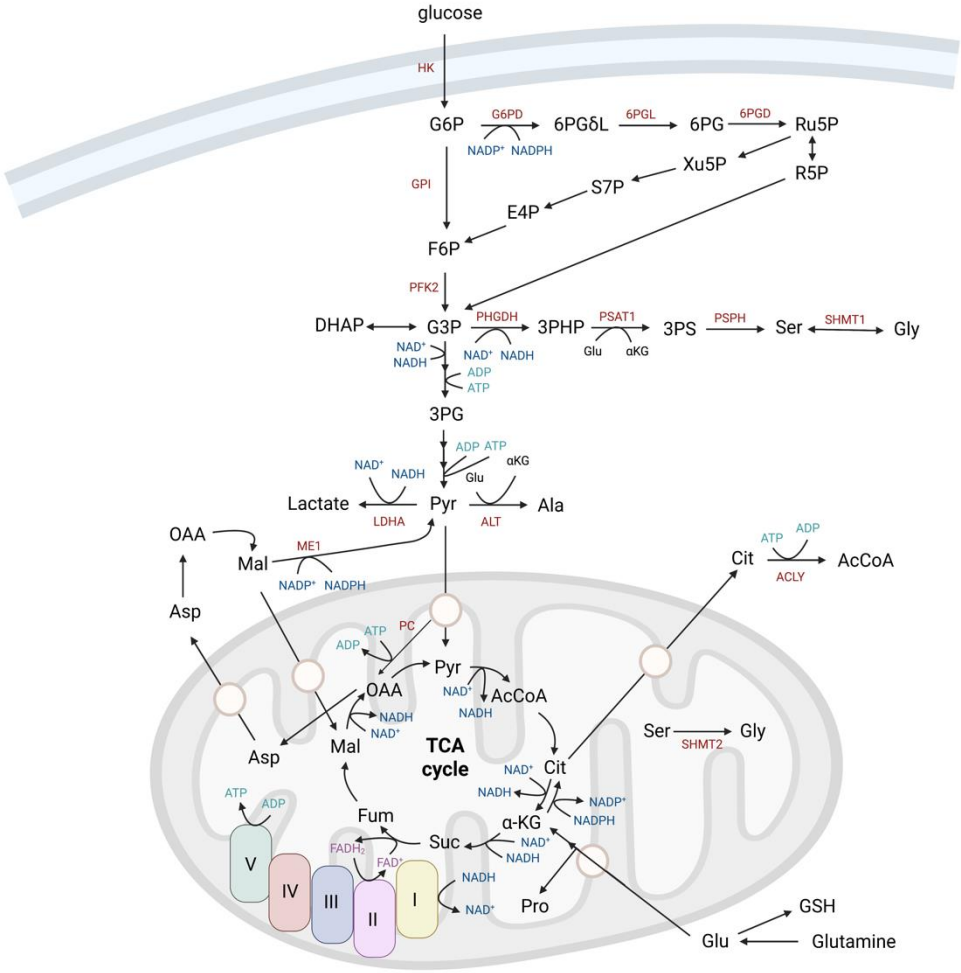

Figure 1.2 Fundamentals of cancer metabolism

The diagram highlights the major pathways involved in the maintenance of biomass production and redox control during cancer proliferation. NAD(P)H/NAD(P)$^+$ Redox couples are shown in blue, FADH/FAD$^+$ is shown in pink, ATP/ADP in green, key metabolic enzymes are shown in red. Abbreviations: G6P, glucose-6-phosphate; F6P, fructose-6-phosphate; G3P, glyceraldehyde-3-phosphate; 3PG, 3-phosphoglycerate; Pyr, pyruvate; Ala, alanine; HK, Hexokinase; GPI, Glucose-6-phosphate isomerase; PFK2, Phosphofructokinase-2; Glu, glutamate; α-KG, α-ketoglutarate; LDHA, Lactate dehydrogenase; ALT, alanine transaminase; DHAP, dihydroxyacetone phosphate; 6PGδL, 6-phosphogluconolactone; 6PG, 6-phosphogluconate; Ru5P, Ribulose-5-phosphate; R5P, Ribose-5-phosphate; Xu5P, Xilulose-5-phosphate; S7P, sedoheptulose-7-phosphate; E4P, erythrose-4-phosphate; G6PD, Glucose-6-phosphate dehydrogenase; 6PGL, 6-phosphogluconolactonase; 6PGD,

6-phosphogluconate dehydrogenase; PHGDH, Phosphoglycerate dehydrogenase; PSAT1, Phosphoserine aminotransferase 1; PSPH, Phosphoserine phosphatase; SHMT1, Serine hydroxymethyltransferase 1; 3-PHP, 3-phosphohydroxypyruvate; 3PS, 3-phosphoserine; Ser, serine; Gly, glycine; Pyr, pyruvate; ME1, Malic enzyme 1; Mal, malate; OAA, oxaloacetate; Asp, aspartate; AcCoa, Acetyl-CoA; Cit, citrate; Suc, succinate; Fum, fumarate; Pro, proline; SHMT2, Serine hydroxymethyltransferase 2; PC, Pyruvate carboxylase; ACLY, ATP citrate lyase; GSH, reduced glutathione.

Whereas serine supports purine biosynthesis, aspartate fosters pyrimidine generation in all cancer cells and, in particular, in ASS1-deficient cancer cells, via CAD activation mediated by mTOR[20]. Indeed, the urea cycle enzyme, argininosuccinate synthetase (ASS1) is involved in aspartate catabolism, by converting nitrogen from aspartate and ammonia to urea[20]. In case of arginine starvation, asparagine synthetase (ASNS) is induced, further consuming intracellular aspartate, and impairing the malate-aspartate shuttle[21]. Intracellular arginine availability is controlled by enhancing the plasma membrane transporters SLC7A1 and 2, or via endogenous synthesis by ASL, another component of the urea cycle[21]. ASL which produces arginine from argininosuccinate, sustains also the synthesis of other arginine-derived metabolites, such as polyamines (putrescine, spermidine, spermine)[21]. The latter metabolites play a role in autophagy, DNA binding, ion channels modulation and cellular proliferation[22]. Especially in Myc-driven tumours, the rate-limiting reaction of polyamine biosynthesis is often increased and involves the enzyme ODC1 which synthesises putrescine from ornithine[22]. Another ornithine-dependent enzyme is ornithine δ-aminotransferase (OAT) which promotes the reversible conversion from ornithine and α-ketoglutarate to glutamate and glutamate-5-semialdheyde (GSA)[23]. The amine and an aldehyde group contained

in GSA can lead to internal imination, resulting in an equilibrium with its cyclic form P5C[23]. The latter is an essential metabolite for sustaining proline biosynthesis, a pathway which will be covered in the next sections[23].

1.1.4 Lipid metabolism in cancer

Comparatively understudied, lipids are complex biomolecules that compose the membrane layers, act as signaling molecules and contribute to the cell bioenergetics[24]. Lipids are hydrophobic molecules, and their intracellular availability is the result of extracellular uptake, endogenous synthesis or catabolism[24]. The majority of lipids used as building blocks for membranes are phospholipids, which can be further divided into sphingolipids – if attached to an amino alcohol – or phosphoglycerides - if linked to glycerol[24]. Not all the fatty acids (FA) are synthesized *de novo* from cells and instead must be taken up through fatty acid transporters, such as CD36 and FATPs[25]. Polyunsaturated fatty acids (PUFAs) are an example of imported FA, as mammalian cells can only desaturate specific positions within the hydrocarbon chain. In mammalian cells, these reactions are catalysed by the stearoyl-CoA desaturases (SCDs) and fatty acid desaturases (FADS)[24]. Enzymes involved in FA desaturation are often deregulated in cancer – SCDs can desaturate palmitate into a less used fatty acid, known as sapienate[26].

De novo fatty acid synthesis is often exploited by cancer cells, as in healthy cells only adipocytes and hepatocytes would normally use this pathway[25]. FA synthesis condensates seven malonyl-CoA molecules and one acetyl-CoA through fatty acid synthase (FASN) to produce palmitate[25]. This molecule can be further elongated by

FA elongases (ELOVL1-6) or undergo the desaturation process and packaged into lipid droplets alongside tryglycerides[25,27]. Alternatively, FA can be used as an energy source through fatty acid oxidation (FAO)[28]. FAO shortens fatty acids of two carbons per cycle to regenerate ATP via ETC[28].

1.1.5 Hypoxia-induced metabolic rewiring

The tumour microenvironment is characterized by gradients of oxygen, creating areas of normoxia, mild and severe hypoxia and necrosis[29]. Normoxia is defined as 21% O_2 as standard experimental condition in all labs over the world and it will be used to refer to 21% O_2 throughout this thesis. In reality, oxygen levels in different organs of the body fluctuate between 3-9% O_2, a condition defined as physiological oxygen (physioxia). Malignant cells frequently grow in low oxygen conditions (hypoxia) - around or lower than 1% O_2 - due to a poorly functional vasculature and/or high growth rates[29]. This environment promotes metabolic heterogeneity in cells, with opportunities for metabolic compensation. As an example, cells nearby blood vessels and therefore in normoxic regions, exhibit high glycolytic rates, followed by lactate secretion[30]. Lactate can be taken up by neighbouring cells and be oxidised as major carbon source for ATP and biomass production[30].

Genetic alterations in cancer cells rewire their metabolism, allowing tumours to survive under different levels of hypoxia[29]. Under normal oxygen tension (21% O_2), Hypoxia-Inducible Factor (HIF)-1α prolyl hydroxylases (PHD; EGLN1-3) catalyze the hydroxylation of specific HIF-1α prolyl residues[29]. These are recognised by the von Hippel-Lindau (pVHL) E3 ubiquitin ligase, leading to polyubiquitination and HIF-1α degradation[29]. Additionally, HIF-1α can be hydroxylated at a C-terminal asparagine

residue by the enzyme FIH[29]. These modifications inhibit HIF-1α activity, although FIH is inhibited at lower oxygen tensions than PHDs[29]. HIF-1α exists in three gene expressing subunits - HIF-1α is expressed ubiquitously, HIF-2α is present only in certain cell types whereas HIF-3α is poorly studied – all these subunits dimerise with the constitutively expressed HIF-1β[31]. Interestingly, increased expression of HIF-1α and HIF-2α is associated with poor survival in cancer patients.

During hypoxia or in the presence of other factors, such as succinate, fumarate or α-KG, PHDs are inhibited[32]. The resulting stabilization of the HIF-1α transcription factor allows the binding of HIF response elements (HREs) and transactivation of a set of genes that shift metabolism towards glycolysis, prime angiogenesis, and alter cell proliferation and invasion[31]. For instance, hypoxia directly mediates the glycolytic switch by enhancing lactate generation and secretion, respectively by upregulation of LDHA and some of the monocarboxylate transporters[29].

Other signaling pathways that alter HIF-1α expression can be engaged in hypoxia. For instance transforming growth factor beta (TGF-β) has been shown to enhance HIF-1α stability in hypoxia via decreasing PHD2 mRNA and protein levels by acting through the SMAD signalling pathway[33]. Interestingly, TGF-β promotes a similar metabolic program as HIF-1α, increasing glucose oxidation and lactate production while downregulating ETC activity[34]. Hypoxia can also influence the activity of oncogenes or oncosuppressors, such as p53. The latter elicits a response toward the degradation of HIF-1α and therefore mitigates HIF-1α-mediated metabolic reprogramming during

severe or chronic hypoxia. p53 therefore contributes to the creation of a graded response at lower oxygen tensions[29].

Some metabolic reactions are directly dependent on oxygen availability, such as cholesterol synthesis or FA desaturation. Cholesterol is produced from acetyl-CoA and requires eleven molecules of oxygen[35]. Therefore, the HIF-1α transcriptional program indirectly accelerates the degradation of 3-hydroxy-3-methylglutaryl-coenzyme A reductase (HMG-CoA reductase), the rate-controlling enzyme of cholesterol synthesis to save molecular oxygen[36]. Similarly, hypoxia downregulates FA desaturation as it requires oxygen as electron acceptor, whereas supporting extracellular import[37]. It is indeed important to maintain an appropriate unsaturated/saturated fatty acid ratio for cell membrane fluidity and integrity – an impairment in this ratio could lead to apoptosis[38,39].

In addition, hypoxia is known to decrease the rate of FAO, in particular medium- and long-chain acyl-CoA dehydrogenases (MCAD and LCAD) to protect the cell from reactive oxygen species[40,41].

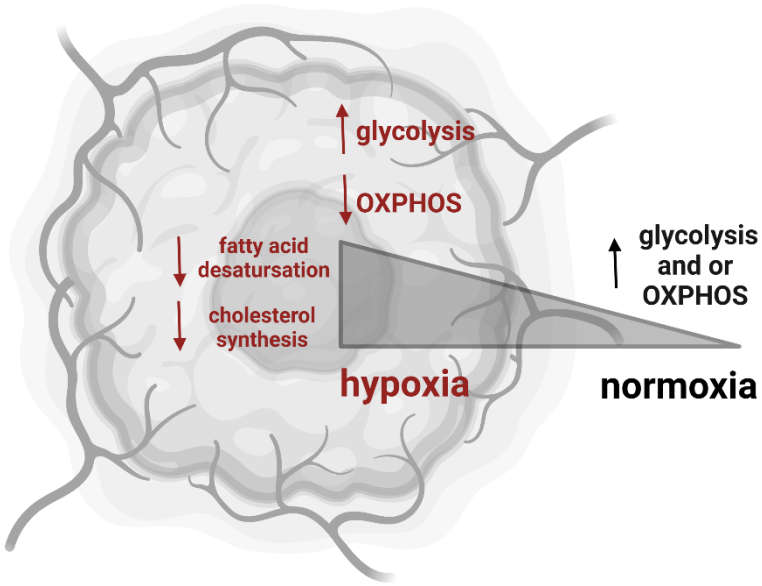

Figure 1.3 Metabolic adaptations of tumours in hypoxic conditions

Outgrowing tumours develop as a spheroid with a decreased oxygen tension towards the core, due to a lack of efficient perfusion. Cancer cells in hypoxic regions increase glycolysis and reduce electron transport chain activity. In addition, fatty acid desaturation and cholesterol synthesis are downregulated to spare oxygen. In normal oxygen conditions glycolysis and/or OXPHOS can be upregulated for ATP production. Abbreviations: OXPHOS, oxidative phosphorylation.

1.2 Redox metabolism in tumours

1.2.1 Redox co-factors and oxidative stress in cancer

Many enzymes require NAD^+/$NADP^+$ as electron acceptors or NADH/NADPH as electron donors to drive their biochemical reactions[42].

The $NADP^+$/NADPH redox couple plays an essential role in cellular anabolism and oxidative stress defense, whereas NAD^+/NADH balances intracellular energy metabolism (e.g. glycolysis, citric acid cycle, oxidative phosphorylation) and is used to drive ATP generation[42,43]. In most mammalian cell types, the intracellular levels of NAD^+ and NADH are higher than $NADP^+$ and NADPH[43]. Furthermore, the balance of the NADH/NAD^+ redox couple is shifted towards NAD^+, while then NADPH/$NADP^+$ is the opposite[43]. Collectively, the NAD^+/NADH ratio dictates a more oxidizing environment in the cytosol, with a range 60-700, whereas mitochondria show a more reduced scenario, with a NAD^+/NADH ratio of 7-8[44]. Two mitochondrial NAD^+ importers have been identified in *Saccharomyces Cerevisiae*, known as Ndt1p and Ndt2p, and recently SLC25A51 was reported as the NAD^+ transporter in the mammalian system[42,45,46]. In human cells, NADH can indirectly shuttle between the cytosol and the mitochondria via the malate-aspartate shuttle and the 3-glycerol-phosphate shuttle[44]. The former moves the reducing potential of NADH from the cytosolic compartment into the mitochondrion, regenerating cytosolic NAD^+, while the latter transfers the reducing potential to form $FADH_2$ instead, regenerating cytosolic NAD^+ without affecting mitochondrial NAD^+/NADH ratio[44]. In the same way for NADP(H) pools, the $NADP^+$ can be regenerated in the cytosol via P5C-proline cycle, and used in the oxidized form as an electron acceptor to sustain the pentose phosphate pathway[47]. Alternatively, the isocitrate-α-ketoglutarate cycle effectively shuttles reducing potential of NADPH from

the mitochondria to the cytosol. This shuttle is coupled to nicotinamide nucleotide transhydrogenase (NNT) which exploits the mitochondrial proton gradient to generate mitochondrial NADPH from NADH[44].

The partial reduction of molecular oxygen creates reactive oxygen species (ROS), highly reactive molecules with one or more unpaired electrons, that can oxidise proteins, lipids and nucleic acids[48]. ROS are generated as a byproduct of normal metabolic reactions or environmental factors and act as signaling molecules, dictating cell proliferation and survival[48]. Anion superoxide (O_2^-) is the product of one electron addition to oxygen and is a significant precursor of ROS[49]. The main source of O_2^- in the majority of cell types is the mitochondrion through electron leak from the electron transport chain (ETC)[49]. O_2^- is so reactive that it readily oxidises cellular macromolecules in the vicinity of its production, and therefore does not travel far through the cell[49]. However, a major means of its detoxification is through dismutation by the mitochondrial enzyme superoxide dismutase 2 (SOD2), forming hydrogen peroxide (H_2O_2)[49]. This oxidant is less reactive and therefore more stable than O_2^- , more frequently oxidizing cytosolic components of the cell, including the nuclear DNA. H_2O_2 is further detoxified by catalase in the cytosol (forming water and O_2), or can be partially reduced to a hydroxyl radical (OH•) in presence of iron[49]. The tight regulation of ROS levels – maintaining a Goldilocks-like 'just right' level – is essential for enabling normal cell function and survival[50,51]. In instances where this homeostasis is perturbed, such as during hypoxia and/or nutrient deprivation, oxidative or reductive stress is observed[50,51]. The former is the best understood of these, and is reversed by utilization of antioxidant systems such as glutathione and thioredoxins[52].The capacity of these

systems are maintained using the pyridine-based redox cofactor, NADPH, as a source of reducing equivalents[52].

Overall, NAD(H) and NADP(H) play a crucial role in ROS generation and scavenging, and therefore maintain cellular metabolism and redox homeostasis in balance. This equilibrium is guaranteed by their biosynthesis, consumption, and compartmentalisation[43].

1.2.2 Redox perturbations in hypoxia

ETC generates more ROS in hypoxia, especially from complex I and III, even if there is less oxygen available intracellularly[53]. This paradox can be explained with the concept of electron “leakage” from the electron transport chain and it causes ROS to act as signalling molecules while reaching the cytoplasm[53,54]. The adaptive response to oxidative stress triggers the activity of the pentose phosphate pathway to regenerate the necessary NADPH to reduce the antioxidant systems, such as glutathione and thioredoxins. Alternatively, cells can use serine and glycine-derived carbons to regenerate NADPH via the folate cycle either in the mitochondria or in the cytosol[55]. Indeed, PHGDH – the enzyme involved in the first step of serine biosynthesis – and SHMT2 - which catalyses the serine-glycine interconversion - were found to be upregulated in breast cancer hypoxic regions[55].

Some mitochondrial enzymes, such as aconitase 2 (ACO2) and alpha-ketoglutarate dehydrogenase (OGDH) are particularly susceptible to oxidation at the Fe-S centres, and are therefore inactivated at lower oxygen tensions[29]. This supports the decrease

of TCA cycle turning in hypoxia. Interestingly, also complex I Fe-S clusters are vulnerable to ROS, inhibiting complex I activity and therefore contributing to an overall increase in mitochondrial NADH[29]. The adaptive response to hypoxia induces a switch from OXPHOS to lactate production, as pyruvate reduction to lactate through LDH regenerates cytosolic NAD^+ that can be imported into the mitochondria to alleviate mitochondrial NADH overload[29]. Alternatively, lower ETC activity also decreases TCA cycle turning by feedback inhibition from NADH[29].

1.3 Proline metabolism in cancer

1.3.1 Proline metabolism and redox

Proline is a non-essential proteinogenic amino acid, essential in stress protection, cellular signalling (apoptosis), microenvironment remodelling and tumour metabolism[56]. For instance, proline acts as protein chaperone, preventing protein aggregation, and therefore ER stress. In addition, proline is involved in oxidative stress protection – the molecule itself reacts directly with H_2O_2 and OH• to generate adducts of proline and 3 or 4-hydroxyproline[57].

Physiologically, proline is synthesised from ornithine or glutamate leading to the intermediate GSA, which non-enzymatically cyclises to P5C. Besides OAT, in prokaryotes and lower eukaryotic organisms, P5C originates from glutamate via the catalytic activity of glutamate 5-kinase (G5K) and γ-glutamyl phosphate reductase (γ-GPR)[56]. In humans, G5K and γ-GPR are combined together to form P5C synthase (P5CS)[56]. This enzyme is dependent on NADPH and ATP to generate P5C. The last step of proline biosynthesis involves NAD(P)H-dependent P5CRs (PYCRs), which

catalyse the reduction of P5C to form proline, driven by the reducing potential of NAD(P)H[56]. Human PYCRs exhibit three isoforms - two mitochondrial, PYCR1 and PYCR2, and one cytosolic, PYCRL[58,59]. Mitochondrial PYCRs display a higher affinity for NADH and a preferred glutamine utilization, whereas PYCRL favours the cofactor NADPH and ornithine as a major source to synthesise proline[58,59,60].

In the context of disease, PYCR2 deficiency results in hypomyelination and microcephaly in humans, whereas PYCR1 deficiency causes cutis laxa[61,62]. Interestingly, no pathological phenotypes were associated with loss of PYCR3. However, the PYCR enzymes may have tumour supporting roles in cancer. PYCR1 has been shown to support tumour growth in a triple-negative breast cancer model when proline is limiting[63]. The same finding was confirmed *in vivo* and from increased mRNA levels in different cancer types, such as kidney adenocarcinoma and hepatocellular carcinoma[63,64,65]. Similarly, PYCR2 mRNA expression is upregulated in colorectal carcinoma and is associated with poor prognosis[66].

PYCR enzymes can also catalyse non-canonical reactions under certain circumstances. It has been suggested that PYCR1 could contribute to lysine catabolism, accepting Δ^1-piperideine-6-carboxylate (P6C) as an alternative substrate in ALDH7A1-deficient fibroblasts and patient urine samples[67]. P6C is an intermediate of lysine metabolism, and has a structure that is very similar to the 5-membered ring of P5C.[39] Alternatively, PYCR1 and, with a ten-fold higher catalytic efficiency PYCR2, can work in reverse at least *in vitro* by oxidating L-Thioproline (L-T4C) into cysteine

and formate, as illustrated by recent kinetic studies[68]. Hence, PYCRs could have undisclosed metabolic functions.

Proline catabolism prevails in the mitochondria via proline dehydrogenase (POX/PRODH1), a flavin-containing enzyme which couples the reduction of coenzyme Q with proline oxidation[56]. Upregulation of PRODH1 by p53, increases ROS levels, resulting in mitochondrial DNA and membrane damage, cytochrome c release and caspase 9 activation[69]. Yet, recent evidence suggests that mitochondrial proline catabolism is fundamental in early stages of breast cancer metastases formation[70]. PRODH exists in two isoforms, PRODH1 and 2, the major activity of the second one being oxidation of *trans*-4-hydroxy-L-proline to 3-OH-P5C, using Ubiquinone-10 as final electron acceptor[56].

Alternatively, aldehyde dehydrogenase 4 family member A1 (ALDH4A1) sustains proline catabolism by catalyzing the NAD^+-dependent conversion of GSA to generate glutamate[56]. As a result of this reaction, NADH acts as an electron donor to support ETC activity, whereas, glutamate can provide carbon to TCA cycle and ammonia for recovering of nitrogen[56]. In addition, glutamate can contribute to glutathione formation, an essential scavenging system against reactive oxygen species[56]. Recent evidence suggests that TCA cycle disruption impairs proline and aspartate biosynthesis whilst increasing glutathione production in kidney epithelial cells. Engagement of glutathione synthesis normalises $NADP^+$ levels and consumes cytosolic ATP, whereas proline biosynthesis via P5CS is impaired due to the lack of mitochondrial ATP upon TCA inhibition[71]. This mechanism was observed in FH- and SDH-deficient cells, but SDHi cells also display impairment in asparagine production and reductive carboxylation.

This suggests that cancer cells can engage in enzyme-specific metabolic compensations[71].

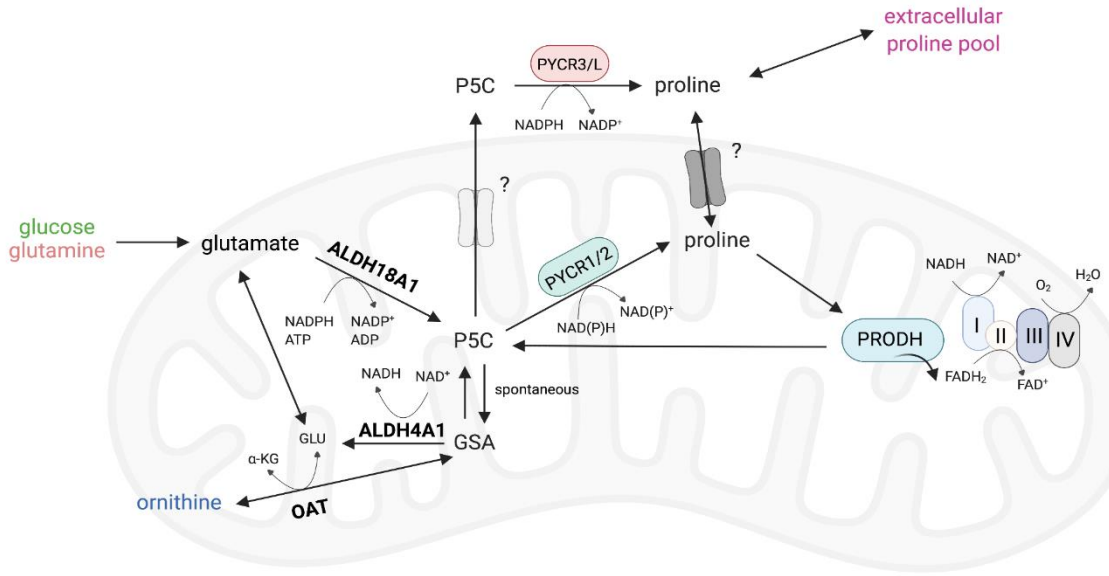

Figure 1.4 Schematic overview of proline metabolism

Proline can be endogenously synthesized from PYCRs and catabolysed by PRODH in the mitochondria. OAT and ALDH18A1 can catalyse the production of P5C respectively from ornithine or glucose and glutamine. Finally, ALDH4A1 can convert GSA into glutamate regenerating mitochondrial NADH. Abbreviations: PYCR1,2, Pyrroline-5-carboxylate reductase 1,2; PYCRL, Pyrroline-5-carboxylate reductase-like; PRODH, Proline dehydrogenase 1; ALDH18A1, Aldehyde dehydrogenase 18 family member A1; ALDH4A1, Aldehyde dehydrogenase 4 family member A1; OAT, Ornithine aminotransferase; α-KG, α-ketoglutarate; glu, glutamate; P5C, 1-pyrroline-5-carboxylate; GSA, glutamate semialdehyde.

1.3.2 Proline in hypoxia

Hypoxia creates a condition of electron excess and therefore cancer cells have developed different strategies to regenerate electron acceptors under this condition. Previous data from our lab suggests that PYCR1 activity is enhanced in hypoxia and in glioma IDH-mutant cells[72,73]. This event sustains the regeneration of mitochondrial NAD^+, partially uncoupling TCA cycle from ETC, and therefore supporting cell survival when electron acceptors are limiting[72,73]. This process has also been demonstrated in fibroblasts stimulated by TGF-β, where proline is used as a means of maintaining an appropriate redox ratio, which, in turn, normalises ROS induced by TGF-β-dependent increase of glucose and glutamine catabolism[74]. Alternatively, hypoxic cells can engage lipid biosynthesis to dissipate electron excess when proline synthesis is impaired. This model has been confirmed *in vivo* where P5CS KO murine breast cancer xenografts showed decreased cell growth when treated with statins – cholesterol synthesis inhibitors[75].

Proline is also a building-block for collagen and the process of collagen deposition can also be influenced by hypoxia in some cell types. In fact, osteoclasts rely on HIF-1α signalling to increase the total collagen turnover by hydroxylating proline and lysine[76]. Collagen hydroxylation is essential to make cartilaginous matrix less susceptible to protease degradation and aberrant HIF-1α activation can lead to collagen overmodification, a priming condition for fibrosis and cancer[76]. The same finding was confirmed in triple-negative breast cancer cells where increased expression of prolyl 4-hydroxylase alpha 1 subunit (P4HA1) – the enzyme responsible

of the hydroxylation of proline into hydroxyproline coupled with the production of succinate from αKG – augments HIF-1α stability by increasing succinate levels[77].

1.3.3 Proline transport

Intracellular proline homeostasis is also balanced by specific proline transporters which control proline fluxes inside and outside the cell[78]. To date, 12 transporters are known to mediate cytoplasmic proline shuttling, displaying a marked tissue specificity[78].
For instance, proline can be exported from the brain to the blood-brain barrier through SLC38A2, alongside glycine and Na^+. This helps buffering the concentration of small neutral amino acids and osmotic pressure in the brain[79]. A similar observation has been found in retina-to-blood transport where SLC38A2 was responsible of proline export in this system[80]. Conversely, SLC6A20 and SLC36A1 mediate proline uptake, respectively in the human retinal pigment epithelium and in a pancreatic cancer cell line model[78,81,82]. Another example of a tissue-specific proline transporter is SLC6A7, a proline importer selectively expressed in human brain[83].

Beyond tissue-selectivity, proline transporters can also be compartment-specific. An example is SLC36A1 which is also expressed in lysosomes and co-transports other small amino acids, such as alanine and γ-aminobutyric acid. The role of this transporter in lysosomes is mainly export coupled to the activity of the H^+-ATPase of the same organelle. Neurons display the highest expression of lysosomal SLC36A1[84]. Interestingly, a mitochondrial proline or P5C transporter has not been identified yet. For proline, it has been hypothesized that one proline transporter exists either coupled to ETC gradient or potentially coupled to a cation such as K^+; and one

proline/glutamate antiporter[85,86]. The latter has a higher Km and can potentially supply mitochondria with proline when the proline uniporter/symporter is saturated[86]. Even if the mitochondrial proline transporters are not known, it has been demonstrated in plants that proline is imported into the mitochondria and P5C exported to allow the P5C-proline shuttling between mitochondria and cytosol[87]. In this way, cells can control ROS and redox balance in both compartments[87,88].

Proline transporters can also fulfill stage-dependent intracellular proline requirements. For instance, proline uptake through SLC38A2 is necessary for embryonic stem cells and osteoblasts differentiation[89,90]. High proline demand during differentiation helps drive the proline-rich protein production of osteoclasts. As a result, SLC38A2-deficient osteoclasts halt cell differentiation and ossification. Interestingly, the same transporter can be stored in the perinuclear space to be quickly relocated to the plasma membrane in case of amino acid deficiency in muscle and adipose cells[89].

External factors can also influence proline transport, for example Ca^{2+} levels, insulin, and other metabolites. Human cells lacking the scaffold component MCUR1 of the mitochondrial calcium uniporter (MCU), have shown a faster influx of proline in the mitochondria and perturbed redox homeostasis[91]. Similarly, insulin influences the translocation of SLC38A2 from the trans-Golgi storage site of the transporter to the plasma membrane in 3T3-L1 adipocytes whereas ceramide, a byproduct of cytokine and sphingolipid metabolism attenuates the expression of SLC38A2[92,93,94].

In the context of disease, SLC36-family supports tumour growth by providing exogenous proline in fruit flies. Mechanistically, cachectic muscles free exogenous proline in the circulation which is then taken up by tumours[82]. Alternatively, SLC36A1 expression has been shown to induce resistance against cell cycle protein inhibitors in melanoma cells. Nevertheless, in this case it is more likely that the resistance is not mediated by amino acid import, but rather the protein itself[95].

1.3.4 Proline availability in the tumour microenvironment

Systemic proline availability is the output of influx and efflux from different organs and diet[60]. Proline, as well as hydroxyproline, comes from the hydrolysis of dietary proteins in the small intestine[96]. Proline and preferentially hydroxyproline can then be consumed by the microbiota to produce propionate and acetate (metabolised by the liver), before they reach the circulation[96]. However, around 60% of proline reaches the plasma after enterocyte utilisation which accounts for approximately 40% of the total diet-derived proline[96]. 50% of circulating proline is then absorbed by the liver with the rest available for uptake and metabolism by other organs[81]. Proline blood concentrations fluctuate between 100-200 μM, which includes contribution from endogenous synthesis[97].

Interestingly, the increased proline plasma levels have been associated with some diseases such as hepatic fibrosis, type 2 diabetes, and obesity[98]. Inborn errors of metabolism can also cause hyperprolinaemia. For example, PRODH deficiency in patients causes hyperprolinaemia type I and the velo-cardio-facial syndrome[99].

Alternatively, loss of ALDH4A1 causes hyperprolinaemia type II and is associated with metabolic dysfunction, especially of the urea cycle[99].

In physiological conditions, some cell types tend to uptake more proline whereas others are more prone to secretion. This is the case of retinal pigment epithelial cells which prefer to take up proline compared to other tissues[100]. Proline can then be metabolised into TCA cycle intermediates which are secreted into the local microenvironment to be taken up by nearby photoreceptor cells[100]. This is an example of symbiotic relationship where both cells can benefit. Alternatively, M2-like macrophages are more likely to consume of collagen, even if the clear mechanism of why this is the case has not been delineated yet[101].

Recent evidence suggests that in breast tumours, cancer-associated fibroblasts (CAFs) upregulate PYCR1 which directs a portion of cellular glutamine to produce proline, which can then be used for collagen synthesis[102]. Indeed, knockdown of PYCR1 in CAFs is sufficient to impair tumour growth and collagen production[102]. Interestingly, this collagen produced could be a source of proline for tumours – this was shown first in pancreatic ductal adenocarcinoma (PDAC), in which cells take up collagen during glutamine deprivation[103].

Exogenous proline availability can compensate for local proline deficiency. For instance, NAD kinase 2 (NADK2) supports proline production by providing the $NADP^+$ required for endogenous proline biosynthesis and loss of NADK2 makes tumours proline auxotrophic[104,105]. Similarly, NADK2-deficient fibroblasts from patients display

reduced NADPH levels and increased proline levels in the circulation[106]. This suggests that while it can compensate for deficiencies in cellular proline levels, exogenous proline cannot compensate for local redox imbalance[106].

Hypoxia also influences local and systemic proline availability, especially during cancer and inflammation. During chronic inflammation, macrophages type M2 and T $CD4^+$ cells release cytokines that drive fibroblasts activation into myofibroblasts[107]. This subtype of fibroblasts produces up to 30% of the total collagen[107,108]. Therefore, aberrant activation of fibroblasts results in a significant increase in collagen deposition, a process known as fibrosis[107]. Chronic inflammation requires therefore a large amount of proline to fuel excess collagen deposition, a phenotype that can be achieved by increasing the activity of proline biosynthesis enzymes. Upregulation of endogenous proline biosynthesis therefore results in cells to require intracellular redox adjustments to compensate[74].

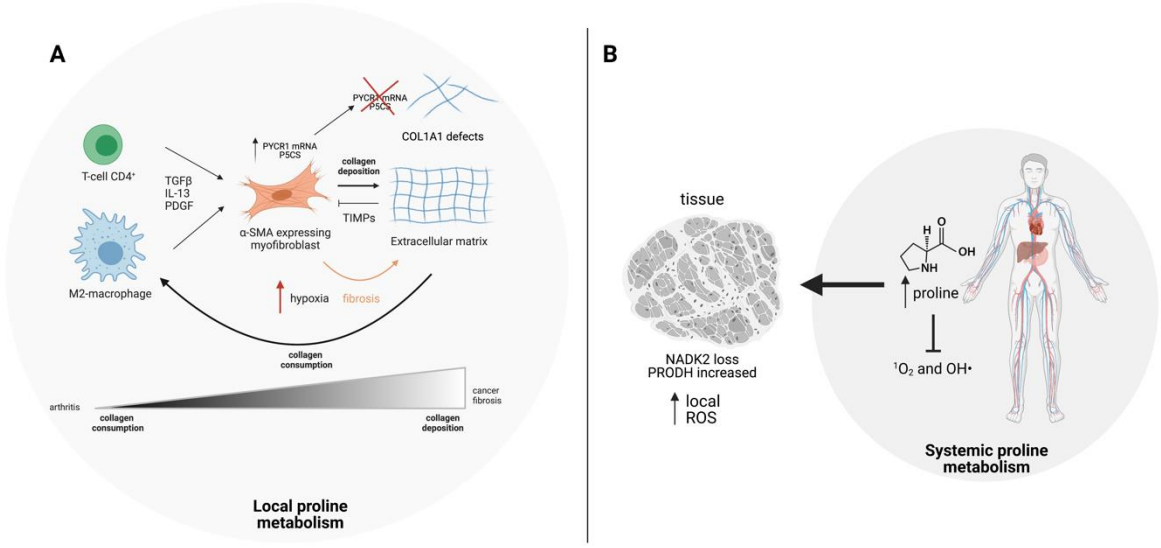

Figure 1.5 Integration between local and systemic proline metabolism

Locally, T-CD4+ cells and M2-macrophages secrete factors that activate fibroblast to increase enzymes involved in proline biosynthesis and collagen deposition. Alternatively, hypoxia can also increase fibrosis. Any imbalance between collagen deposition and consumption lead to disease, such as cancer. Systemically, proline availability can fulfill local proline needs, but cannot compensate for regional redox imbalance. Abbreviations: TGF-β, Transforming growth factor β; IL-13, Interleukin-13, PDGF, platelet-derived growth factor; TIMPs, Tissue inhibitor metalloprotease; PYCR1, Pyrroline-5-carboxylate reductase 1; P5CS, Pyrroline-5-carboxylate synthase; α-SMA, alpha smooth muscle actin; NADK2, NAD Kinase 2; PRODH, Proline dehydrogenase; ROS, reactive oxygen species.

1.4 Tools to investigate cancer metabolism

1.4.1 Metabolomics

Metabolomics allows the determination of comprehensive intra- and extracellular metabolite levels in different biological samples, including tissue and fluids[109].

Recent technological advancement in the instrumentation support metabolomics studies and the downstream software has supported the huge progress in our understanding of cancer metabolism over the past 20 years, and now provides the underpinnings of a broad knowledge base of how metabolism is altered in a number of diseases[110]. For instance, metabolic profiling highlighted that IDH1 and IDH2 – the enzymes that convert isocitrate to α-KG – when mutated, catalyse an alternative reaction that produces D-2-hydroxyglutarate from α-KG[111]. High abundance of this metabolite competes with α-KG as a substrate in histone and DNA demethylases reactions, as previously highlighted. Failure of accomplishing those reactions causes a problem with activation of the genetic differentiation program. This, in turn, can support malignancy in IDH-mutant tumours[112,113]. Today, levels of D-2-hydroxyglutarate can be used to follow disease progression[114].

One of the instruments that enables the measurement of the metabolome is gas-chromatography mass spectrometry (GC-MS). Gas chromatography (GC) separates analytes by vaporising the sample into a chromatographic column[115]. The sample is then carried though the column via an inert gas, such as helium (mobile phase)[115]. The GC is divided into two sub-groups one where the stationary phase of the column is solid (packed column) and one where it is liquid (capillary column)[115]. The separation of metabolites in the column happens according to their chemical properties and their

ability to bind to the column[116]. After passing through the column, analytes are charged (ionised) and enter a vacuum chamber where repelling electrodes constrain the ions through focusing lenses[116]. This leads the sample to reach the analyser part of the mass spectrometer where ionised molecules can also be fragmented[116]. The metabolites inside the mass spectrometer can then reach the detector based on their mass to charge ratio (m/z)[116]. According to the fragmentation pattern, also called as "mass spectrum", is then possible to identify a specific molecule[116].

Liquid chromatography mass spectrometry (LC-MS) uses a liquid mobile phase to carry the analytes through the column[117]. As for the GC system, the sample is then ionised before entering the mass analyser[117].

There are different types of mass spectrometers, one example of which is the triple quadrupole. In this type of mass analyser, 2 sets of 4 parallel rods (first and second quadrupole) apply a magnetic field which makes the ionised molecules oscillate through the rods before reaching the detector[116,117]. In addition, through manipulation of the voltages it is possible to operate the analyser in different modes - either scanning the entire m/z range, or monitoring a specific m/z value[116,117]. Between the first and the second quadrupole there is another one designed for collision cell[116,117]. This quadrupole is configured to maintain the low pressure required for the collision gas (argon) to fragment ionised molecules[116,117,]. The advantage of having a triple quadrupole to aid in metabolite identification is reduced in GC-MS, as the chromatography alone is sufficient to resolve most of the analytes that make it through the column due to the more limited number of metabolites that are resolved by a single

method. Only recently the technology has allowed GC systems to be coupled to triple quadrupole or more advanced mass analysers.

Time-of-flight (TOF) mass analyser has more resolving power than triple quadruple MS systems. The TOF accelerates ions through a flight tube at a high voltage[118]. The ions reach a detector after passing through a reflector and the detector can acquire spectra very quickly[118]. TOF can be equipped with a quadrupole and a collision cell, this set-up is known as Q-TOF[118].

Further increased resolution can be achieved by ion trap analysers, such as Orbitrap. This mass analyser traps the ions by making them oscillate around a spindle electrode closed in a vacuum chamber[119]. m/z ratio is measured by the frequency of harmonic oscillation of the ions parallel to the axis of the spindle[119]. Fourier transform algorithms are then applied to reconstruct the metabolite spectrum in a manner analogous to NMR spectroscopy[119].

1.4.2 Isotope tracing

Changes in the concentration of -intra and extracellular metabolites achieved by metabolomics do not necessarily provide insight into the specific metabolic flux of a single/multiple reactions[120,121]. Therefore, if metabolomics allows the quantitation of the total production/consumption of a certain metabolite, isotope tracing maps the flux of one or multiple reactions catalysed by different enzymes[120,121]. The specific flux of a certain reaction/pathway is measured by enriching metabolites with heavy labelled isotopes (isotope tracers), such as ^{13}C; a naturally occurring carbon isotope with an

additional neutron that causes a mass shift of one. Most frequently, the heavy isotopes selected are stable – i.e. non-radioactive, as this reduces the technical complexity of dealing with radioactivity within the analytical pathway. By tracking the fate of the heavy isotope in cellular metabolism, is possible to frame a snapshot of the activity of a specific enzyme, by looking at the flux rate over time [120,121]. This is also defined as isotopic steady state or dynamic labelling, which examines the enrichment of an isotopic tracer into metabolites before becoming stable (metabolic steady state). During metabolic steady state, intracellular fluxes and metabolite abundances are maintained constant, as the cell number and concentration of nutrients in cell culture condition do not change or are minimal (metabolic pseudo-steady state). Under this condition, it is possible to establish relative or absolute pathway usage. In the latter case, the extracellular flux exchange is taken into account over time as well as media volume, according to this formula:

$$\frac{C_f - C_i}{N * h * V}$$

C_f = final concentration
C_i = initial concentration
N = cell number
h = hours
V = media volume

In addition, it is possible to multiply the total abundance of a molecule to the most abundant isotopologue - part of the mass isotopologue distribution (MID) – to map out the incorporation of each carbon source into the metabolite of interest. The MID highlights how the isotope tracer is distributed within a molecule. Metabolic flux analysis (MFA) allow us to infer the contribution of specific metabolic reactions from the MID pattern of a metabolite[122]. To further confirm that a specific reaction has been correctly unpicked, more specialist positional labelling can be used in which a

metabolic with one or more heavy isotopes incorporated into specific parts of the molecule (^{13}C, ^{15}N, ^{2}H or ^{18}O) is used. For instance, 1,2-$^{13}C_2$-glucose can be used to identify the metabolic flux from glycolysis into the pentose phosphate pathway (PPP)[121].

Given that heavy labelled tracers are also naturally present in all nutrient sources, even if in minimal part, it is necessary to correct for their abundance[123]. Natural abundance can be estimated experimentally from the biological sample with additional use of standards or mathematically inferred[123].

In vivo isotope tracing has revealed metabolic heterogeneity, within tissues, including cancers[124]. For example, dissected mouse brain slices uncovered a similar labelling pattern from $^{13}C_6$-glucose in the hippocampus and the cortex[124]. However, 1,2-^{13}C-acetate tracing showed differential labelling between these brain areas, with increased m+2 labelling into the TCA cycle intermediates in the hippocampus compared to the cortex[124]. To be able to have confidence in those measurements, an assumption of *in vivo* steady state is important, which in turn requires constant infusion of the tracer of interest and determining the tracer/tracee ratio from the blood sampling at different time points[125]. In this way, it is possible to adjust for the tracer dilution in the sample (tracer dilution model) at the point of sampling[125]. Alternatively, it is possible to determine the quantification of flux *in vivo* by using the tracer incorporation model. According to this method, it is possible to calculate the fractional or absolute synthesis rate of a specific product assuming that the precursor is at steady state[125]. The product enrichment is monitored over time and increases until it is the same as the precursor[125].

The fractional synthesis rate (FSR) can be calculated by dividing the enrichment of the product over time divided by the pool size of the precursor[125]. The absolute synthesis rate (ASR) can be obtained by multiplying FSR to the pool size of the product[125].

1.5 Thesis aims

Cancer proliferation often demands oxygen to the extent that the vasculature cannot supply, leading to tumor hypoxia. In hypoxic regions cancer cells reprogram their metabolism to survive and this often results in poor prognosis and treatment resistance. A better understanding of how cancer cells restructure their metabolism in hypoxia is therefore required to develop more selective treatment strategies for patients and overcoming relapses.

Proline levels often increase in hypoxic tumours, but how cancer cells re-route proline metabolism towards this adjustment and if this is important for tumour survival and growth is not yet understood. This thesis aims to investigate how cancer cells restructure proline metabolism to survive in hypoxia, identifying targetable vulnerabilities, such as the less studied cytosolic proline biosynthesis enzyme PYCRL and the proline transporter SLC38A2 in glioma. In addition, we investigate how proline biosynthesis is regulated in hypoxic regions to better understand this metabolic adaptation in cancer. In addressing these questions, we hope to expand the knowledge of this metabolic network to open further opportunities for cancer treatment in the future.

CHAPTER 2:

PYCRL regenerates NAD^+ to support proliferation and survival in hypoxic cancer cells

2.1 Introduction

The mitochondrial proline biosynthesis enzymes (PYCR1,2 and ALDH18A1) have been extensively studied for their importance in supporting tumour growth in different cancer types, such as kidney, liver and neuroblastoma. Recently, NADK2 has been shown to support mitochondrial proline biosynthesis by providing $NADP^+$ to sustain ALDH18A1 activity and, in turn, mitochondrial PYCRs. On the other hand, the cytoplasmic proline-producing enzyme PYCR3 is less studied and whether it plays a role in tumour progression is still unknown.

Previous data from our lab have shown that PYCR1 is essential in redox control in IDH1 mutant in gliomas[126]. Mechanistically, PYCR1 regenerates the NAD^+ required for proliferation when the electron transport chain activity is impaired in IDH1 mutant glioma. Nevertheless, the role of this enzyme and other PYCRs has not been uncovered yet in IDH-wt hypoxic gliomas and other cancer types.

2.2 Results

2.2.1 Intracellular and extracellular proline levels are increased in hypoxia

To investigate the role of proline in hypoxic cancer cells, A172 glioblastoma stem-like cells and HCC1806 triple-negative breast cancer stem-like cells were used to assess intracellular and extracellular proline levels (Figure 2.1A-D) under different oxygen tensions. The selection of these cell lines comes from a screening done by a collaborator in Luxembourg, indicating that PYCRL mRNA expression was increased specifically in cancer stem cells and further confirmed in our lab (data not shown). Intracellular and extracellular proline levels were indeed increased in hypoxia (1% or 0.3%), suggesting that cancer cells increase endogenous synthesis, rather than promoting extracellular uptake. To further understand the sources of intracellular proline, ^{13}C-enriched carbon sources, such as $^{13}C_5$-glutamine, $^{13}C_5$-ornithine, $^{13}C_6$-glucose were employed, with the contribution of extracellular proline taken into account through the use of $^{13}C_5$-proline (Figure 2.1E-F). Figure 2.1F indicates that approximately 60% of intracellular proline is exogenous, whereas 20% is endogenously synthesised. The remaining proline can come from other sources, such as protein breakdown.

To understand which of the three proline biosynthesis enzymes is responsible of increased proline production in hypoxia, protein levels were assessed by western blot at different oxygen tensions (21%O_2, 1%O_2, 0.3%O_2) in HCC1806 and A172 cell lines (Figure 2.2 A-B). Among the three enzymes, PYCRL was the only one upregulated in glioblastoma at lower oxygen tensions. The difference, however, was less in HCC1806 triple-negative breast cancer cell line, suggesting that PYCR protein expression may be cancer dependent.

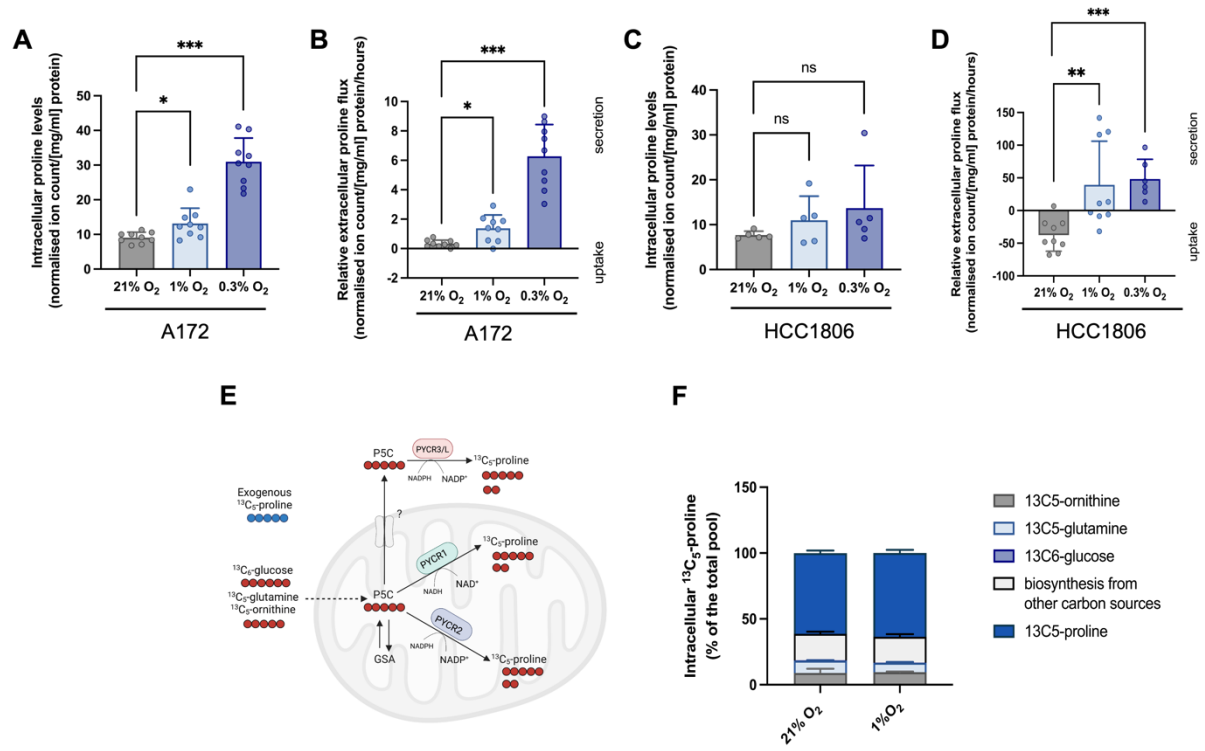

Figure 2.1 Intracellular and extracellular proline levels increase in hypoxia

(A-B) Intracellular and extracellular proline levels in A172 glioblastoma cell line at different oxygen tensions. (C-D) intracellular and extracellular proline levels in HCC1806 triple-negative breast cancer cells. (E) Diagram showing endogenous (red dots) and exogenous (blue dots) sources of proline. (F) Carbon sources contributing to intracellular proline levels in A172 glioblastoma cell line in normoxia (21% O_2) and hypoxia (1% O_2). Error bars indicate ± S.E.M. and each experiment was conducted with three biological replicates. The Mann-Whitney test was used to determine the statistical significance *** p<0.001, * p<0.05, ** p<0.01.

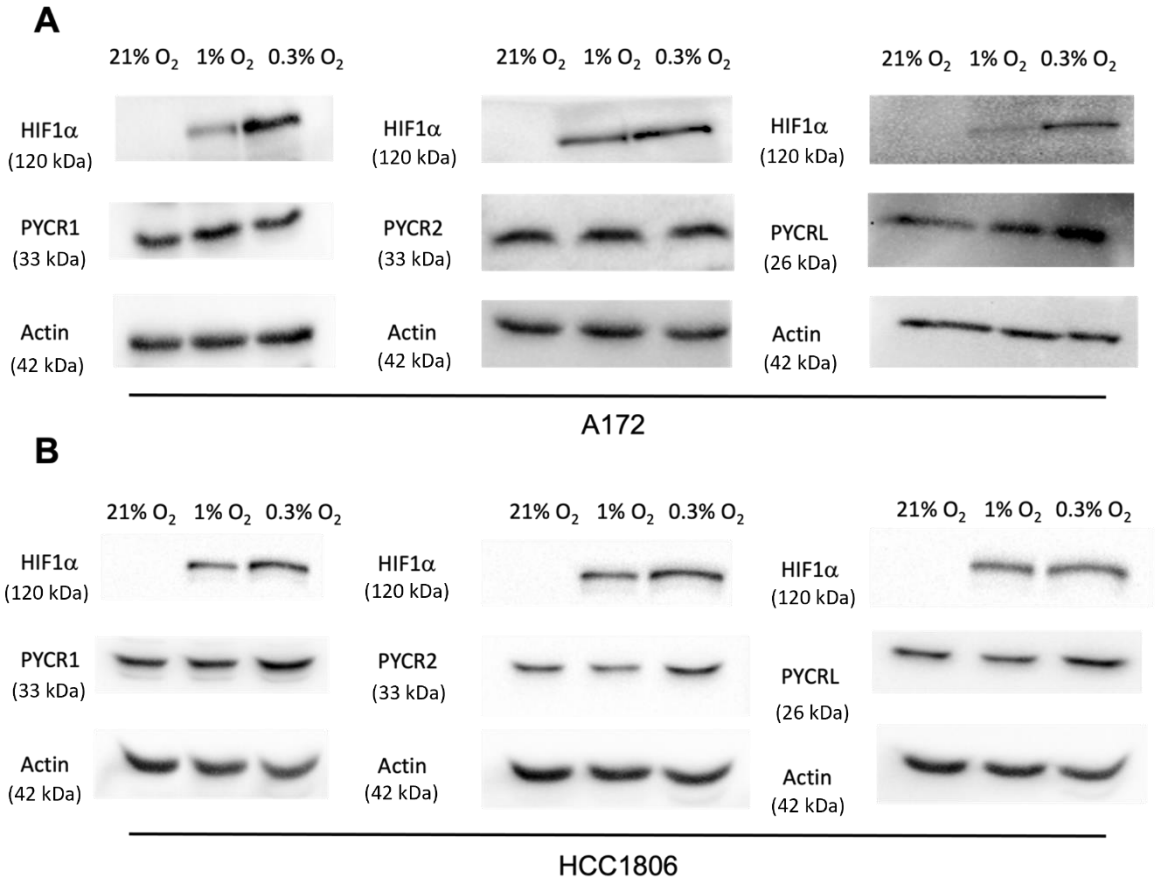

Figure 2.2 PYCRL protein expression is upregulated in glioblastoma at lower oxygen tensions
(A) Western blot in A172 glioblastoma cell line shows the expression levels of PYCR1, PYCR2 and PYCRL in normoxia and hypoxia. (B) PYCRs protein expression levels in HCC1806 triple-negative breast cancer cell line at different oxygen tensions.

2.2.2 PYCRL is upregulated in hypoxic glioblastoma though TGF-β signaling

To further investigate how PYCRL protein levels were regulated in hypoxic glioblastoma cells, A172 cell line was treated with the PHD2 inhibitor, IOX2 at a concentration of 50 μM (Figure 2.3A). Surprisingly, stabilization of HIF-1α mediated by IOX2 does not change PYCRL expression levels, indicating that the protein upregulation of this enzyme is PHD2 and HIF-1α-independent. In the literature is shown that hypoxic fibroblasts induce PYCR1 and 2 expression via TGF-β[74]. To understand if this condition is also applicable to glioblastoma, TGF-β levels were assessed at lower oxygen tensions, showing the highest increase at 0.3% O_2 (Figure 2.3B). A172 cells were then treated with 15 ng/ml of TGF-β and/or adding the TGF-β inhibitor LY-2109761 (Figure 2.3C). While PYCRL protein levels were moderately increased with addition of TGF- β, the inhibitor remarkably reduced PYCRL protein levels, suggesting that PYCRL upregulation is at least in part TGF-β–mediated, with a role for basal autocrine/paracrine signalling. Proline production was gauged after supplementation with TGF-β and was shown to be increased, further confirming a TGF-β–PYCRL axis in A172 glioblastoma cell line (Figure 2.3D).

Interestingly, treatment with increasing concentrations of nutlin (a p53 activator), decrease PYCRL protein levels in different p53 wild-type glioblastoma cell lines (Figure 2.4A-C). This indicates that multiple signaling pathways are likely to be involved in PYCRL regulation, depending on the cellular context.

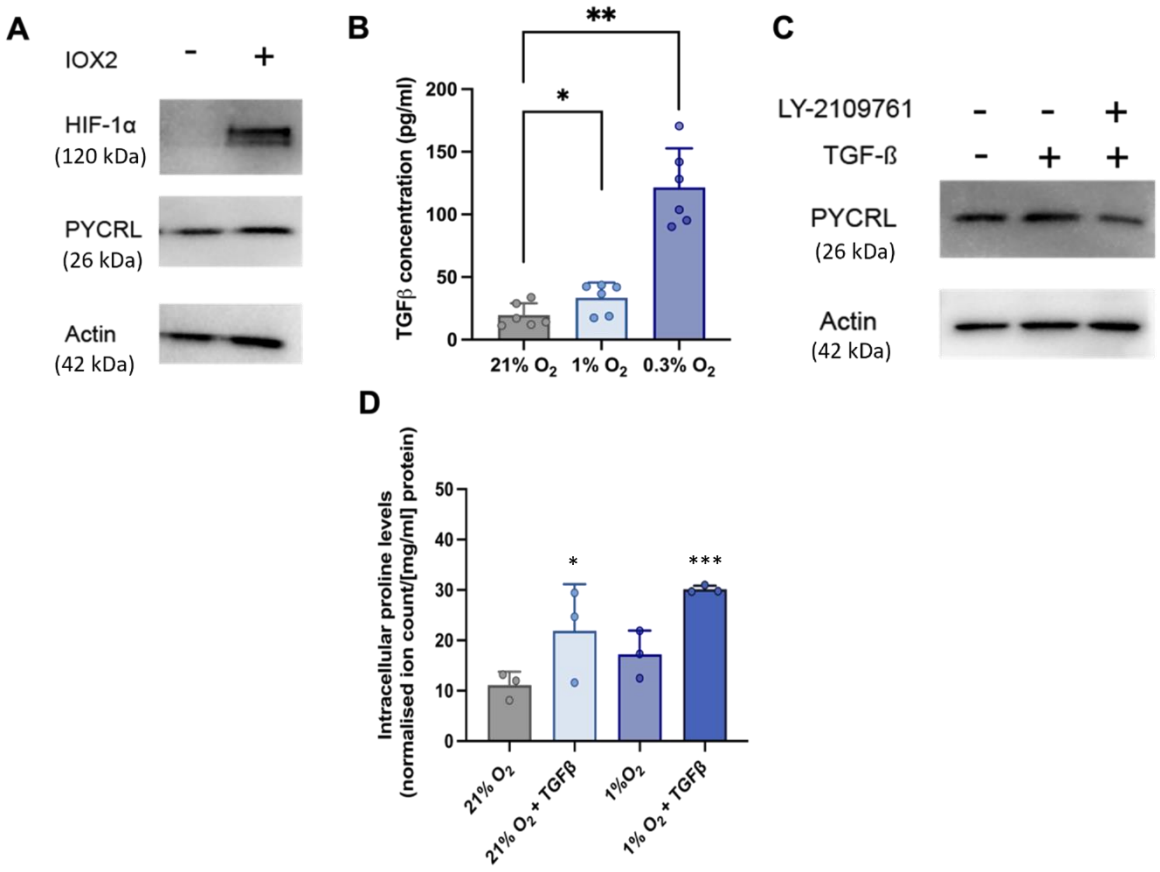

Figure 2.3 PYCRL is upregulated in hypoxic glioblastoma through TGF-β signalling

(A) PYCRL protein expression with or without the PHD2 inhibitor IOX2 (50 μM). (B) TGF-β concentrations at lower oxygen tensions measured by ELISA in the media. (C) PYCRL expression levels when A172 cells are treated with 15 ng/ml of TGF-β or with the TGF-β inhibitor LY-2109761. (D) Intracellular proline levels were assessed by GC-MS with or without TGF-β at 21% O_2 or at 1% O_2. Error bars indicate ± S.E.M. and each experiment was conducted with three biological replicates. The Mann-Whitney test was used to determine the statistical significance *** $p<0.001$, * $p<0.05$, ** $p<0.01$.

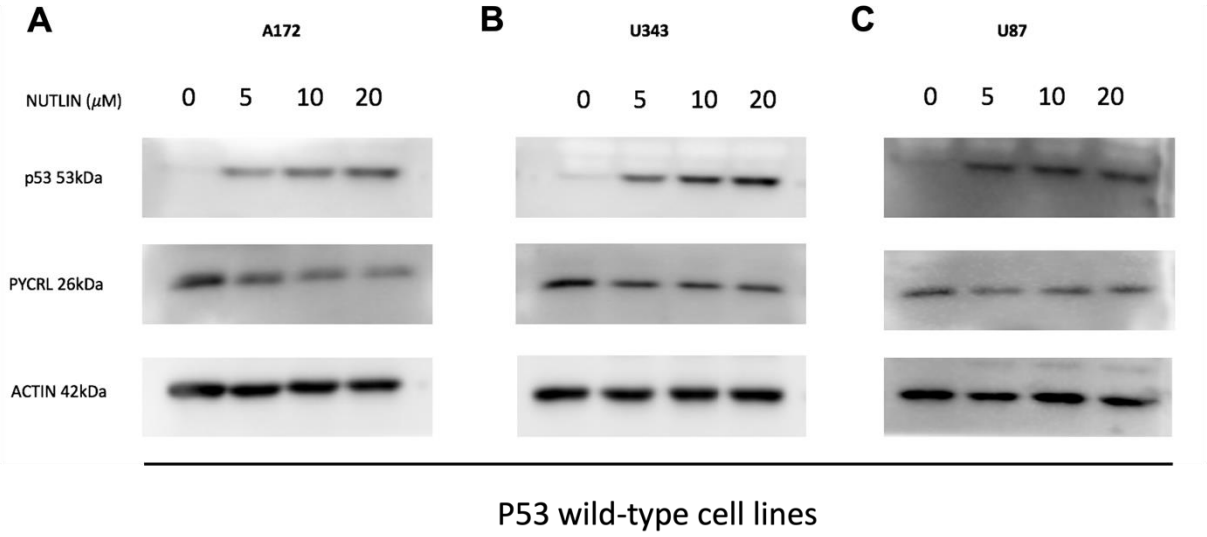

Figure 2.4 PYCRL protein levels are downregulated by p53 activation

(A-C) A172, U343 and U87 p53-wt glioblastoma cell lines were treated with increasing concentrations of nutlin, a well-known activator of p53.

2.2.3 PYCRL enzymatic activity is upregulated in hypoxia

To better understand the metabolic role of PYCRL in IDH-wt glioblastoma, two different cell types, A172 and NCH421k were engineered with an inducible construct that permitted the knockdown of PYCRL upon exposure to doxycycline (DOX). PYCRL protein levels were assessed by western blot after 48h of DOX treatment, confirming a successful knock-down (Figure 2.5A-B). We further confirmed a successful downregulation of PYCRL activity in A172 cell line in hypoxic conditions and in glioblastoma stem cells, NCH421k (Figure 2.5C-F). NCH421k cells grow as a 3D spheroid, mimicking glioblastoma growth in *vivo*, where tumours develop a hypoxic core.

To further confirm that PYCRL can contribute to proline production, HEK293 were engineered to be PYCR1 and 2 deficient (Figure 2.6B). HEK293 PYCR1/2 double-knockout (DKO) labelled with 4D-glucose were used as a tool to understand PYCR co-factor preference[127]. Indeed, 4D-glucose allows the measurement of incorporation of deuterated NADH into m+1 proline. Our data show that PYCRL can use NADH as a co-factor in normoxia, and to a minor extent in hypoxia (Figure 2.5G). DKO cells were then cultured in the absence of exogenous proline and incorporation into m+5 proline from m+5 glutamine or m+5 ornithine was gauged in figure 2.6A. This graph, in addition to the total intracellular and extracellular proline levels shown in figures 2.6C and D, suggests that PYCRL is sufficient to maintain proline production when PYCR1 and 2 are absent. However, figure 2.6E shows that despite proline levels being maintained in this model, the cells still exhibit a growth defect connected to the absence of PYCR1

and 2, confirming that these enzymes play an important role in cell proliferation independent of their proline-synthetic activity[73,74].

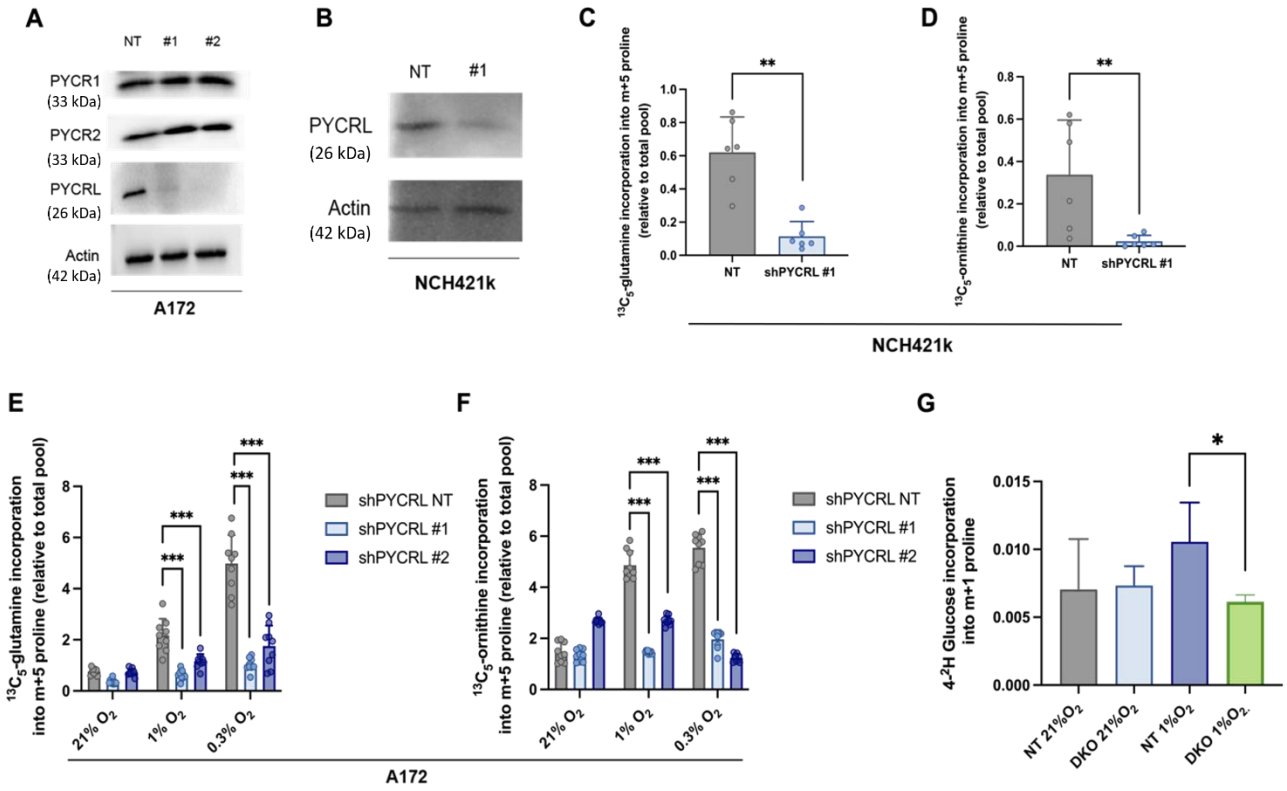

Figure 2.5 PYCRL-deficient cells confirm a block in proline production in hypoxic conditions
(A,B) Western blot showing doxycycline induced PYCRL KD, respectively in A172 and NCH421k glioblastoma cell lines. (C-F) m+5 proline levels either from m+5 glutamine or m+5 ornithine, respectively in NCH421k cells and A172 cell line in the presence or absence of PYCRL. (G) 4D-glucose incorporation into intracellular m+1 proline in HEK293 cells NT or PYCR1/2 double-knockout (DKO) in normoxia or hypoxia. Error bars indicate ± S.E.M. and each experiment was conducted with three biological replicates. The Mann-Whitney test was used to determine the statistical significance *** p<0.001, * p<0.05, ** p<0.01.

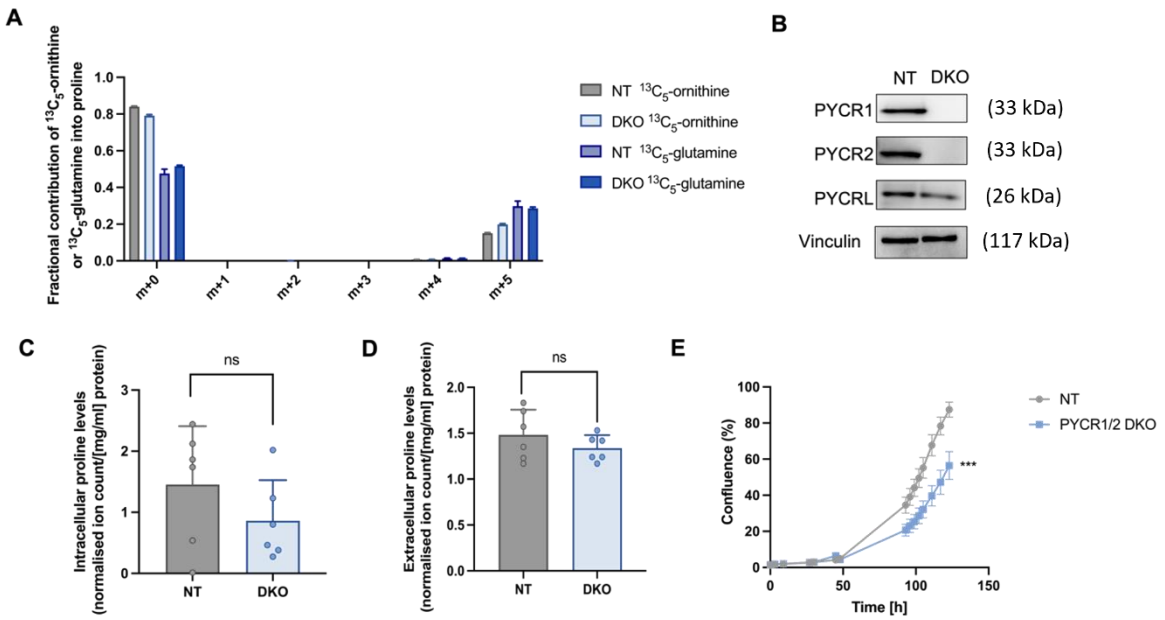

Figure 2.6 PYCRL maintains adequate intracellular proline levels in PYCR1/2 deficient cells

(A) Mass isotopologue distribution of $^{13}C_5$-ornithine or $^{13}C_5$-glutamine into proline in HEK293 cell line with or without PYCR1/2 double-knockout. (B) Western blot showing PYCR1,2 and L protein levels in HEK293 cells. (C-D) Intracellular and extracellular proline levels in PYCR1/2 deficient cells. (E) % cell confluence in PYCR1/2 double-knockout HEK293 cells compared to non-targeting control. Error bars indicate ± S.E.M. and each experiment was conducted with three biological replicates. The Mann-Whitney test was used to determine the statistical significance *** p<0.001, * p<0.05, ** p<0.01.

The enzymatic function of PYCRL was further explored to assess if this enzyme, alongside PYCR1 and 2 could work in reverse, or whether PRODH was contributing to this catabolic activity. To do this, proline deuterated in the positions that could be lost during PYCRs or PRODH reaction ($^2H_3$-2,5,5-proline) was supplemented to A172 glioblastoma cells (Figure 2.7A). When deuterated intracellular proline enrichment was measured by GC-MS, no m+2 proline was detected (Figure 2.7B). This result suggests that PYCRs cannot work in reverse and that PRODH does not use exogenous proline to catalyse its reaction. The absence of deuterium incorporation into lactate or

palmitate – respectively representing NADH or NADPH, if deuterated during proline reactions – further confirmed that PYCRs work canonically and that PRODH activity is not linked to exogenous proline carbons.

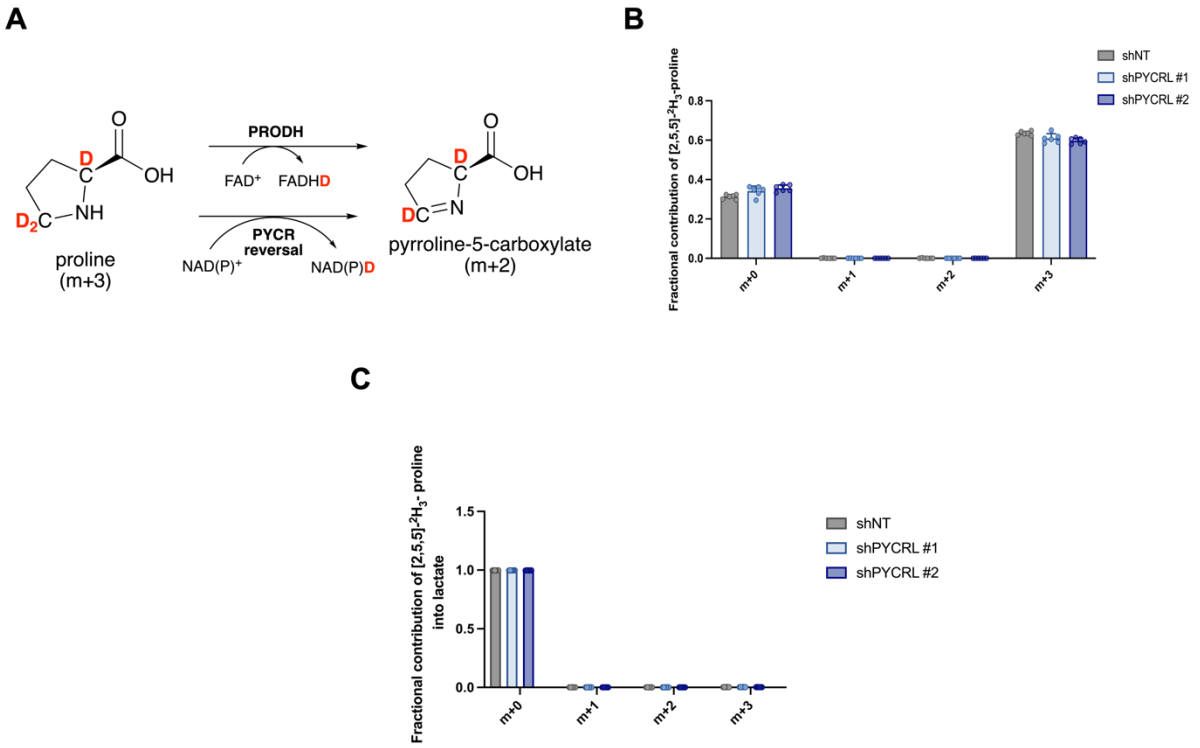

Figure 2.7 PYCRs cannot work in reverse and there is no PRODH activity from exogenous proline in standard culture conditions

(A) Diagram showing PRODH reaction in the presence of deuterated proline or hypothetical reversal of PYCRs activity. (B) Mass isotopologue distribution (MID) of $^{2}H_{3}$-proline labelling into intracellular proline in A172 glioblastoma cell line. (C) MID of $^{2}H_{3}$-proline into lactate. Experiments in figure (B) and (C) were performed in the presence of 200 μM of exogenous $^{2}H_{3}$-proline. Error bars indicate ± S.E.M. and each experiment was conducted with three biological replicates. The Mann-Whitney test was used to determine the statistical significance *** p<0.001, * p<0.05, ** p<0.01.

2.2.4 Metabolomics in PYCRL KD reveals a defect in nucleotide synthesis

After assessing PYCRL enzymatic activity, a metabolomic analysis was conducted in A172 KD cells to reveal potential metabolic differences compared to the non-targeting control (Figure 2.8A). Interestingly, nucleotides such as IMP as well as nucleotide precursors, such as AICAR and carbamoyl-aspartate were lower in PYCRL-deficient cells. This result was further confirmed by pathway enrichment analysis and principal component analysis (Figure 2.8B-C). Figure 2.9A-E further illustrates that PYCRL-deficient cells display a defect in aspartate-dependent reactions.

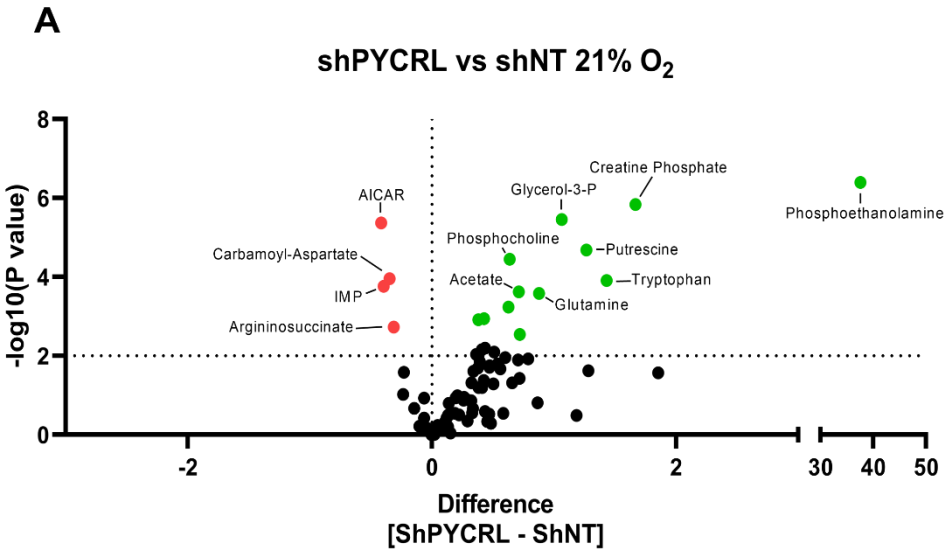
A
shPYCRL vs shNT 21% O2
-log10(P value)
Difference
[ShPYCRL - ShNT]
AICAR
Carbamoyl-Aspartate
IMP
Argininosuccinate
Creatine Phosphate
Glycerol-3-P
Phosphocholine
Putrescine
Acetate
Tryptophan
Glutamine
Phosphoethanolamine

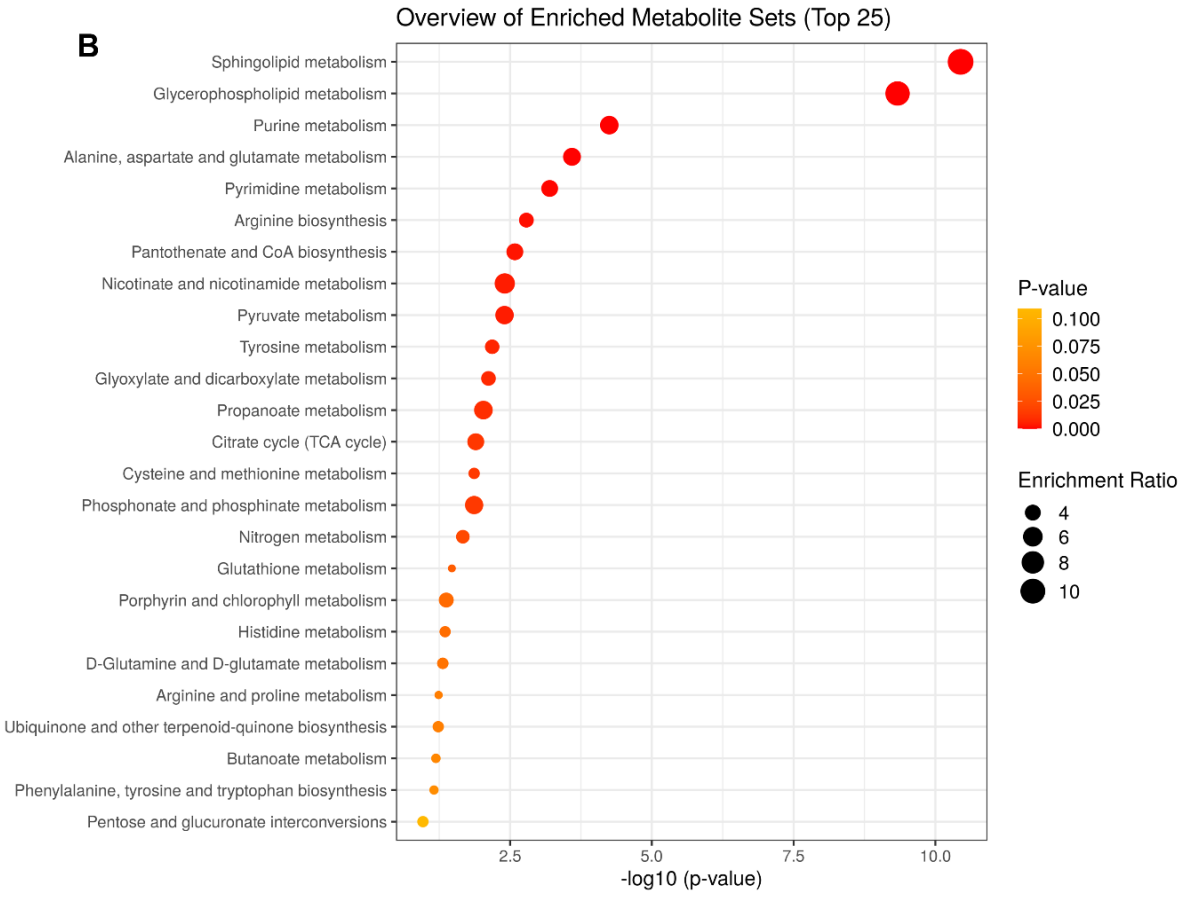
B
Overview of Enriched Metabolite Sets (Top 25)
Sphingolipid metabolism
Glycerophospholipid metabolism
Purine metabolism
Alanine, aspartate and glutamate metabolism
Pyrimidine metabolism
Arginine biosynthesis
Pantothenate and CoA biosynthesis
Nicotinate and nicotinamide metabolism
Pyruvate metabolism
Tyrosine metabolism
Glyoxylate and dicarboxylate metabolism
Propanoate metabolism
Citrate cycle (TCA cycle)
Cysteine and methionine metabolism
Phosphonate and phosphinate metabolism
Nitrogen metabolism
Glutathione metabolism
Porphyrin and chlorophyll metabolism
Histidine metabolism
D-Glutamine and D-glutamate metabolism
Arginine and proline metabolism
Ubiquinone and other terpenoid-quinone biosynthesis
Butanoate metabolism
Phenylalanine, tyrosine and tryptophan biosynthesis
Pentose and glucuronate interconversions
-log10 (p-value)
P-value
Enrichment Ratio

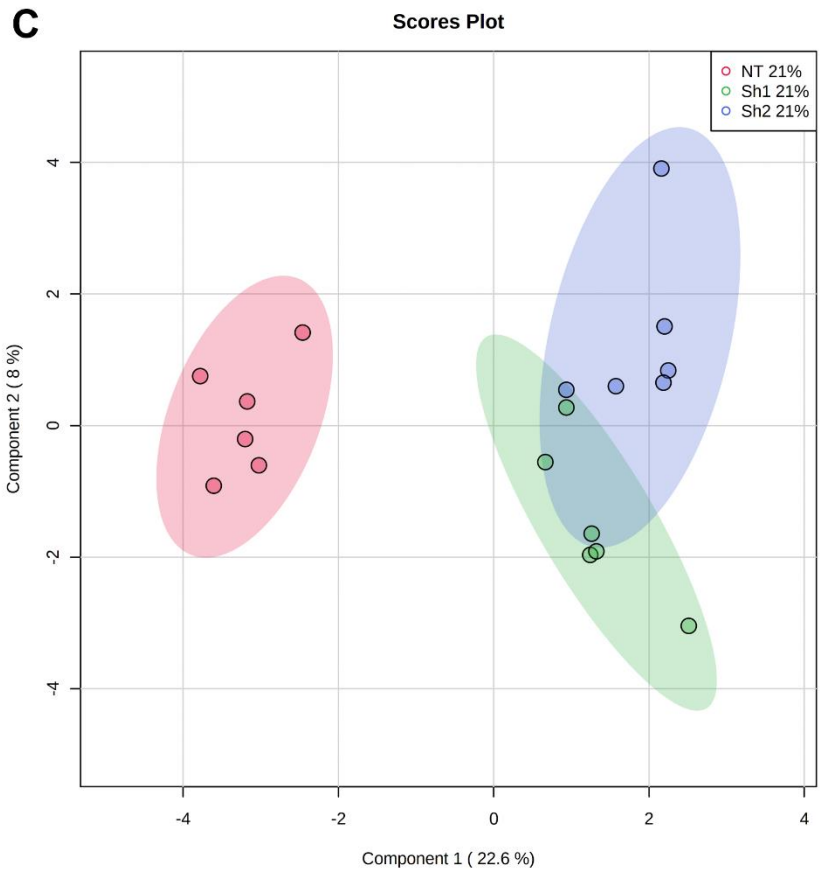

Figure 2.8 Metabolomics in PYCRL-deficient cells reveals a defect in nucleotide biosynthesis

(A) Volcano plot showing metabolites levels in doxycycline induced PYCRL-deficient A172 glioblastoma cell line. (B) Pathway enrichment analysis based on the metabolomic dataset in doxycycline induced PYCRL KD cells. (C) Principal component analysis (PCA) showing the clustering of NT control and doxycycline induced PYCRL KD based on metabolomics data. Data analysis conducted by Dr. Adam Boufersaoui. Each experiment was conducted with three biological replicates. Multiple unpaired t-test analysis was conducted to determine significance in figure (A), indicating in red or green $p<0.05$.

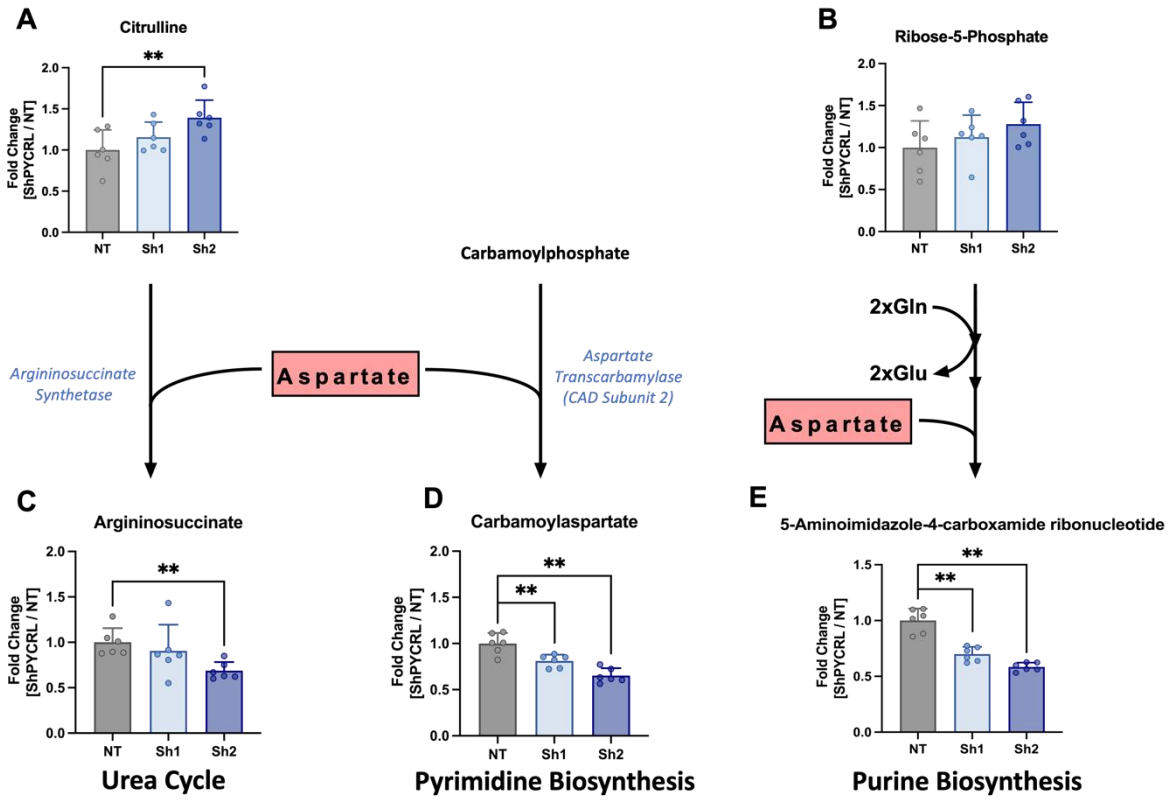

Figure 2.9 PYCRL KD cells display a reduced abundance in purines and pyrimidines precursors

(A-B) Citrulline and Ribose-5-phosphate abundance with or without doxycycline induced PYCRL KD. (C-E) Metabolite abundances of aspartate-dependent reactions in the presence or absence of doxycycline induced PYCRL. Data produced and analysis conducted by Dr. Adam Boufersaoui. Abbreviations: Gln: glutamine; Glu: glutamate. Error bars indicate ± S.E.M. and each experiment was conducted with three biological replicates. The Mann-Whitney test was used to determine the statistical significance *** p<0.001, * p<0.05, ** p<0.01.

2.2.5 PYCRL KD perturbs NADH/NAD$^+$ redox homeostasis

It has been shown that the major source of aspartate inside the cell is the mitochondrial TCA cycle. Investigation of $^{13}C_5$-glutamine labelling into TCA cycle intermediates was consistent with this: PYCRL KD led to a decrease in the levels of these metabolites, including aspartate, suggesting that TCA cycle turning is impaired in PYCRL KD cells (Figure 2.10A-E)[128]. The TCA cycle activity is tightly connected to ETC activity and redox homeostasis. These parameters were investigated in figure 2.11A-D. PYCRL KD demonstrated an increased NADH/NAD$^+$ ratio in normoxia and hypoxia (Figure 2.11A), revealing a perturbation in redox homeostasis. ETC activity was also altered in PYCRL-deficient cells towards increased oxygen consumption in normoxia and a decreased activity in hypoxia, where oxygen is less available (Figure 2.11B). Decreased ETC activity was also confirmed in hypoxia, by a noticeable accumulation of reduced CoQ_{10} at 1% O_2, and partly in reduced CoQ_9 abundance (Figure 2.11C). Further examination of the main output of ETC activity – oxidative phosphorylation - showed a drop in ATP levels in hypoxia upon PYCRL knockdown, suggesting that while the bioenergetic defects do not result in ATP depletion in normoxia, the additional stress of hypoxia tips the cells into energetic deficit (Figure 2.11D).

The perturbation in redox homeostasis elicited by PYCRL KD led to the hypothesis that cells can use the malate-aspartate shuttle to shuttle excess of NADH into the mitochondria, to allow this redox cofactor to be recycled by ETC (Figure 2.12B). Indeed, A172 glioblastoma cells prefer to regenerate NAD$^+$ through ETC activity as illustrated in figure 2.12A. When the malate-aspartate shuttle is halted by AOA treatment, cells try to recover NAD$^+$ by engaging LDH activity and increased lactate

production is observed. Another cytosolic NAD^+ regenerating shuttle, the glycerol-3-phosphate shuttle, is impaired in PYCRL KD cells, as illustrated by glycerol-3-phosphate accumulation in figure 2.12.C.

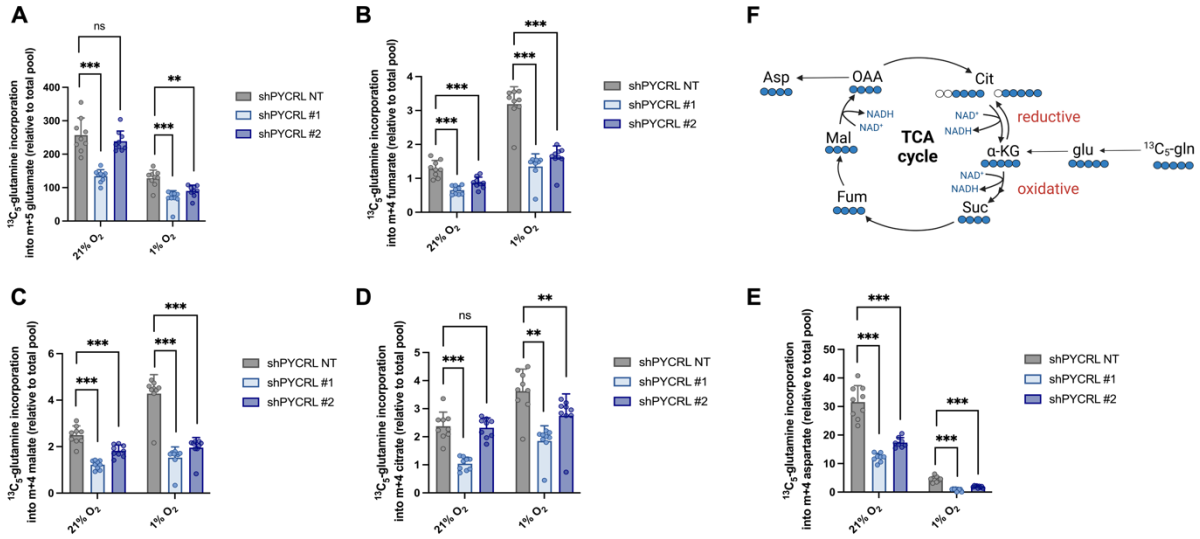

Figure 2.10 PYCRL KD reveals a defect in TCA cycling

(A-D) TCA cycle intermediates in doxycycline induced PYCRL NT or shPYCRL #1 or #2 measured by GC-MS. (E) m+5 glutamine incorporation into m+4 aspartate relative to total pool. (F) Diagram showing $^{13}C_5$-glutamine incorporation into TCA cycle intermediates and into aspartate. Abbreviations: Cit, citrate; Glu, glutamate; Gln, glutamine; Suc, succinate; Fum, fumarate; Mal, malate; OAA, oxaloacetate; asp, aspartate; α-KG, α-ketoglutarate. Error bars indicate ± S.E.M. and each experiment was conducted with three biological replicates. The Mann-Whitney test was used to determine the statistical significance *** p<0.001, * p<0.05, ** p<0.01.

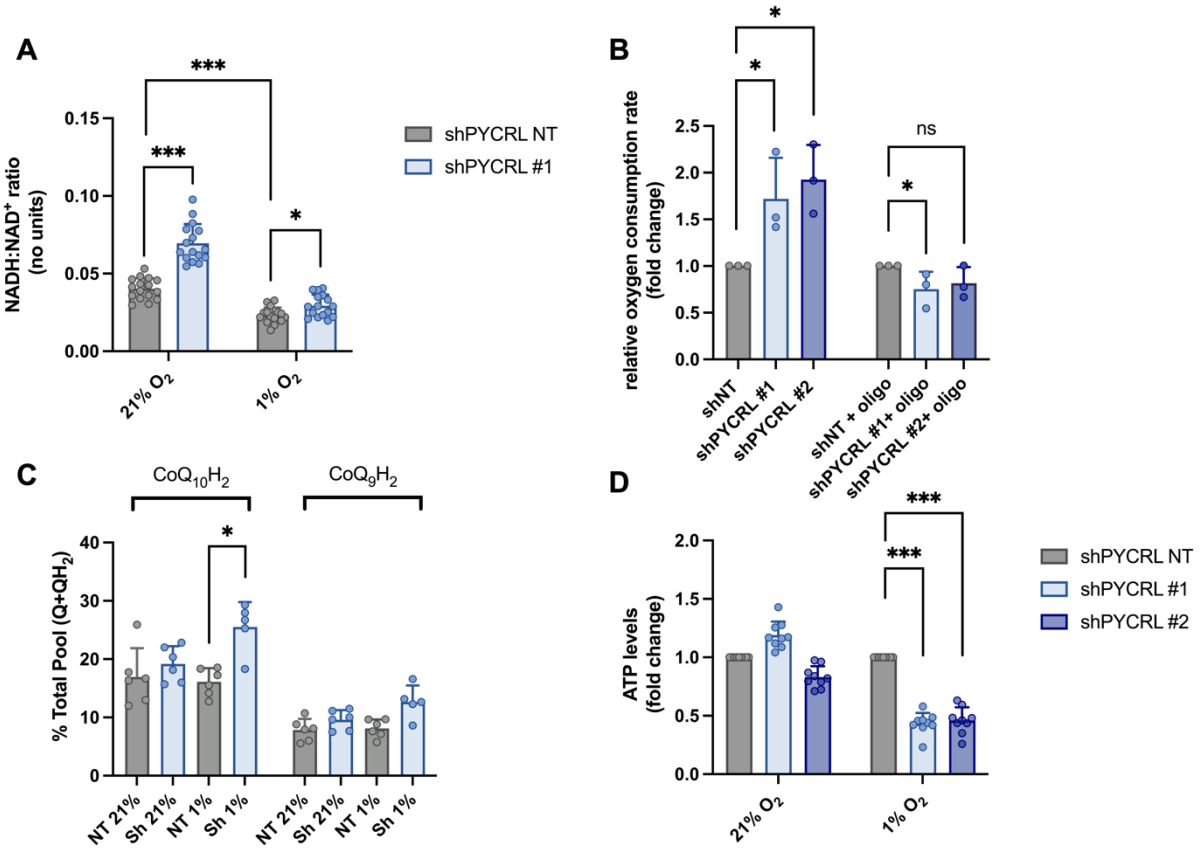

Figure 2.11 PYCRL inhibition alters NADH/NAD⁺ redox homeostasis and ETC activity

(A) Diagram showing NADH/NAD⁺ ratio with doxycycline induced PYCRL NT or shPYCRL #1 in A172 glioblastoma cell line at 21% or 1% O_2. (B) Relative oxygen consumption rate in the presence or absence of doxycycline induced PYCRL, with or without oligomycin (complex V inhibitor) in A172 glioblastoma cell line. (C) Abundance of reduced ubiquinone 9 or ubiquinone 10 pools with or without doxycycline induced PYCRL KD in normoxia or hypoxia. (D) Fold change of ATP levels measured in doxycycline induced non-targeting control or PYCRL-deficient A172 cells. Data for figure 2.11A and C were analysed by LC-MS by Dr. Adam Boufersaoui. Error bars indicate ± S.E.M. and each experiment was conducted with three biological replicates. The Mann-Whitney test was used to determine the statistical significance *** p<0.001, * p<0.05, ** p<0.01.

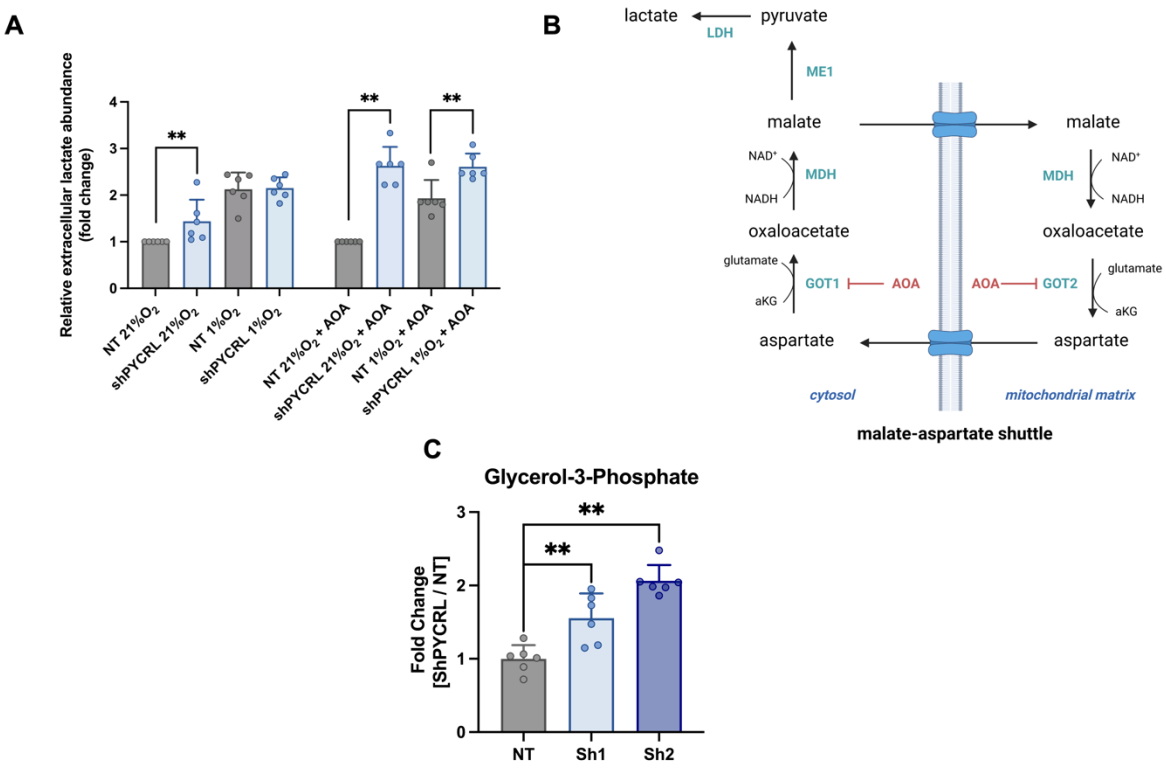

Figure 2.12 PYCRL KD cells shuttle NADH excess into the mitochondria through the malate-aspartate shuttle

(A) Extracellular lactate levels in doxycycline induced PYCRL NT or KD A172 cells with or without the pan-transaminase inhibitor AOA (2,5 mM) at 21% O_2 or 1% O_2. (B) Diagram showing the metabolic intermediates and enzymes involved in the malate-aspartate shuttle. Treatment with AOA blocks the activity of GOT1 and GOT2. (C) Glycerol-3-phosphate measured in A172 glioblastoma cell line in doxycycline induced NT or shPYCRL #1 or #2. Error bars indicate ± S.E.M. and each experiment was conducted with three biological replicates. The Mann-Whitney test was used to determine the statistical significance *** p<0.001, * p<0.05, ** p<0.01.

2.2.6 PYCRL KD reduces cell proliferation and survival in glioblastoma

Given the metabolic and redox perturbation elicited by PYCRL further experiments were conducted to assess if this condition correlates with a growth defect. Indeed, PYCRL KD results in reduced cell growth compared to non-targeting control which is not rescued by supplementation with physiological proline levels in either normoxic or hypoxic conditions (Figure 2.13A-B). To more closely recapitulate the *in vivo* condition, A172 cells were grown in an ultra-low attachment plate to encourage the formation of spheroids. PYCRL-deficient cells show impaired spheroidal growth and increased internal hypoxia – as indicated by the hypoxic marker pimonidazole (Figure 2.13C-D). In addition, the apoptotic marker cleaved Caspase-3 was increased, whereas the proliferation marker Ki67 was decreased in PYCRL KD A172 glioblastoma cells (Figure 2.13D). Overall, these results suggest that loss of PYCRL decreases glioblastoma cell proliferation and survival in normoxic and hypoxic conditions.

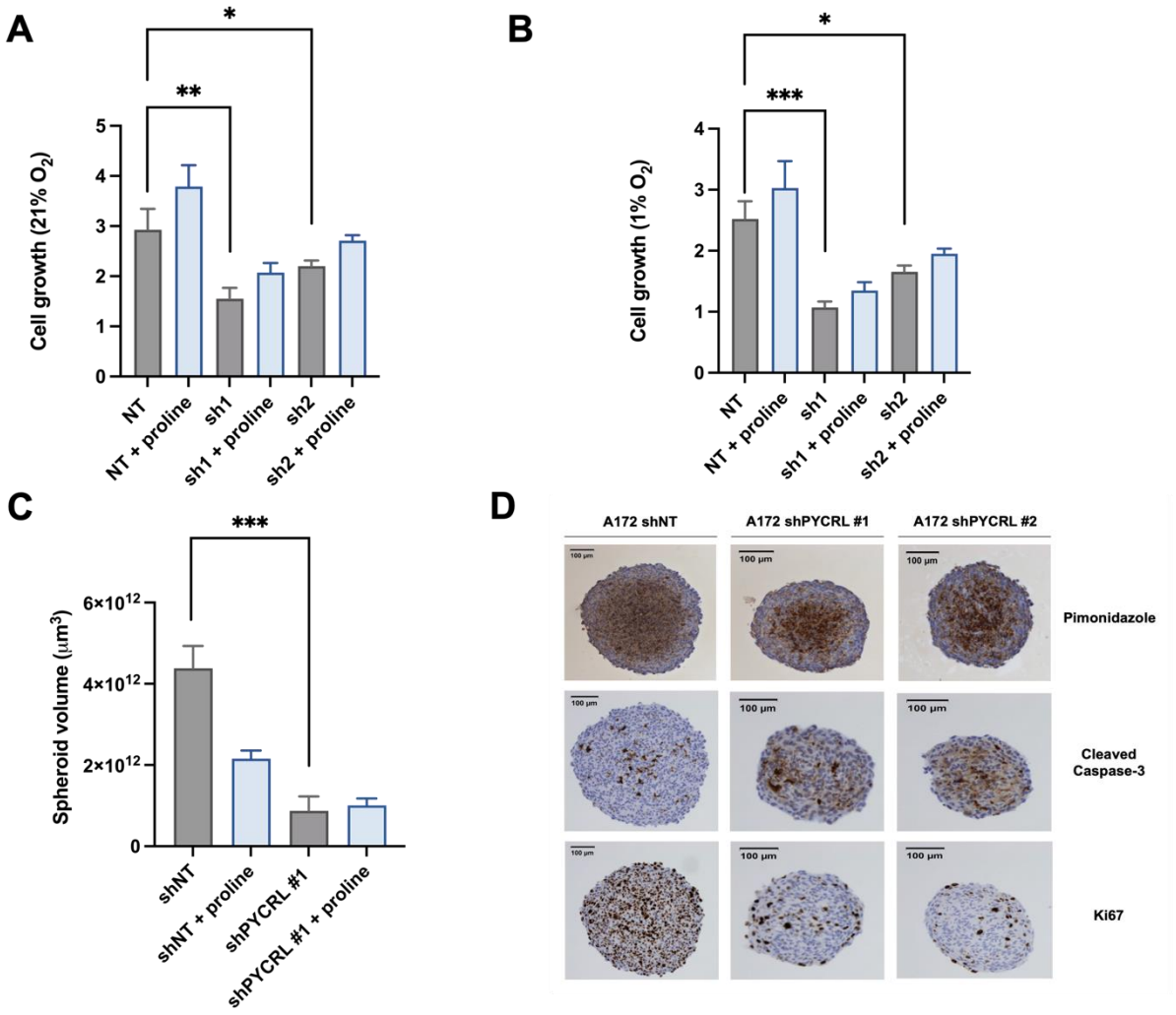

Figure 2.13 PYCRL KD reduces cell proliferation and survival in A172 glioblastoma cells

(A-B) Cell growth in doxycycline induced PYCRL NT and shPYCRL #1 and #2 cells, measured in the presence or absence of exogenous proline (200 μM), respectively in normoxia and in hypoxia. (C) Spheroid volume measured in doxycycline induced PYCRL control or inhibited A172 cells, with or without proline supplementation (200 μM). (D) IHC of A172 doxycycline induced shNT, shPYCRL #1, shPYCRL #2 cells stained with the hypoxic marker pimonidazole, or cleaved Caspase-3 (apoptosis marker), or Ki67 (proliferation marker). Error bars indicate ± S.E.M. and each experiment was conducted with three biological replicates. The Mann-Whitney test was used to determine the statistical significance *** $p<0.001$, * $p<0.05$, ** $p<0.01$.

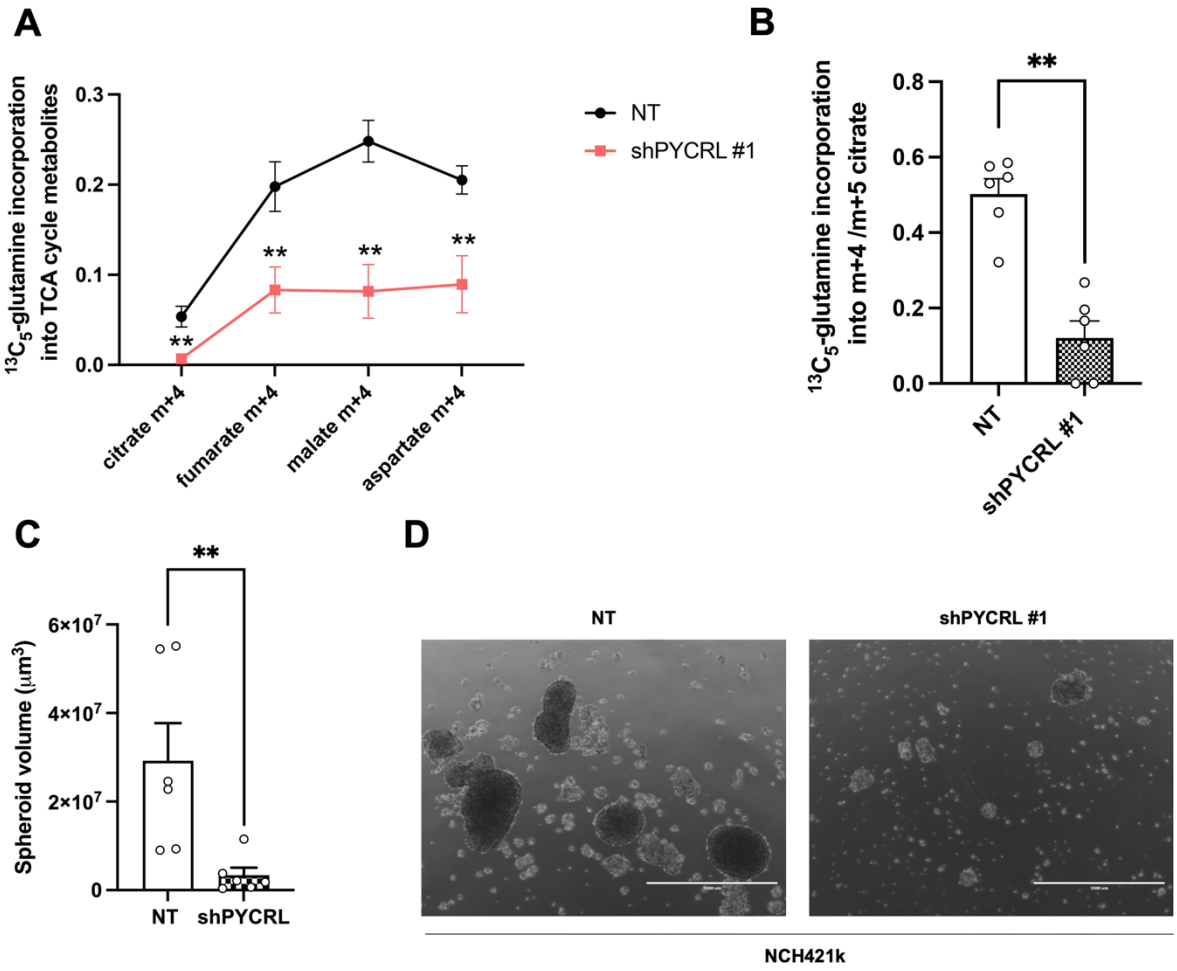

Figure 2.14 NCH421k glioblastoma stem cells phenocopy the metabolic perturbation and reduced proliferation observed in A172 glioblastoma cell line

(A) m+5 glutamine incorporation into TCA cycle intermediates measured by GC-MS in NCH421k glioblastoma stem cell line in doxycycline induced non-targeting control or PYCRL KD cells. (B) m+4/m+5 citrate from glutamine carbons (reductive carboxylation) with or without doxycycline induced PYCRL KD in NCH421k cells. (C-D) Spheroid volume measurement and brightfield microscopy image of NCH421k cells with or without doxycycline induced PYCRL KD (scale bar 5000 μM). Error bars indicate ± S.E.M. and each experiment was conducted with three biological replicates. The Mann-Whitney test was used to determine the statistical significance *** p<0.001, * p<0.05, ** p<0.01.

Another cell line was used to further confirm the phenotype observed in A172 glioblastoma cell line upon loss of PYCRL. NCH421k is another glioblastoma stem cell line that grows as a 3D spheroid. Even this cell line displays the same reduction in TCA cycle activity and a decrease in reductive carboxylation when PYCRL is KD (Figure 2.14A-B). In addition, spheroid volume was also decreased in NCH421k PYCRL-deficient cells, confirming the previous finding in A172 cell line. We also observed that PYCRL KD cells take up more exogenous aspartate (Figure 2.15A). Indeed, supplementation with exogenous aspartate seems to improve cell growth in PYCRL-deficient cells (Figure 2.15B). Lastly, we used data from the International Mouse Phenotypic Consortium (IMPC) to show that PYCRL KO mouse does not cause any pathological phenotype and therefore makes PYCRL a safe target for cancer treatment (Figure 2.16).

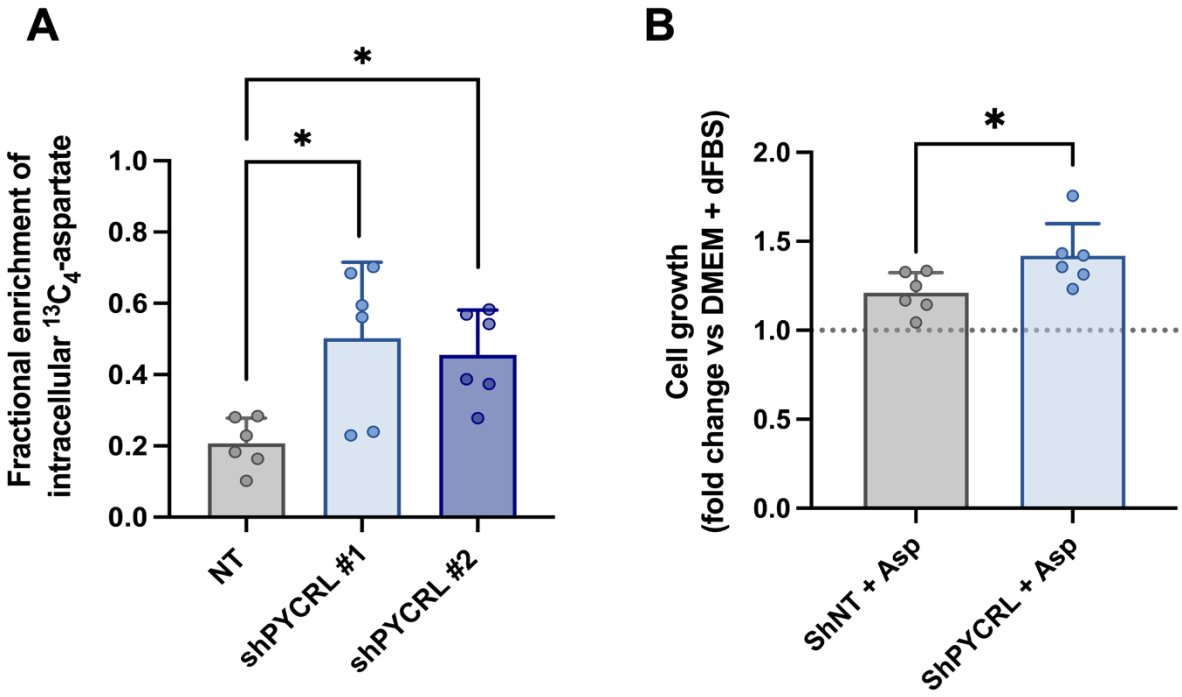

Figure 2.15 Aspartate supplementation partially rescues growth in PYCRL-deficient cells

(A) Intracellular $^{13}C_4$-aspartate levels when doxycycline induced PYCRL NT or shPYCRL #1 or #2 are supplemented with 500 μM of $^{13}C_4$-aspartate. (B) Cell growth measured in doxycycline induced shNT or shPYCRL A172 cells supplemented with aspartate (Asp) 500 μM. Error bars indicate ± S.E.M. and each experiment was conducted with three biological replicates and two technical replicates. The Mann-Whitney test was used to determine the statistical significance *** p<0.001, * p<0.05, ** p<0.01.

Figure 2.16 PYCRL KO mouse shows no phenotypic changes

Data obtained from the International Mouse Phenotypic Consortium (IMPC) show mice tested for different parameters, such as grip strength and eye morphology to assess changes in PYCRL KO mouse compared to wild-type control.

2.3 Discussion

Recent evidence has highlighted the importance of proline biosynthesis in tumors for the maintenance of redox homeostasis rather than proline synthesis per sè[75,72,74,73]. Our results further suggest that the cytosolic proline-producing enzyme PYCRL balances the cytosolic NAD^+ pool, and this has consequences for the NAD^+/NADH ratio, especially in hypoxia. Indeed, inhibition of PYCRL leads to an accumulation of NADH shuttled into the mitochondria through the malate-aspartate shuttle. Increased mitochondrial NADH hampers TCA cycle activity, which, in turn, renders aspartate limiting for nucleotide biosynthesis. Therefore, PYCRL-deficient tumors proliferate less and display increased hypoxia and apoptosis (Figure 2.17).

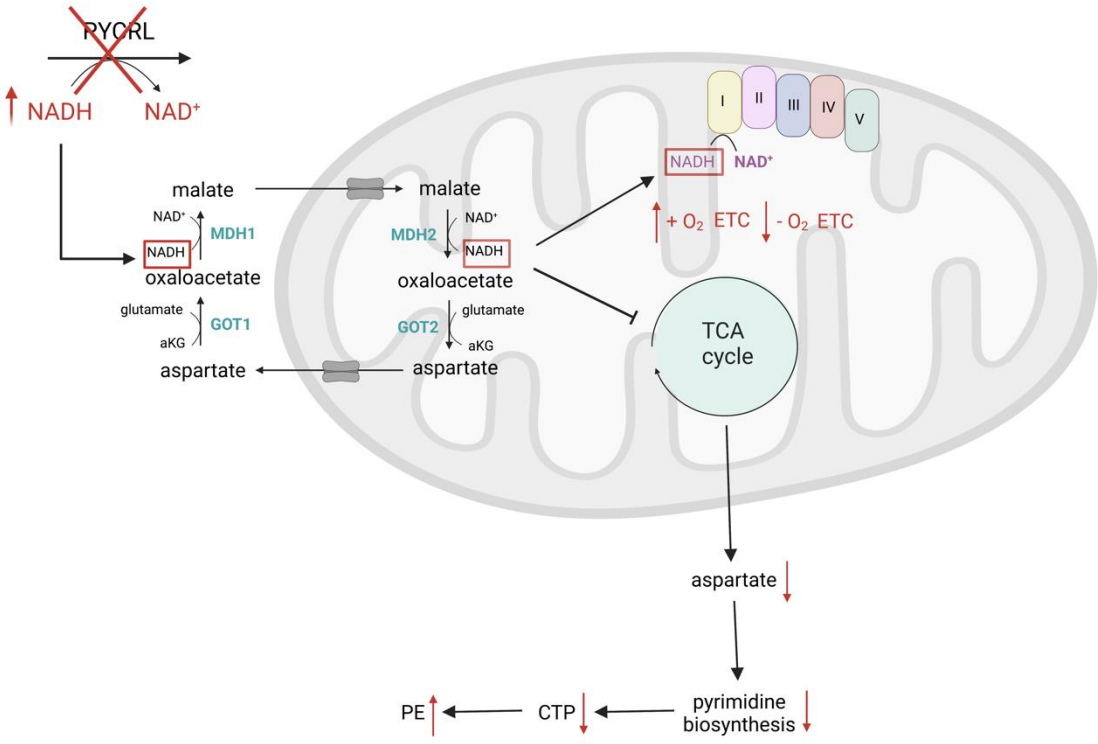

Figure 2.17 Schematic diagram showing the metabolic changes associated with PYCRL loss

Loss of PYCRL increases cytosolic NADH availability, leading the malate-aspartate shuttle to import NADH excess into the mitochondria. Increased NADH in the mitochondria halts TCA cycle activity, whereas the ETC tries to regenerate NAD^+ when oxygen is available. TCA cycle inhibition leads to decreased aspartate availability which in turn impairs pyrimidine biosynthesis. As a result of these metabolic changes, cell proliferation decreases and the stress molecule phosphoethanolamine is increased.

The redox perturbation that originates from PYCRL KD is visible in normoxia and hypoxia and is independent from proline availability (Figure 2.11A). Inhospitable environments, such as hypoxia provide a challenge to cells for their maintenance of appropriate redox homeostasis, therefore even a smaller change in $NADP^+$/NADPH or NAD^+/NADH ratios has a more widespread consequences, including reduced cell survival. In this context, PYCR2 has been recently discovered to catalyse a “reverse” reaction to produce cysteine, which might explain why in recent publications tumors lacking PYCR2 do not display any change in proline production or redox, although this has to be confirmed in a mammalian system[72,68].

In our system NADH availability seems to be more crucial than ATP demand. Indeed, the drop in ATP levels when PYCRL was KD was observed in hypoxia, but not in normoxia (Figure 2.11D), even if the cell growth defect was observed in normoxia and in hypoxia (Figure 2.13A-B). This suggests that ATP is not the limiting molecule for proliferation in the absence of PYCRL. A similar result was observed in another study where tumors were described to adjust the ATP pool according to the NAD^+ demand[129].

In our study we supplemented the media with ornithine, as the importance of this amino acid for PYCRL activity was highlighted in previous studies[58]. In addition, ornithine has been confirmed to be present in the plasma in different human and rat studies[130,131]. This further suggests that proline can be continuously synthesized from ornithine by PYCRs in the absence of glutamine or even from arginine when Arginases 1 or 2 are expressed.

It has been shown that some cancers are dependent on proline for survival and that a lack of NADPH in the mitochondria can be corrected by proline supplementation[105,104,132]. To whether extent proline-dependent cancers require proline for survival or rely on the proline biosynthesis pathway for redox control, or both, requires further exploration. Additionally, further studies are required to shed light on the role of PYCRL both in tumor and stroma and how proline exchange – either through import or export – influences the activity of the proline biosynthesis pathway.

One limitation of the study is not being able to have shown the actual subcellular compartmentalisation of NAD(H) perturbation as the sample preparation for cellular fractionation will alter those ratios *per se*. In addition, for time constraints, it was not possible to explore the function of the stress molecule phosphoethanolamine in PYCRL-deficient cells.

CHAPTER 3:

PYCRL loss promotes lipid desaturation as alternative route for NAD^+ regeneration

3.1 Introduction

NAD^+ is an important co-factor for breakdown of reduced nutrients, such as lipids and to produce new molecules such as amino acids and nucleotides[129]. There are multiple pathways that are capable of regenerating NAD^+. For instance, two of the best describes means of oxidising NADH to regenerate NAD^+ are the mitochondrial ETC and the cytosolic reduction of pyruvate to produce lactate through LDH activity[129]. Impairment in either of these two pathways can lower the NAD^+/NADH ratio to an extent that halts cell growth, even if intracellular ATP is sufficient[129]. Other NAD^+ contributors are mitochondrial glutamate dehydrogenase GDH, the enzyme that uses α-ketoglutarate and ammonia to generate glutamate coupled to NADH oxidation, or the desaturation reactions catalysed by the delta-5 and -6 desaturases (D5D, D6D, encoded by FADS1 and FADS2 genes)[133,134]. These enzymes are required for the synthesis of highly unsaturated fatty acids (HUFAs). D5D and D6D introduce a double bond along the carbon backbone using molecular oxygen and cytosolic NADH. The rate of this reaction has been suggested to increase when the electron transport chain is impaired, for instance in response to rotenone treatment (complex I inhibitor) or in hypoxic conditions[134]. Even if lactate turnover in the whole body is greater than HUFA synthesis which accounts for 0.03/0.08 mol/day of NAD^+ recycling, it does not consider local tissue or disease-specific NAD^+ requirements and genetics[134]. For instance, it has recently been shown that mitochondrial MTHFD2, one of the enzymes involved in folate metabolism, can catalyse a non-canonical oxidative reaction after loss of the gene *UQCR11*. In *UQCR11*-deleted ovarian cancer, MTHFD2 can regenerate NAD^+ instead of $NADP^+$, using malate-aspartate shuttle-derived NADH[135].

Similarly, in glioblastoma stem cells, PYCRL can use NADH as a co-factor to catalyse cytosolic proline biosynthesis, as shown in chapter 2. Chapter 3 further explores mechanisms engaged for NAD^+ regeneration after PYCRL loss. For instance, lipid desaturation is required to offset increased cytosolic NADH.

3.2 Results

3.2.1 Loss of PYCRL reduces lipid synthesis

In Chapter 2 I found that loss of PYCRL led to metabolic consequences, including reduced TCA cycle oxidative activity and a disturbed redox homeostasis. This suggested that PYCRL activity was functionally linked to a number of metabolic sub-networks that may be connected via the downstream effects of the significant change in redox homeostasis observed in the system. Interestingly, further analysis of some of the metabolic tracer studies presented in chapter 2 suggested other effects, such as reduced reductive carboxylation, as illustrated by the m+5/m+4 citrate ratio from $^{13}C_5$-glutamine in normoxic or hypoxic conditions (Figure 3.1A-B). The combined effect of reduced TCA cycle oxidative and reductive activity would be predicted to reduce citrate synthesis, with knock-on effects on *de novo* fatty acid synthesis. We therefore investigated palmitate synthesis from dual tracing of $^{13}C_6$-glucose and $^{13}C_5$-glutamine and found that it was decreased in A172 PYCRL KD cells (Figure 3.1D-E). Palmitate (C16:0) is synthesised by the condensation of acetyl-CoA and malonyl-CoA catalysed by FASN, and itself can be elongated to form longer fatty acids, such as stearate (C18:0). Alternatively, FASN can also synthesise myristate (C14:0) and to a lesser extent stearate (Figure 3.2). Indeed, *de novo* synthesis of both stearate and myristate was decreased in shPYCRL both in normoxic and hypoxic conditions (Figure 3.3A-C,

Figure 3.4A-C). We also examined synthesis of cholesterol, another non-polar metabolite synthesized from acetyl-CoA (via the mevalonate pathway) using eleven molecules of molecular oxygen. Our data show that this pathway is also highly suppressed in PYCRL-deficient cells. Overall, we suggest that anabolism from acetyl-CoA is significantly and globally repressed in the absence of PYCRL, potentially to spare oxygen for other NAD^+ regenerating reactions, such as lipid desaturation.

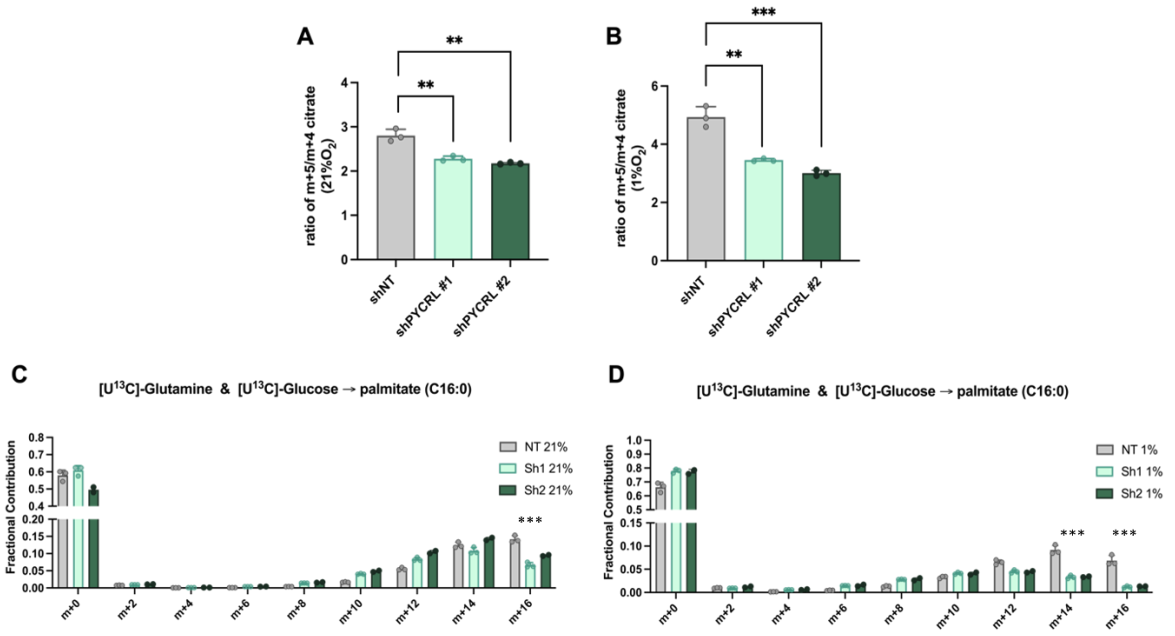

Figure 3.1 Loss of PYCRL reduces palmitate synthesis from $^{13}C_6$-glucose and $^{13}C_5$-glutamine

(A-B) Ratio of m+5/m+4 citrate as a redout of reductive carboxylation, with or without doxycycline induced PYCRL KD, respectively in normoxia or hypoxia. (C-D) Dual $^{13}C_5$-glutamine and $^{13}C_6$-glucose tracing into palmitate (C16:0) in the presence or absence of doxycycline induced PYCRL KD. Error bars indicate ± S.E.M. and each experiment was conducted with three biological replicates. The Mann-Whitney test was used to determine the statistical significance *** p<0.001, * p<0.05, ** p<0.01.

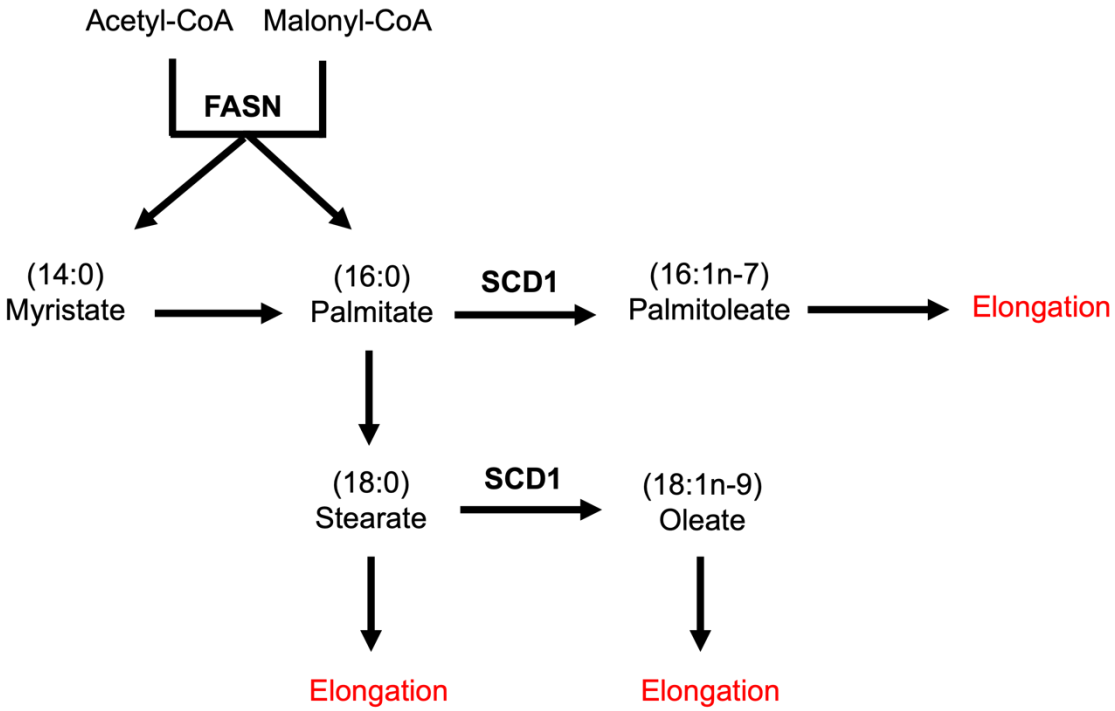

Figure 3.2 Schematic overview of the lipid biosynthesis pathway

Diagram showing the synthesis of myristate (14:0) and palmitate (16:0). Palmitate can then be elongated into stearate (C18:0). Both palmitate and stearate can be desaturated by SCD1, given respectively palmitoleate and oleate. During the process of elongation, other desaturases such as FADS1-3 can introduce double bonds into fatty acid backbones, thus contributing to a panoply of intracellular lipids.

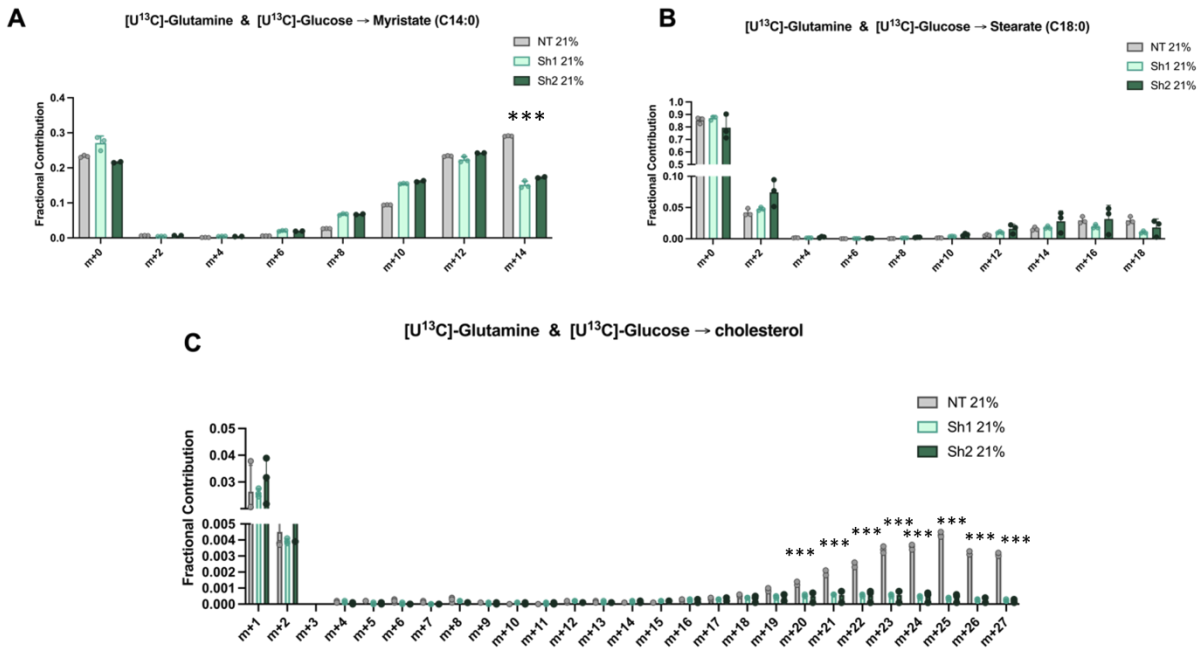

Figure 3.3 Myristate, stearate and cholesterol are depleted in PYCRL KD cells in normoxia

(A-C) Fractional contribution from dual $^{13}C_5$-glutamine and $^{13}C_6$-glucose into myristate, stearate and cholesterol in normoxia with or without doxycycline induced PYCRL. Error bars indicate ± S.E.M. and each experiment was conducted with three biological replicates. The Mann-Whitney test was used to determine the statistical significance *** p<0.001, * p<0.05, ** p<0.01.

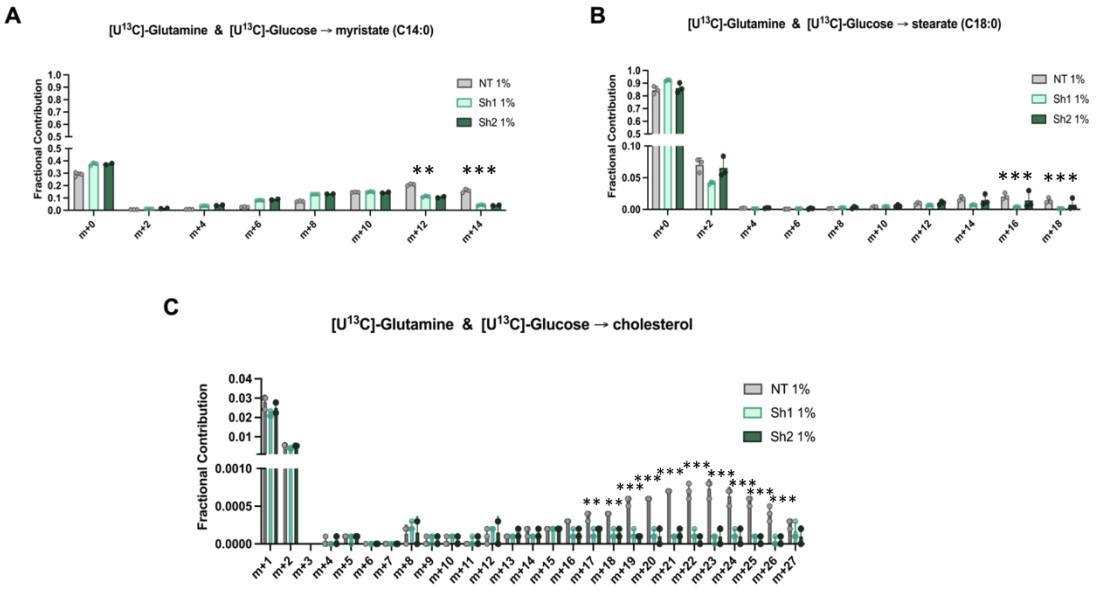

Figure 3.4 Myristate, stearate and cholesterol are depleted in PYCRL KD cells in hypoxic conditions. (A-C) Dual labelling from $^{13}C_5$-glutamine and $^{13}C_6$-glucose into different lipid species, such as myristate, stearate and cholesterol, with or without doxycycline induced PYCRL knockdown in hypoxia. Error bars indicate ± S.E.M. and each experiment was conducted with three biological replicates. The Mann-Whitney test was used to determine the statistical significance *** p<0.001, * p<0.05, ** p<0.01.

3.2.2 Loss of PYCRL promotes lipid desaturation for NAD^+ regeneration

Given that loss of PYCRL reduces the synthesis of many fatty acids, such as palmitate and stearate, we hypothesized that exogenous lipids might compensate to maintain viability and proliferation. Indeed, metabolic modelling with the Fatty Acid Source Analysis (FASA) program suggested a moderate increase in exogenous fatty acid uptake in PYCRL KD compared to non-targeting control (Figure 3.5A)[136]. Interestingly, it was noticeable that despite the less endogenous synthesis, intracellular fatty acids tented to be more frequently desaturated, as illustrated in Figure 3.5B. This finding was in agreement with a previous publication showing that in conditions of ETC impairment increased desaturation was observed as a means of compensating for NADH accumulation[134]. Indeed, FADS1-3 can use NADH and molecular oxygen to recycle NAD^+ (Figure 3.5C).

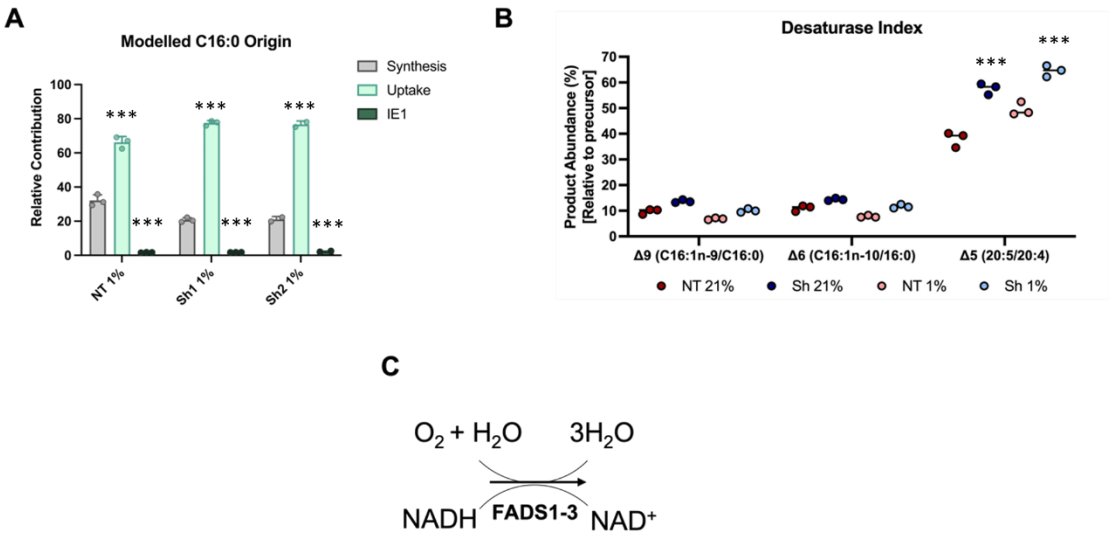

Figure 3.5 Loss of PYCRL promotes lipid desaturation for NAD^+ regeneration

(A) Metabolic modelling with FASA software shows synthesis, uptake, and elongation in A172 doxycycline induced non-targeting control and shPYCRL cells. (B) Desaturase index calculated as percentage of product abundance relative to precursor in doxycycline induced shNT and shPYCRL cells in normoxia or hypoxia. (C) Schematic diagram showing the reaction catalysed by the enzymes FADS1-3 where NADH oxidation is coupled to O_2 consumption. Error bars indicate ± S.E.M. and each experiment was conducted with three biological replicates. The Mann-Whitney test was used to determine the statistical significance *** $p<0.001$, * $p<0.05$, ** $p<0.01$.

3.2.3 Intracellular lipids are stored as lipid droplets in PYCRL KD

It is known that accumulation of desaturated fatty acids promotes lipid droplets formation inside the cell[137]. Lipid droplets are storage organelles, containing a triacylglycerol or cholesterol ester core enwrapped by a phospholipid monolayer. The phospholipid monolayer is mainly composed by phosphatidylcholine and, to a minor extend, by phosphoethanolamine[138]. Interestingly, phosphoethanolamine was previously identified in chapter 2 after a screening in A172 shPYCRL cells, and it is known in the literature to promote lipid droplets stability[139]. As illustrated by Figure 3.6A from BODIPY staining, lipid droplets tend to accumulate in PYCRL-deficient cells in normoxic conditions and even further in hypoxia (Figure 3.6A-B).

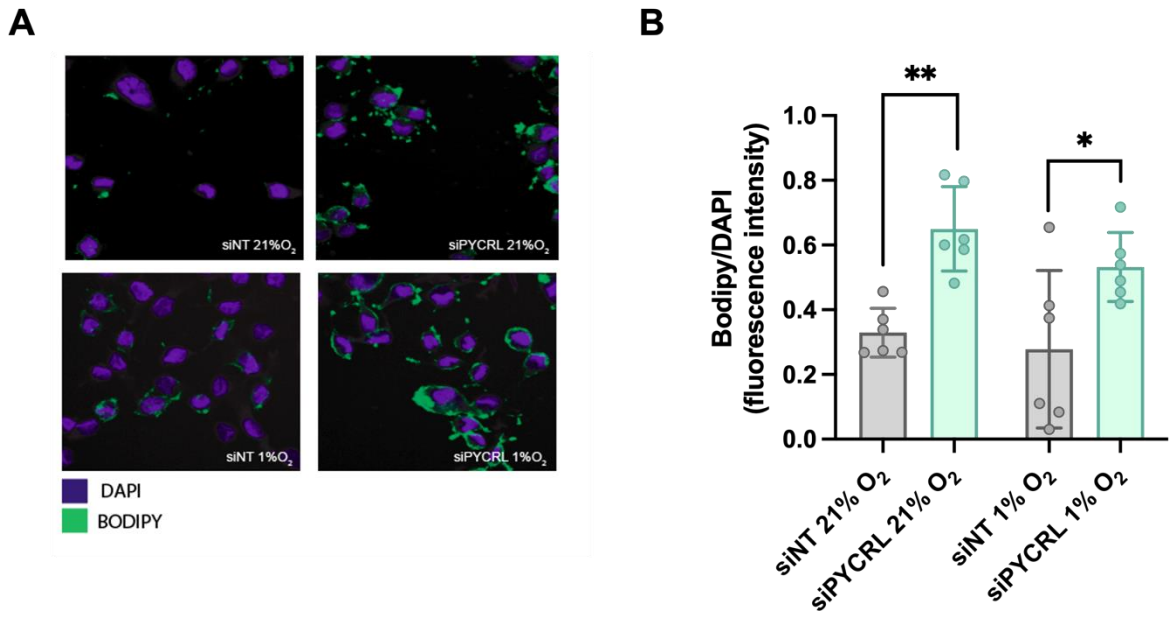

Figure 3.6 Intracellular lipids are stored as lipid droplets in PYCRL KD

(A) Staining with Bodipy highlights lipid droplet content inside cells (green), DAPI staining for nucleus (blue) in A172 cells doxycycline induced non-targeting control (siNT) or PYCRL knockdown (siPYCRL) in normoxia or hypoxia. (B) Quantification of Bodipy staining of lipid droplets per cell with ImageJ. Error bars indicate ± S.E.M. and each experiment was conducted with three biological replicates and technical duplicates. The Mann-Whitney test was used to determine the statistical significance *** $p<0.001$, * $p<0.05$, ** $p<0.01$.

3.2.4 Acetate supplementation partially rescues growth in hypoxic PYCRL KD

Given that acetyl-CoA levels are decreased in hypoxia, but not in normoxia (Figure 3.7A-C), we hypothesised that exogenous supplementation of the acetyl-CoA precursor, acetate, could restore growth in shPYCRL cells. This would be the case if in PYCRL-deficient cells ATP is not limiting as ACSS1 or ACSS2 expressed in A172 glioblastoma cell line (Figure 3.7D), are ATP-dependent enzymes. Indeed, supplementation with 5 mM of acetate was able to partially restore cell growth in hypoxic PYCRL KD cells (Figure 3.7E). although little effect was observed in normoxia. This implies that sufficient ATP is available in PYCRL KD cells and may not be a limiting factor for cell growth, through the endogenous synthesis of acetyl-CoA from citrate – also an ATP-dependent reaction. To understand how acetate was able to restore cell growth in shPYCRL cells, GC-MS analysis was performed in A172 cells. Surprisingly, supplementation with acetate in PYCRL KD cells was observed to contribute to citrate and glutamate. This is indicative of glutamate synthesis from α-KG, which can be either from transamination or GDH.

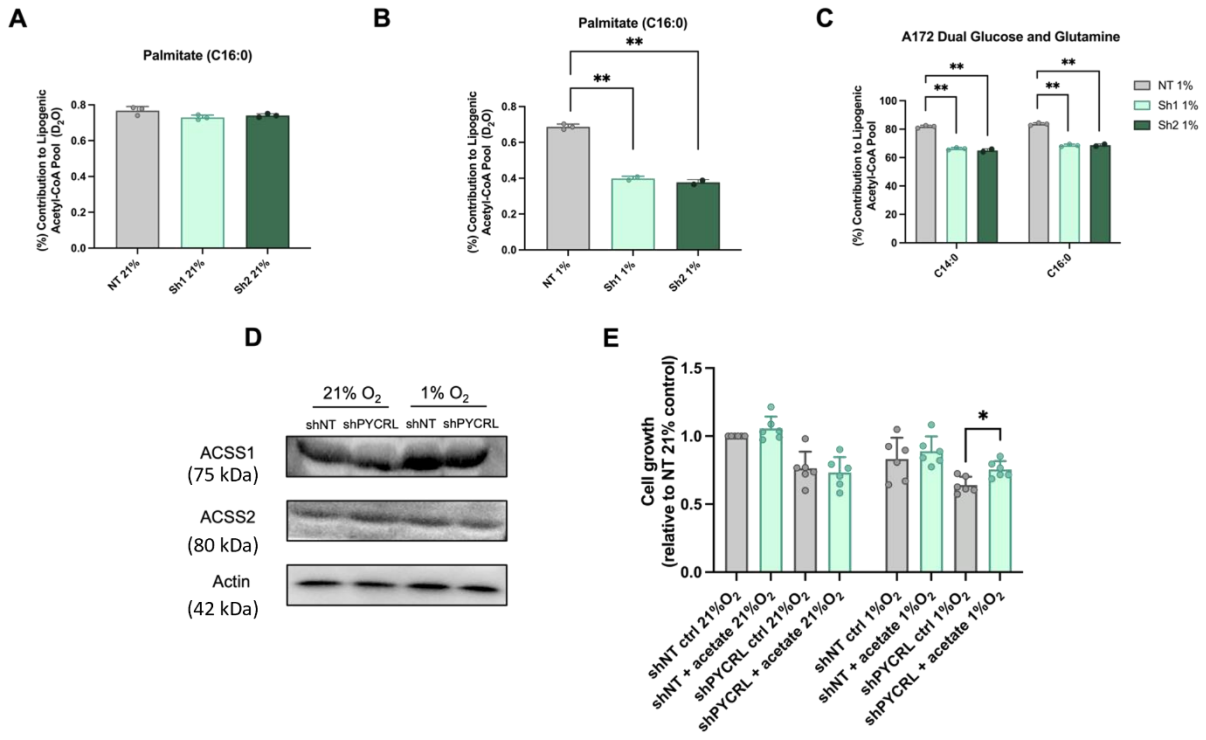

Figure 3.7 acetate supplementation partially rescues growth in hypoxic PYCRL KD

(A-C) Acetyl-CoA pool modelled with FASA from either deuterated water or dual $^{13}C_6$-glucose and $^{13}C_5$-glutamine tracing in A172 cells with or without doxycycline induced PYCRL KD in normoxia or hypoxia. (D) Western blot showing ACSS1 and ACSS2 protein expression in A172 glioblastoma cell line in doxycycline induced shNT or shPYCRL at different oxygen tensions. (E) Cell growth measured with sulforhodamine B in A172 cell with or without 5 mM of acetate, in the presence or absence of doxycycline induced PYCRL KD in normoxic or hypoxic conditions. Error bars indicate ± S.E.M. and each experiment was conducted with three biological replicates. The Mann-Whitney test was used to determine the statistical significance *** p<0.001, * p<0.05, ** p<0.01.

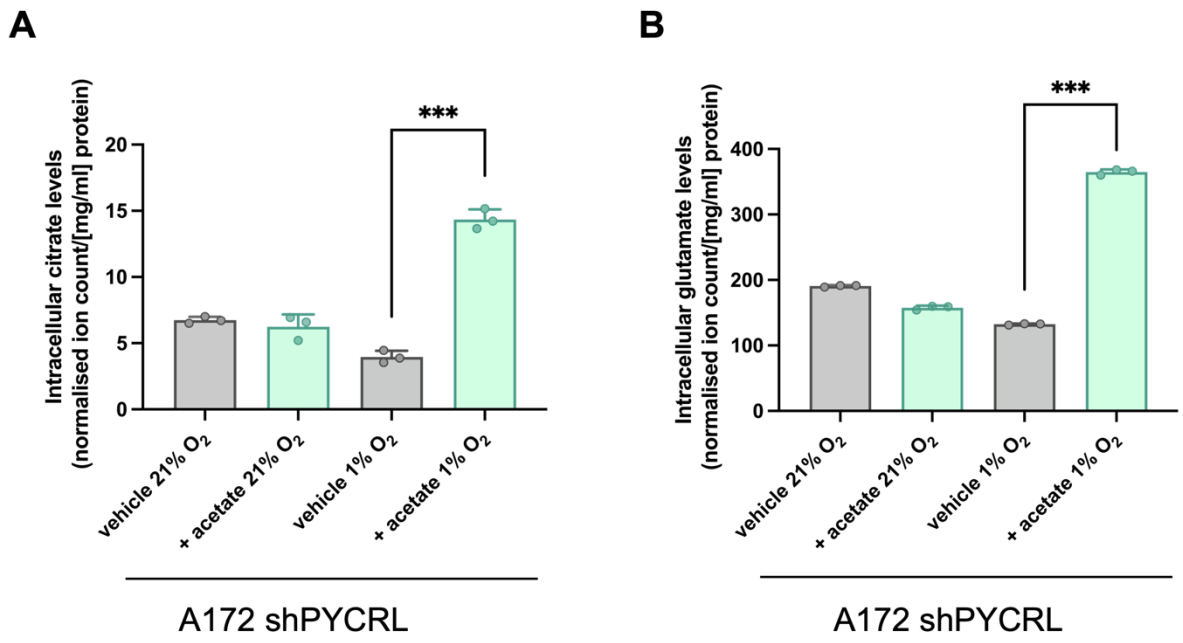

Figure 3.8 acetate supplementation regenerates citrate and glutamate in PYCRL KD under hypoxic conditions. (A) Intracellular citrate levels measured by GC-MS in A172 cells supplemented with 5 mM of acetate or vehicle in doxycycline induced shPYCRL cells at different oxygen tensions. (B) GC-MS-measured abundance of glutamate in doxycycline induced PYCRL-deficient cells in the presence or absence of 5 mM acetate at 21% O_2 or 1% O_2. Error bars indicate ± S.E.M. and each experiment was conducted in three biological replicates. The Mann-Whitney test was used to determine the statistical significance *** $p<0.001$, * $p<0.05$, ** $p<0.01$.

3.2.5 PYCRL-deficient cells exhibit a lack of glutathione availability

Glutamate has multiple fates inside the cell, two of which are contributions to TCA cycle and glutathione biosynthesis. The latter is part of a defense mechanism against ROS through the maintenance of a biochemically reduced pool of glutathione. Given that glutamate is low in PYCRL-deficient cells (Figure 3.9A), it was hypothesised that this could affect the synthesis of GSH, and therefore the pool size. Indeed, the total glutathione pool was reduced in shPYCRL cells in normoxia and even further in hypoxic conditions (Figure 3.9B). Interestingly, when the ratio of glutathione reduced/glutathione oxidised (GSH:GSSG) was measured, there was an increase in this ratio (Figure 3.9C). This could be potentially explained by a previous ROS accumulation that would have triggered the reduction of glutathione pool, that even if lower, was still sufficient to allow cell survival. Indeed, the $NADP^+$/NADPH ratio is also perturbed towards increased $NADP^+$ (Figure 3.9D). NADPH is the co-factor necessary to maintain the antioxidant systems in a reduced state to effectively eliminate ROS. The use of a pool of guide siRNAs to knockdown PYCRL did not alter PYCR1 and 2 protein expression, further confirming that changes in glutathione levels are due specifically to a lack of PYCRL (Figure 3.9E). To investigate in which compartment GSH levels were affected, A172 cells were transfected with siNNT. NNT is a mitochondrial enzyme that transhydrogenates NADH to NADPH. The NADPH produced can, in turn, be used for mitochondrial only GSH reduction (Figure 3.10A). shPYCRL in siNNT condition (Figure 3.10B) did not alter further glutathione levels, suggesting that GSH loss may localise to the cytoplasmic compartment. Successful knock down of NNT was displayed in figure 3.10C.

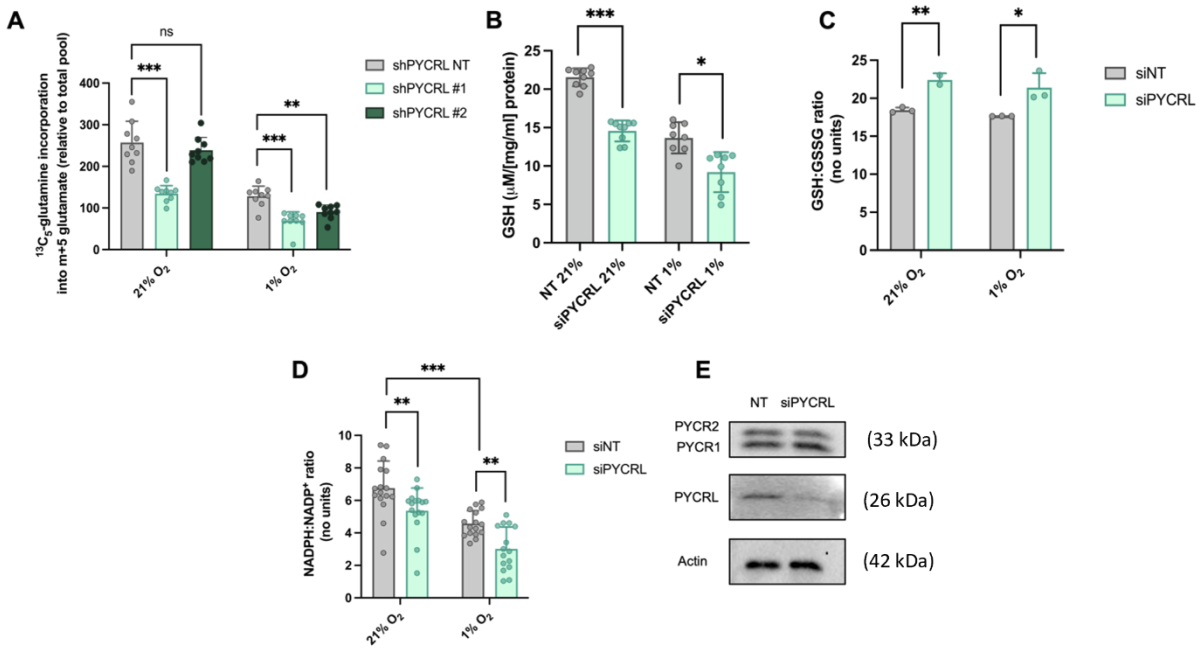

Figure 3.9 Reduced glutamate availability limits glutathione biosynthesis in PYCRL KD

(A)$^{13}C_5$-glutamine incorporation into glutamate relative to the total glutamate pool in doxycycline induced shPYCRL NT or shPYCRL #1 and #2 measured by GC-MS in normoxic or hypoxic conditions. (B) total GSH measured in siNT or siPYCRL cells at 21% O_2 or 1% O_2. (C) GSH:GSSG ratio measured in siNT or siPYCRL cells at different oxygen tensions. (D) NADPH:$NADP^+$ ratio in non-targeting control or in PYCRL-deficient cells in normoxia or hypoxia. (E) Western blot showing PYCR1,PYCR2 and PYCRL protein levels with or without PYCRL KD. Error bars indicate ± S.E.M. and each experiment was conducted with three biological replicates. The Mann-Whitney test was used to determine the statistical significance *** p<0.001, * p<0.05, ** p<0.01.

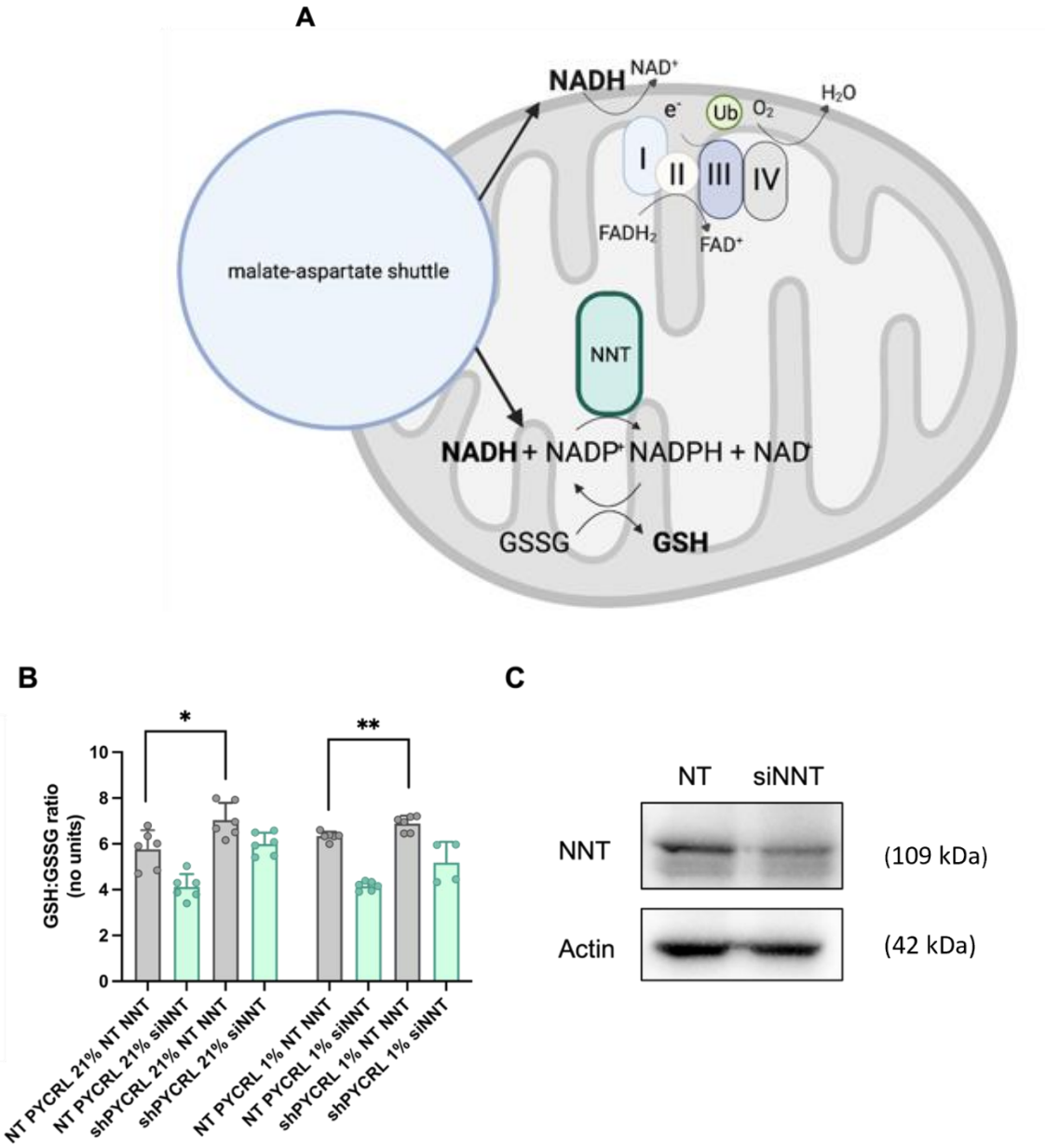

Figure 3.10 The glutathione pool depleted in PYCRL KD cells is mainly cytosolic

(A) Schematic overview of how silencing of NNT can affect only the mitochondrial glutathione pool. (B) GSH:GSSG ratio in doxycycline induced shNT or shPYCRL cells at different oxygen tensions. (C) Western blot showing successful NNT knockdown in A172 glioblastoma cells. Error bars indicate ± S.E.M. and each experiment was conducted with three biological replicates. The Mann-Whitney test was used to determine the statistical significance *** p<0.001, * p<0.05, ** p<0.01.

3.2.6 Glutathione depletion synergises with PYCRL KD in halting cell growth

Given that PYCRL KD lowers the cytoplasmic glutathione pool, it was important to investigate if treatment with 1 mM of the glutathione biosynthesis inhibitor, buthionine sulfoximine (BSO), synergises with loss of PYCRL. Figure 3.11 shows that shPYCRL and BSO treatment contribute to further decrease cell growth in shPYCRL cells, both in normoxia or in hypoxia.

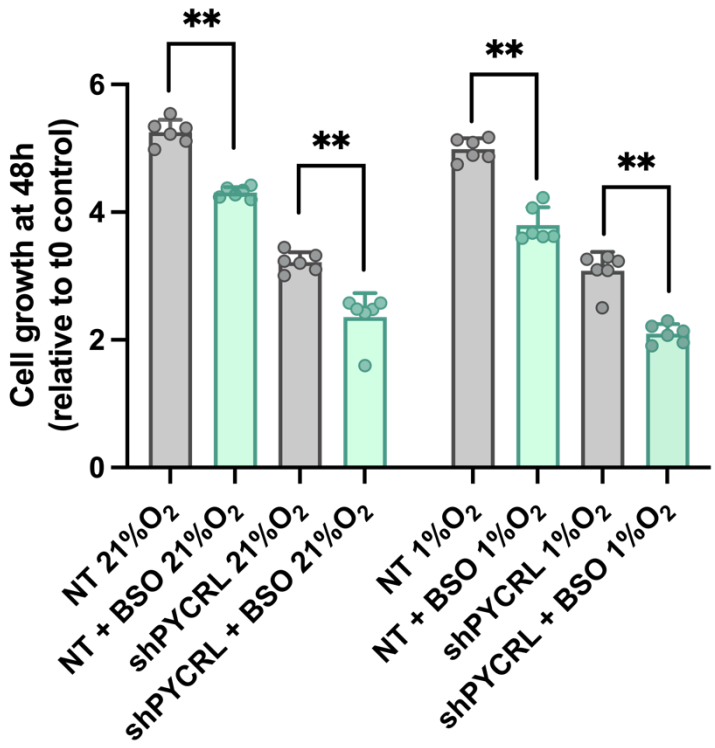

Figure 3.11 BSO treatment synergises with PYCRL KD in halting cell growth

Cell growth relative to t0 in doxycycline induced non-targeting control or shPYCRL A172 cell line with or without BSO treatment (1 mM) in normoxic or hypoxic conditions. Error bars indicate ± S.E.M. and each experiment was conducted with three biological replicates and technical duplicates. The Mann-Whitney test was used to determine the statistical significance *** p<0.001, * p<0.05, ** p<0.01.

3.3 Discussion

In the previous chapter we showed that loss of PYCRL leads to NADH accumulation. In this chapter, we explored further how cancer cells cope with an impaired NAD^+/NADH homeostasis, focusing on alternative pathways of regenerating NAD^+. In our system NAD^+ availability seems to be the major determinant of cell phenotype, rather than energy or anabolic precursor availability. Indeed, when acetate is supplemented in the media, despite the requirement of ACSS1/2 for ATP, a partial rescue in growth in hypoxic conditions was still observed (Figure 3.7E).

In addition, the data show that NADP(H) and NAD(H) pools, despite the compartmentalisation, are interconnected, and that an impairment in NAD^+/NADH can also affect $NADP^+$/NADPH pools. Indeed, mitochondrial NADH accumulation decreases TCA cycle activity which, in turn, makes citrate less available for NADPH-dependent endogenous lipid synthesis (Figure 3.1A-B).

Interestingly, compensating for NADH accumulation also affects the intracellular O_2 budget, which is preferentially allocated towards oxygen requiring NAD^+ regenerators, such as lipid desaturation (Figure 3.5B), whilst reducing flux through significantly oxygen-consuming pathways, such as cholesterol synthesis (Figure 3.3C and 3.4C).

Overall, PYCRL loss leads to a decrease in glutamate, which, in turn, is less available for glutathione synthesis, TCA cycling and potentially for transamination reactions. Indeed, it appears that endogenous glutamate synthesis may increase to drive NAD^+ regeneration through GDH, but it still not sufficient to maintain an adequate flux through

the glutathione pathway (Figure 3.12). Indeed, treatment with the glutathione synthesis inhibitor BSO sensitises the cells to PYCRL KD (Figure 3.11). Less glutathione availability causes increased potential damage from ROS, which might justify why the NADPH pool is depleted and while the glutathione available is decreased (despite an increase in GSH/GSSG) (Figure 3.9B and figure 3.9C). Nevertheless, further studies are required to clarify the mechanism that interconnects glutathione reduction, less NADPH availability, and the fate of endogenously synthesised glutamate carbons.

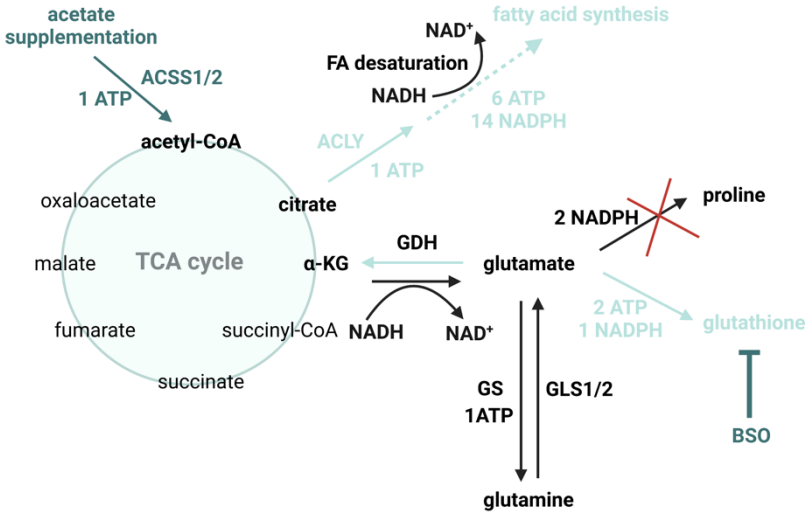

Figure 3.12 Schematic overview of the NAD⁺ regenerating pathways engaged by loss of PYCRL
Increased lipid desaturation in PYCRL KD contributes to NAD⁺ recycling in the cytosol. Acetate supplementation can restore the TCA cycle intermediates citrate and glutamate, supporting GDH activity in reversal, thus regenerating mitochodrial NAD⁺. Treatment with BSO halts glutathione synthesis and synergises with shPYCRL which *per se* limits glutamate availability for glutathione production.

CHAPTER 4:

A more oxidized redox state promotes proline import through SLC38A2 for glioma cell survival in hypoxic regions

4.1 Introduction

Glucose and acetate are the major metabolites available in the brain, that are promptly consumed by cancer cells to fuel glycolysis and oxidative phosphorylation (OXPHOS) in the mitochondria[140]. Conversely, proline is less abundant in the brain as excess impairs pre-synaptic transmission and normal neuronal function[141].

Different compartments in the brain maintain different proline levels. For instance, in healthy individuals, proline levels in the CSF, (the liquid that fills subarachnoid space and cerebral ventricles), are maintained at a concentration of 1.3 μM[142]. In mice, proline CSF levels fluctuate around 4.2 μM, whereas in the brain interstitial fluid reach a concentration of approximately 1.8 μM[143]. In blood, proline levels are around 60 μM in mice, and around 239 μM in healthy humans[143,144].

During glioblastoma progression the blood-brain barrier (BBB) can be disrupted and amino acids that were tightly regulated can be available as carbon sources for tumour growth. Indeed, when the BBB integrity is compromised, the result is an altered vasculature known as the brain-tumour barrier (BTB)[145]. Through this leakier and more permeable vasculature, amino acids and other molecules present in the blood can access the brain. Given its “leakier” nature, the BTB vasculature accumulates waste products and is less efficient in carrying oxygen, contributing to the formation of hypoxic regions throughout the tumour[145].

It is now well understood that proline metabolism is important as a vent for intracellular redox control. Nevertheless, it has been reported that some tumours can use proline for growth. For instance, the proline transporter SLC36A1 is required for tumour growth

in a *Drosophila* model, and in the absence of NADK2 - the mitochondrial enzyme involved in mitochondrial $NADP^+$ regeneration from NAD^+ - some tumours become proline auxotroph[82,104,105]. In the latter case, lack of mitochondrial $NADP^+$ impairs endogenous proline biosynthesis through ALDH18A1 – the enzyme that produces P5C from glutamine and uses NADPH as a co-factor to catalyse its reaction. Under these conditions, intracellular P5C might become limiting in these cells that privilege proline import to fulfill proline-dependent protein requirements. It is therefore important to assess in which conditions tumours prefer proline import to endogenous proline biosynthesis to reconcile apparently contrasting findings.

To date, 12 transporters are described as putative proline transporters. In a recent study, it was hypothesised that in rat glioblastoma C6 cells proline uptake was mediated by a Na^+-dependent mechanism[146]. In addition, through mathematical modelling of U87 glioblastoma cell line it was possible to assess that SLC38A1 is the most important proline importer in normoxic conditions[147]. Nevertheless, how proline transport in the more resistant brain tumour hypoxic regions occurs is still unknown.

In this fourth chapter, we discuss the mechanism through which glioblastoma cells privilege proline import over endogenous proline biosynthesis and we use the newly identified proline importer in hypoxia SLC38A2 as a way of manipulating the system to uncover an underlying metabolic vulnerability.

4.2 Results

4.2.1 Proline supplementation might support cell proliferation in more oxidised cellular contexts

Recent evidence has highlighted that some cancer cells proliferate more rapidly when proline is supplemented into the media[104,105]. To test this hypothesis and verify if that could occur in gliomas, four different glioma cell lines available in the lab were supplemented with 200 μM of exogenous proline. Surprisingly, U87 and HOG-IDH mutant showed increased growth, mainly in hypoxic conditions, but also in normoxia in the HOG IDH-mutant astrocytoma cell line (Figure 1A-D). Given that IDH-mutant cells have the peculiarity of regenerating more $NADP^+$, the total redox status of these cell lines was measured by LC-MS. Figure 4.2 shows that U87 and HOG-IDH mutant exhibit the highest fold change of the redox ratio shifted towards oxidation compared to HOG IDH-wildype and T98G glioblastoma cell lines. This result appears to be in line with the previous finding where U87 and HOG IDH-mutant showed increased growth in hypoxia after proline supplementation and also the fact that endogenous proline synthesis, especially through the glutamine route, requires NAD(P)H. This led us to the hypothesis that proline import can become important under inhospitable environments in cancer cells whose redox flexibility is more constrained, for instance in hypoxia and IDH-mutant cells.

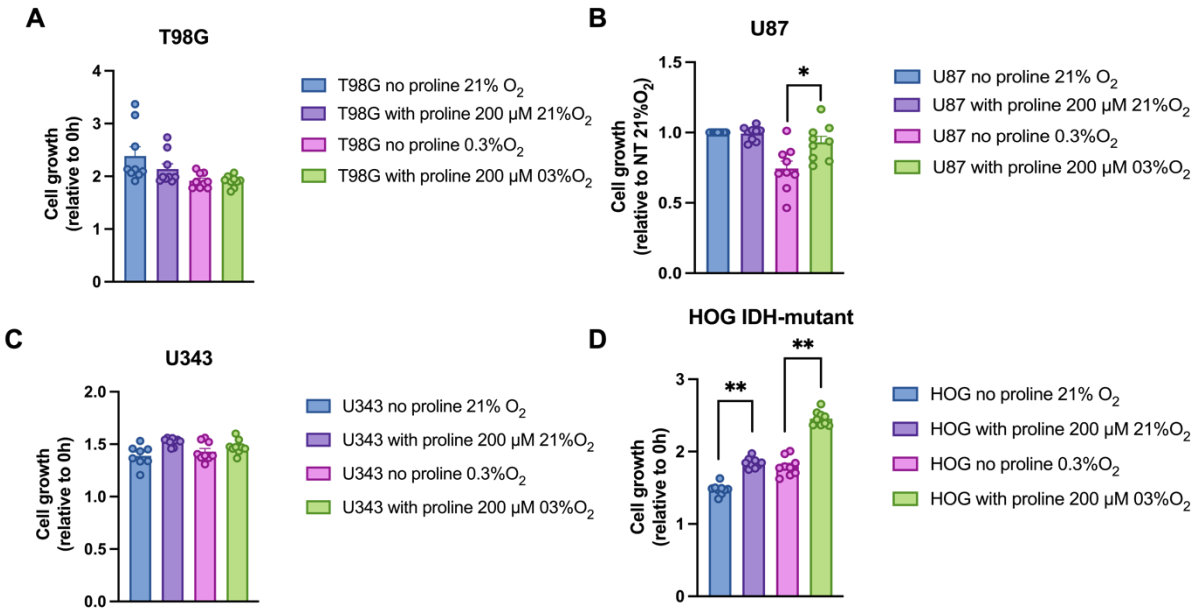

Figure 4.1 Some glioblastoma cell lines grow more after proline supplementation in hypoxia

(A-D) Cell growth relative to 0h or NT 21%O_2 in T98G, U87, U343, HOG IDH-mutant with or without proline supplementation at 21% O_2 or 0.3%O_2. Error bars indicate ± S.E.M. and each experiment was conducted with three biological replicates and technical duplicates. The Mann-Whitney test was used to determine the statistical significance *** p<0.001, * p<0.05, ** p<0.01.

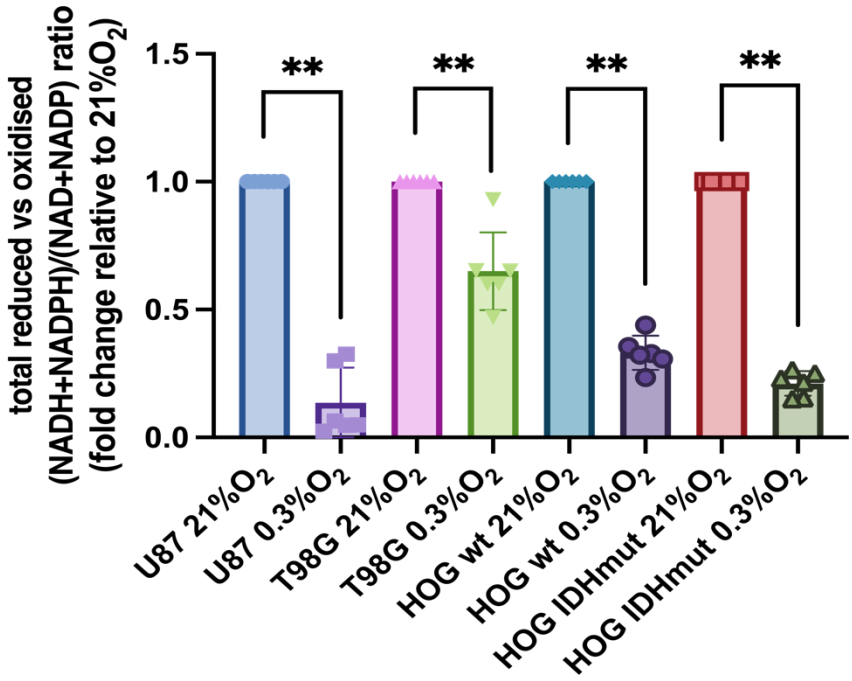

Figure 4.2 U87 and HOG-IDH mutant show increased oxidation in hypoxia compared to other cell lines.

Fold change (relative to the normoxic condition per each cell line) of the redox ratio (NADH+NADPH)/(NAD^++$NADP^+$) in U87, T98G, HOG IDH-wildtype and HOG IDH-mutant. Error bars indicate ± S.E.M. and each experiment was conducted with three biological replicates and technical duplicates. The Mann-Whitney test was used to determine the statistical significance *** $p<0.001$, * $p<0.05$, ** $p<0.01$.

4.2.2 The proline transporter SLC38A2 protein levels increase in hypoxia

To identify the enzyme responsible of proline import in hypoxic cells, protein levels of putative brain proline transporters was investigated by western blot. Figure 4.2A-D show the protein expression of SLC1A4, SCL6A20, SLC36A1 and SLC36A4 in U87 cells at different oxygen tensions. No change in expression of these potential proline transporters was observed, including SLC38A1 (Figure 4.4A). SLC38A2 was the only transporter whose protein expression levels change at 0.3%O_2 (Figure 4.4B). Interestingly, protein expression levels of the transporters SLC6A20 and to a lesser extent SLC36A4, are expressed in triple-negative breast cancer cells HCC1806, but are absent in breast-derived normal fibroblasts (NF) or cancer-associated fibroblasts (CAFs), suggesting disease specificity in expression of these transporters.

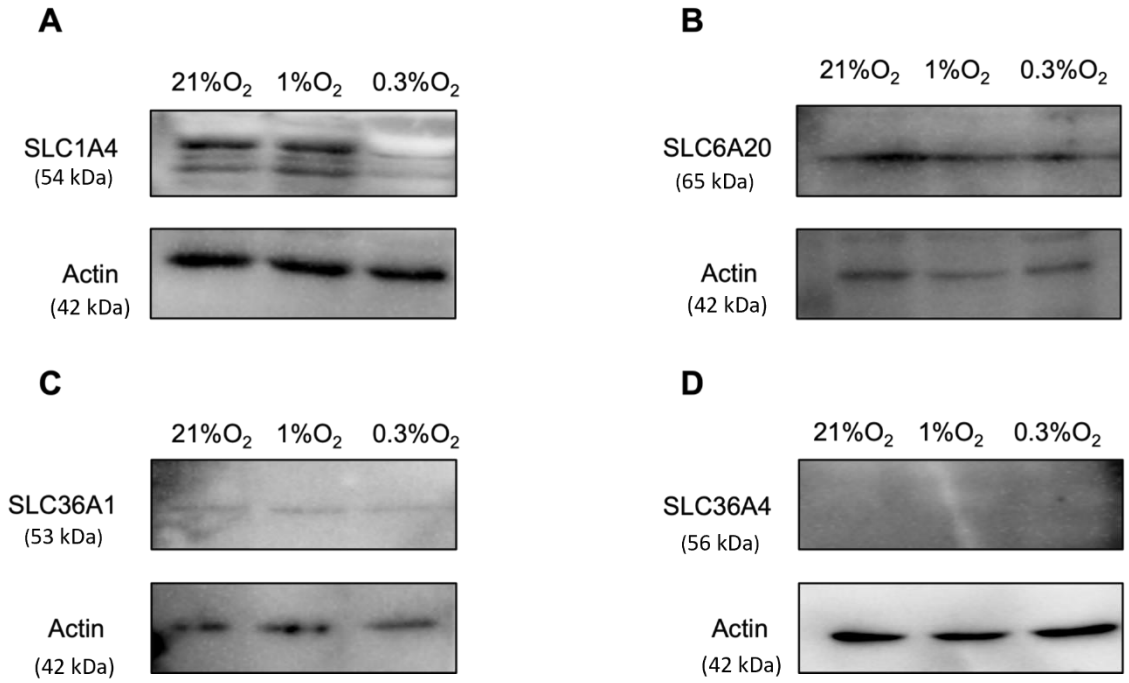

Figure 4.3 Proline transporters protein expression in U87 cell line at 21%O_2 1%O_2 0.3%O_2.
(A-D) Protein expression levels of putative proline transporters, respectively of SLC1A4, SLC6A20, SLC36A1, SLC36A4 at different oxygen tensions in U87 cell line.

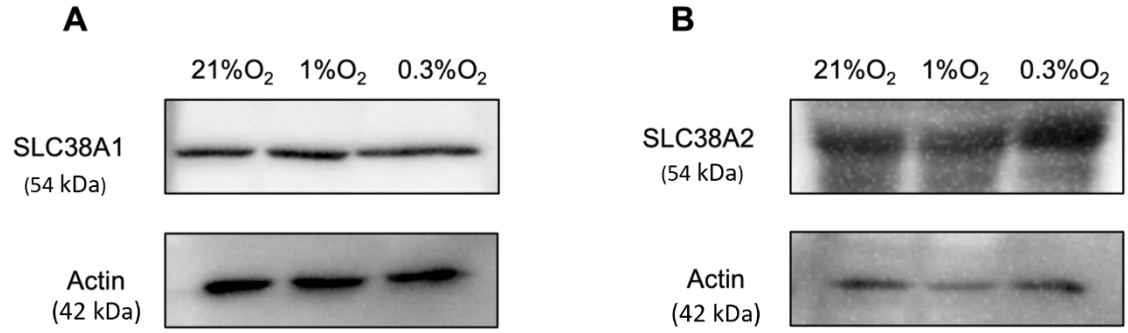

Figure 4.4 SLC38A2 protein levels increase under hypoxic conditions.

(A-B) Protein expression levels of, respectively, SLC38A1 and SLC38A2 at different oxygen tensions ($21\%O_2$, $1\%O_2$, $0.3\%O_2$) in U87 cell line.

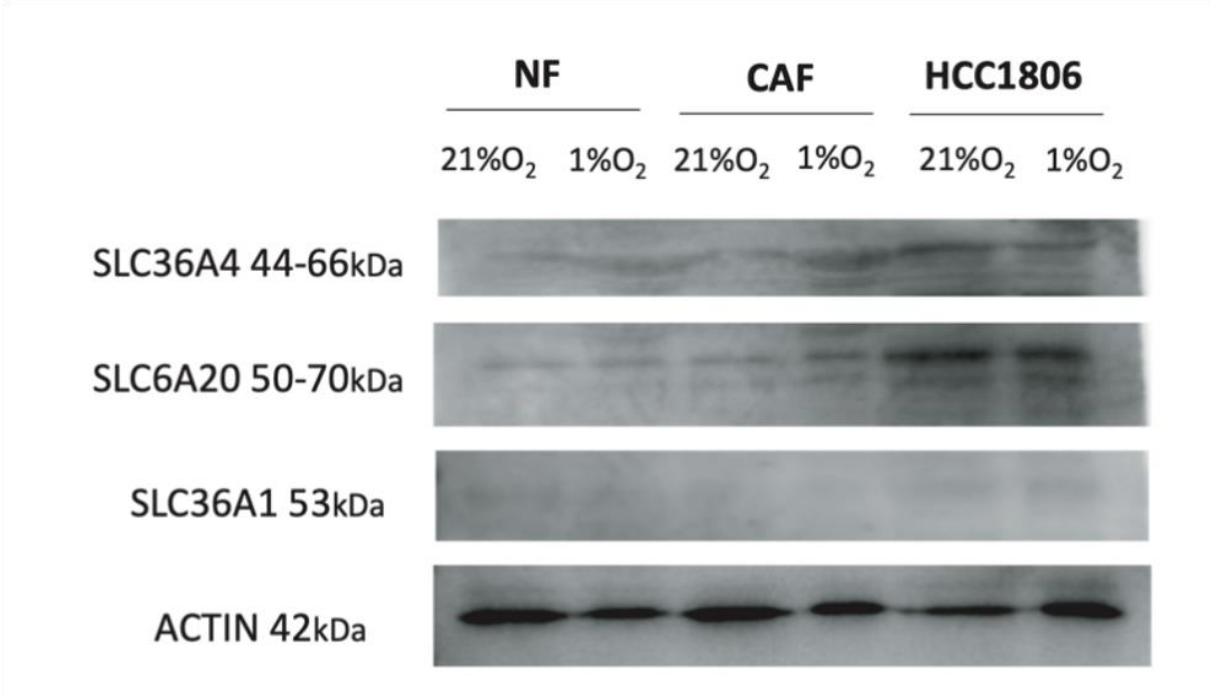

Figure 4.5 Cancer cells and fibroblasts show different protein expression of proline transporters
Non-associated cancer fibroblasts (NF), cancer-associated fibroblasts (CAF) and triple-negative breast cancer cell line HCC1806 assessed for the protein levels of the putative proline transporter SLC36A4, SLC6A20 and SLC36A1 at 21%O_2 and 1%O_2.

4.2.3 SLC38A2 imports the majority of proline under hypoxic conditions

To investigate if SLC38A2 plays a role in proline import, the U87 cell line was engineered with a shRNA construct, inducible by doxycycline to achieve knockdown of SLC38A2 (Figure 4.6B). After successful knockdown of SLC38A2, we found that the cells incorporate less proline in normoxic conditions and the reduced flux of $^{13}C_5$-proline into the cells was even more accentuated in hypoxia 0.3% O_2 (Figure 4.6A). Reduced flux of fully labelled proline was accompanied by a small decrease in total intracellular proline levels (Figure 4.7A) and to a bigger extent a decrease in intracellular aspartate levels (Figure 4.7C). Given that SLC38A2 was shown to be a glutamine importer in triple-negative breast cancer, total intracellular levels of glutamine were examined after SLC38A2 KD in U87 cells. Figure 4.7B shows no change in intracellular glutamine levels, confirming that SLC38A2 is not responsible for maintaining intracellular concentrations of this amino acid. We also utilized a siRNA against SLC38A2 in U87 cell line to test whether the metabolic consequences were reproducible (Figure 4.7). The metabolic changes associated with SLC38A2 knockdown were then assessed in other two cell lines. We confirmed that the major drop in aspartate was observed in the redox-compromised HOG IDH-mutant cell line, which also demonstrated increased growth with proline supplementation in hypoxia (Figure 4.8D). A smaller decrease in aspartate levels was observed after knockdown of SLC38A2 in the HOG IDH-wildtype cell line (Figure 4.8B). The data from both HOG IDH-wildtype and mutant confirm that SLC38A2 imports proline in hypoxia, as intracellular $^{13}C_5$-proline levels relative to the total pool drop after the transporter knockdown (Figure 4.8A and C). In addition, successful proline import in parental U87 cells as well as the kinetics of the transport were assessed using $^{13}C_5$-proline uptake

over time (Figure 4.9 A-B), under which conditions SLC38A2 protein expression was not altered by proline supplementation (Figure 4.9C). In agreement with a drop in aspartate observed, we found that exogenous proline supplementation did not fuel the TCA cycle, suggesting that the main fate of exogenous proline might be incorporation into proteins (Figure 4.10A-C).

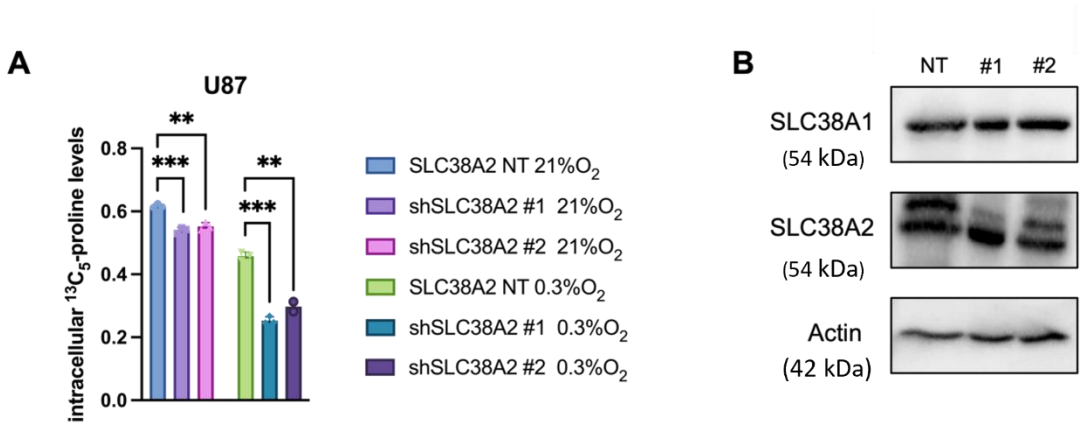

Figure 4.6 SLC38A2 imports most of the proline under hypoxic conditions

(A) Intracellular 13C5-proline levels measured by GC-MS with or without doxycycline induced in U87 SLC38A2 non-targeting control, shSLC38A2 #1 or #2 in normoxic or hypoxic conditions. (B) Western blot confirming successful knockdown of SLC38A2 in U87 glioblastoma cell line. Non-targeting control (NT), shSLC38A2 #1 (#1), shSLC38A2 #2 (#2). Error bars indicate ± S.E.M. and each experiment was conducted with three biological replicates. The Mann-Whitney test was used to determine the statistical significance *** $p<0.001$, * $p<0.05$, ** $p<0.01$.

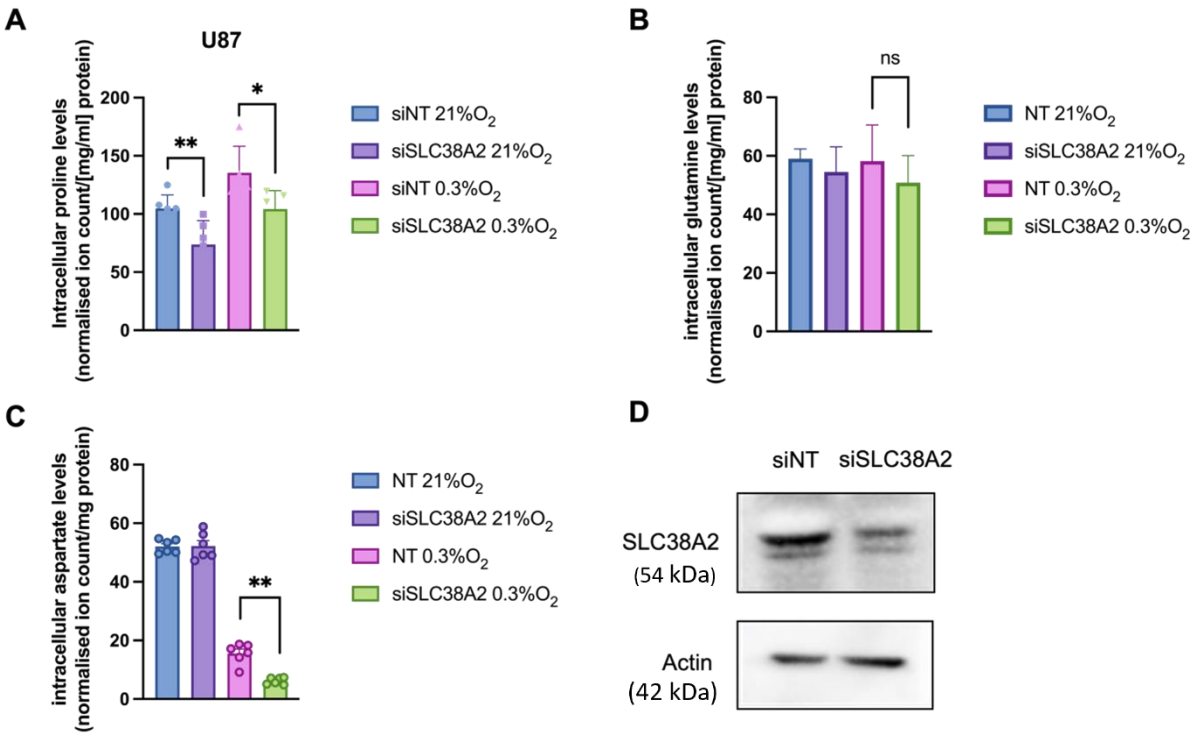

Figure 4.7 SLC38A2 KD decreases aspartate levels

(A-C) Intracellular proline, glutamine and aspartate levels measured by GC-MS in the presence or absence of SLC38A2 in U87 cells at 21%O_2 or 0.3%O_2. (D) Western blot showing successful SL38A2 KD after siRNA transfection in U87 glioblastoma cell line. Error bars indicate ± S.E.M. and each experiment was conducted with three biological replicates. The Mann-Whitney test was used to determine the statistical significance *** $p<0.001$, * $p<0.05$, ** $p<0.01$.

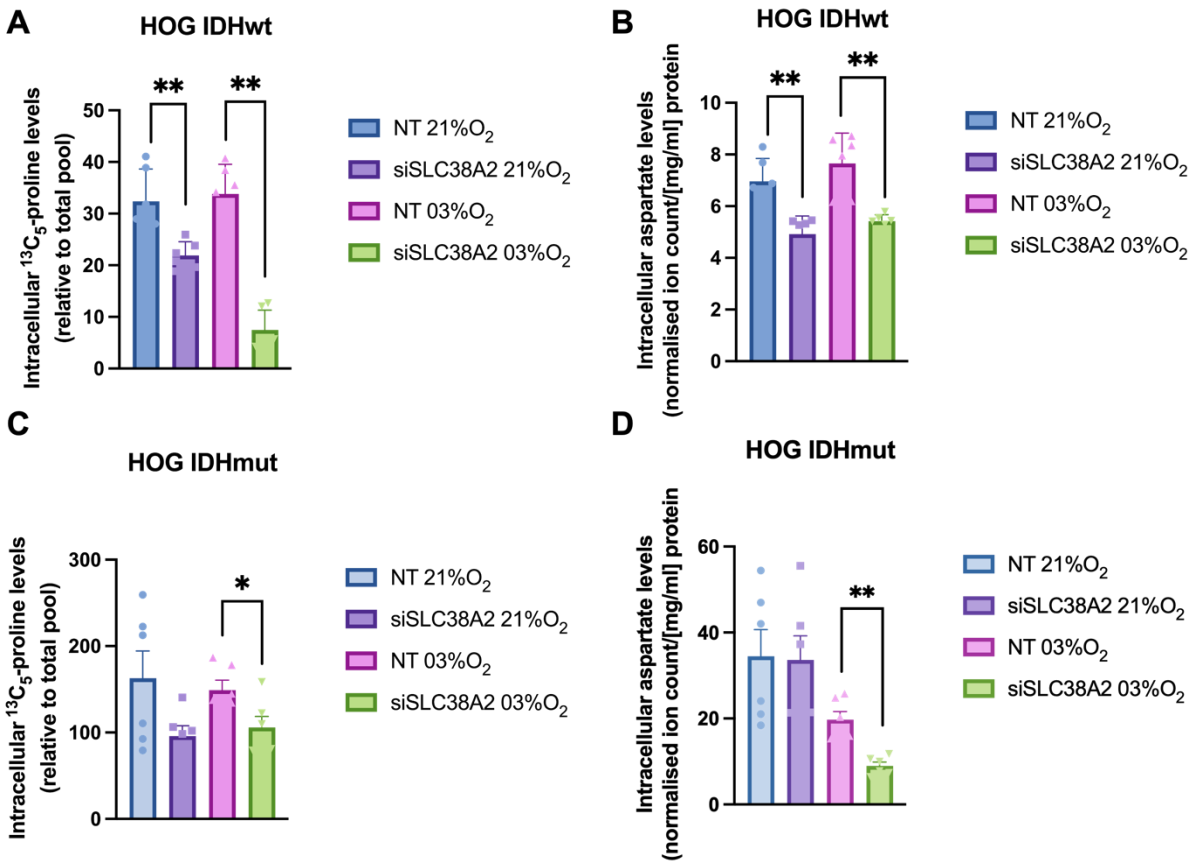

Figure 4.8 aspartate levels drop in redox compromised cell lines

(A and C) Intracellular $^{13}C_5$-proline levels, respectively in HOG IDH-wildtype and HOG IDH-mutant with or without siSLC38A2 in normoxic or hypoxic conditions. (B and D) Intracellular aspartate levels measured by GC-MS, respectively in HOG IDH-wildtype and in HOG IDH-mutant in siNT or siSLC38A2 cells at different oxygen tensions. Error bars indicate ± S.E.M. and each experiment was conducted with three biological replicates. The Mann-Whitney test was used to determine the statistical significance *** p<0.001, * p<0.05, ** p<0.01.

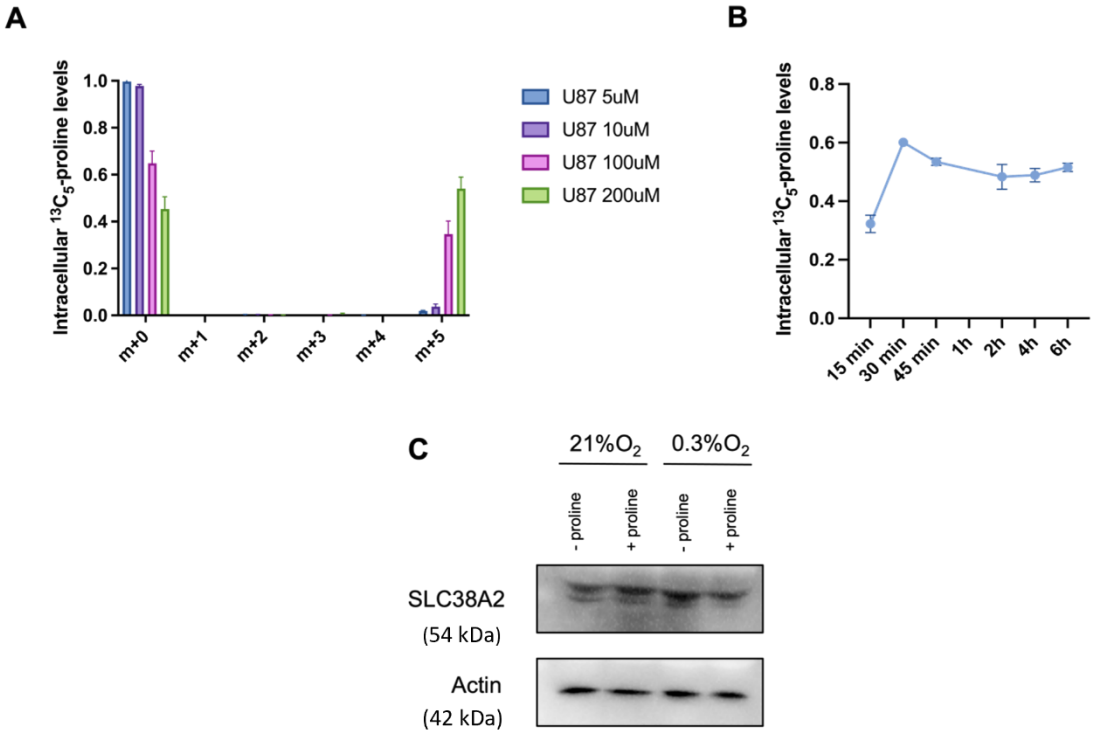

Figure 4.9 Proline can be imported quickly in U87 cell line and SLC38A2 protein levels are not affected by proline supplementation.

(A) Intracellular labelled proline measured after supplementation with increasing concentration of $^{13}C_5$-proline in U87 glioblastoma cell line. (B) Intracellular $^{13}C_5$-proline levels (200 μM) measured at different time points in U87 glioblastoma cell line. Error bars indicate ± S.E.M. and each experiment was conducted with three biological replicates. The Mann-Whitney test was used to determine the statistical significance *** p<0.001, * p<0.05, ** p<0.01.

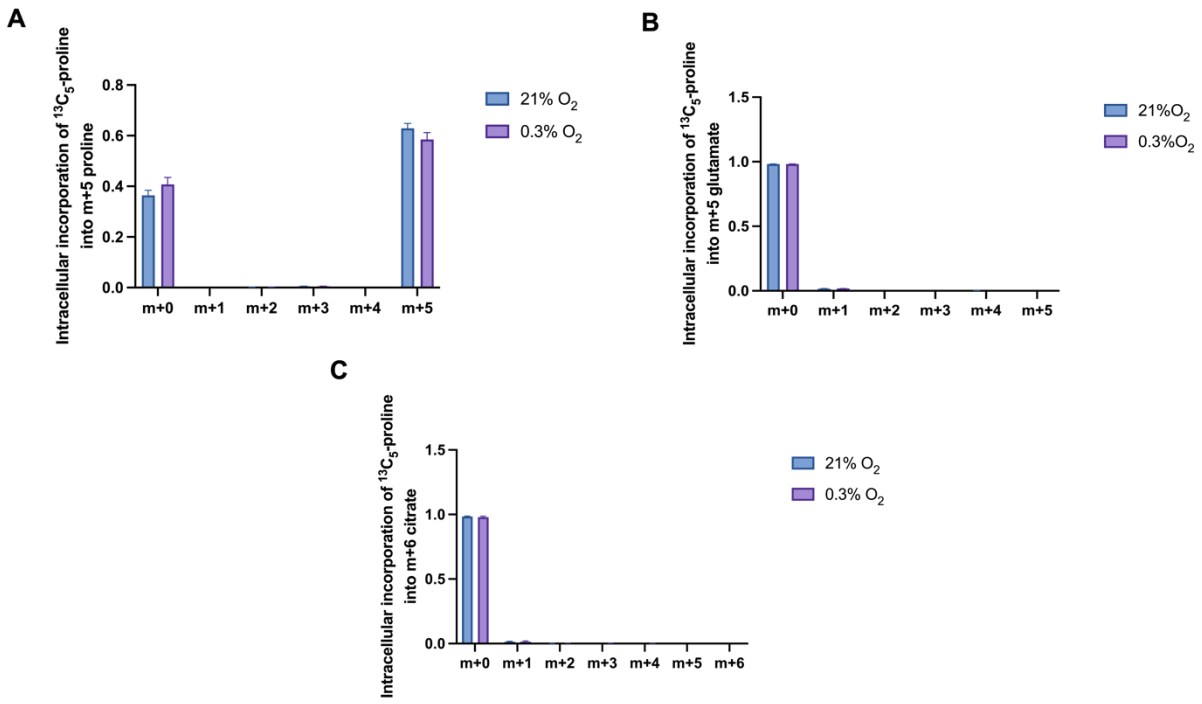

Figure 4.10 Exogenous proline does not label the TCA cycle

(A-C) $^{13}C_5$-proline incorporation into, respectively m+5 proline, m+5 glutamate, m+6 citrate at 21% O_2 or 0.3% O_2 in U87 glioblastoma cell line. Error bars indicate ± S.E.M. and each experiment was conducted with three biological replicates. The Mann-Whitney test was used to determine the statistical significance *** p<0.001, * p<0.05, ** p<0.01.

4.2.4 SLC38A2 KD causes nucleotide deficiency and impaired cell growth in hypoxia

Given that intracellular aspartate levels decrease after SLC38A2 KD, other metabolic changes connected with loss of the transporter were investigated using a targeted LC-MS metabolomics method. Interestingly, we observed that SLC38A2 deficiency resulted in a reduction in nucleotides intermediates, particularly of the purines (Figure 4.10A). Interestingly, nucleotide synthesis as well as proline production for the urea cycle are dependent on aspartate levels (Figure 4.10B), which are limiting after SLC38A2 KD as shown in the previous paragraph. Given the loss of nucleotides can be associated with growth defects, cell growth in U87 cells was measured by sulforhodamine B assay. Figure 4.11 suggests that U87 glioblastoma cells grow less in hypoxic conditions after SLC38A2 KD, while no change in growth was observed in normoxic conditions (Figure 4.11A). To assess if the lack of aspartate was responsible of the metabolic rewiring, 500 μM of $^{13}C_4$-aspartate was supplemented in U87 cells both in non-targeting control and siSCL38A2. Interestingly, we found that siSLC38A2 cells take up more labelled aspartate (Figure 4.12A), which contributes to labelled fumarate, strongly suggesting its use in the urea cycle and/or nucleotide biosynthesis reactions (Figure 4.12B). In addition, exogenous aspartate contributes to TCA cycle labelling, in particular into malate and citrate as shown in figure 4.12C-D. This suggests that labelled aspartate can also be imported into the mitochondria via the malate-aspartate shuttle. Overall, these data show that the decrease in aspartate downstream of reduced SLC38A2 expression is likely limiting for both nucleotide synthesis as well as anabolism and redox homeostasis via the TCA cycle.

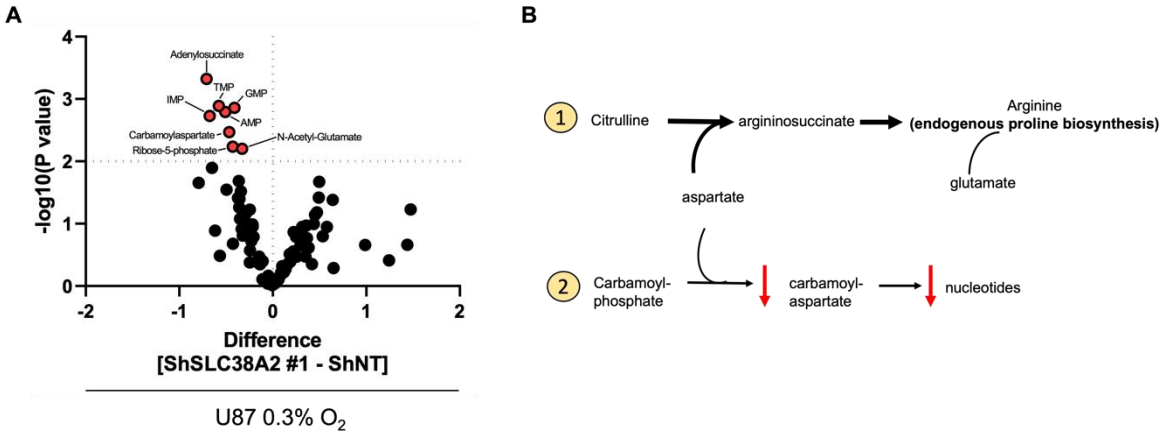

Figure 4.11 SLC38A2 KD causes nucleotide deficiency

(A) Metabolite abundance measured by LC-MS in doxycycline-induced SLC38A2 KD #1 vs non-targeting control U87 cell line in hypoxia 0.3% O_2. (B) Diagram showing key aspartate-requiring reactions: proline biosynthesis from the urea cycle and nucleotide biosynthesis. Each experiment was conducted with three biological replicates. Multiple unpaired t-test analysis was conducted to determine significance in figure (A), indicating in red $p<0.05$.

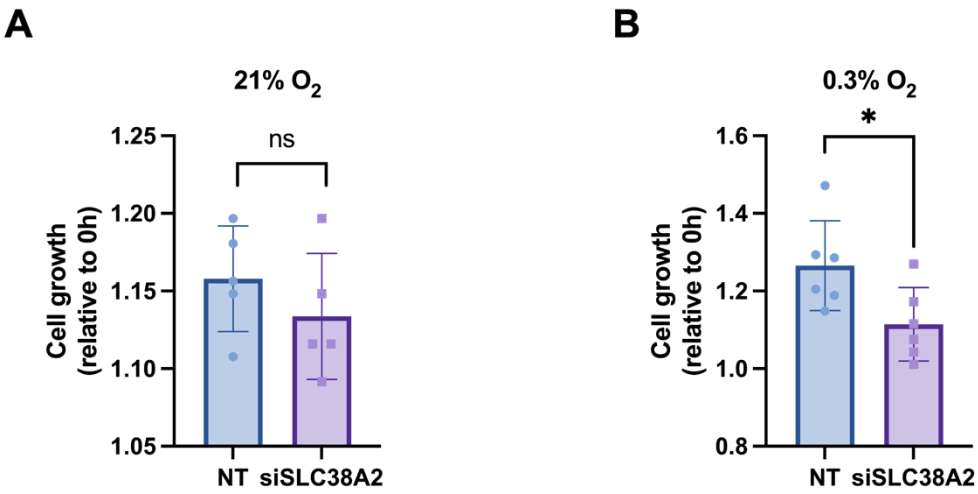

Figure 4.12 SLC38A2 KD causes impaired cell growth in hypoxia

(A-B) Cell growth measured by SRB in U87 siNT and siSLC38A2, respectively in normoxic or hypoxic conditions. Conditions were normalised to the time 0h control. Error bars indicate ± S.E.M. and each experiment was conducted with three biological replicates and technical duplicates. The Mann-Whitney test was used to determine the statistical significance *** p<0.001, * p<0.05, ** p<0.01.

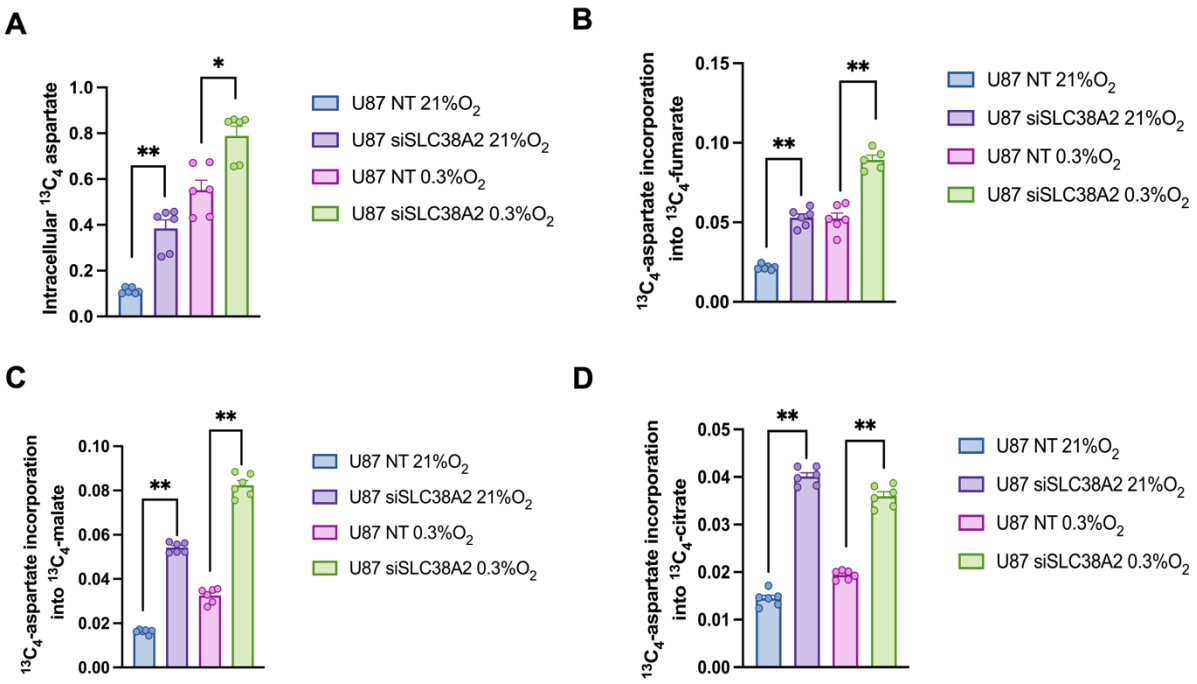

Figure 4.13 SLC38A2 KD cells increase aspartate uptake

(A) Intracellular $^{13}C_4$-aspartate levels in siNT or siSLC38A2 U87 cells in normoxia or hypoxia. (B-D) $^{13}C_4$-fumarate incorporation into, respectively $^{13}C_4$-fumarate, $^{13}C_4$-malate, $^{13}C_4$-citrate in the presence or absence of SLC38A2 in U87 cell line at different oxygen tensions. Error bars indicate ± S.E.M. and each experiment was conducted with three biological replicates. The Mann-Whitney test was used to determine the statistical significance *** p<0.001, * p<0.05, ** p<0.01.

4.2.5 SLC38A2 co-localises with the hypoxic marker CA9 in human brain tumour tissue

Given that SLC38A2 expression levels are increased under hypoxic conditions, the same experiment was conducted in primary brain tumour tissue to assess if the finding was reproducible *ex vivo*. Figure 4.13A shows human brain tissue stained with SLC38A2 (red), the hypoxic marker CA9 (green) or in blue for nuclear staining. Subsequently, Pearson's R value which indicates to what extent two markers are colocalising, was estimated in the same tissue. Surprisingly, a positive correlation 0.75 was calculated by the ImageJ FIJI software, confirming significant co-localisation between SLC38A2 and hypoxic areas (Figure 4.13B), in agreement with our *in vitro* data. The same finding was represented in a scatter plot (Figure 4.13B).

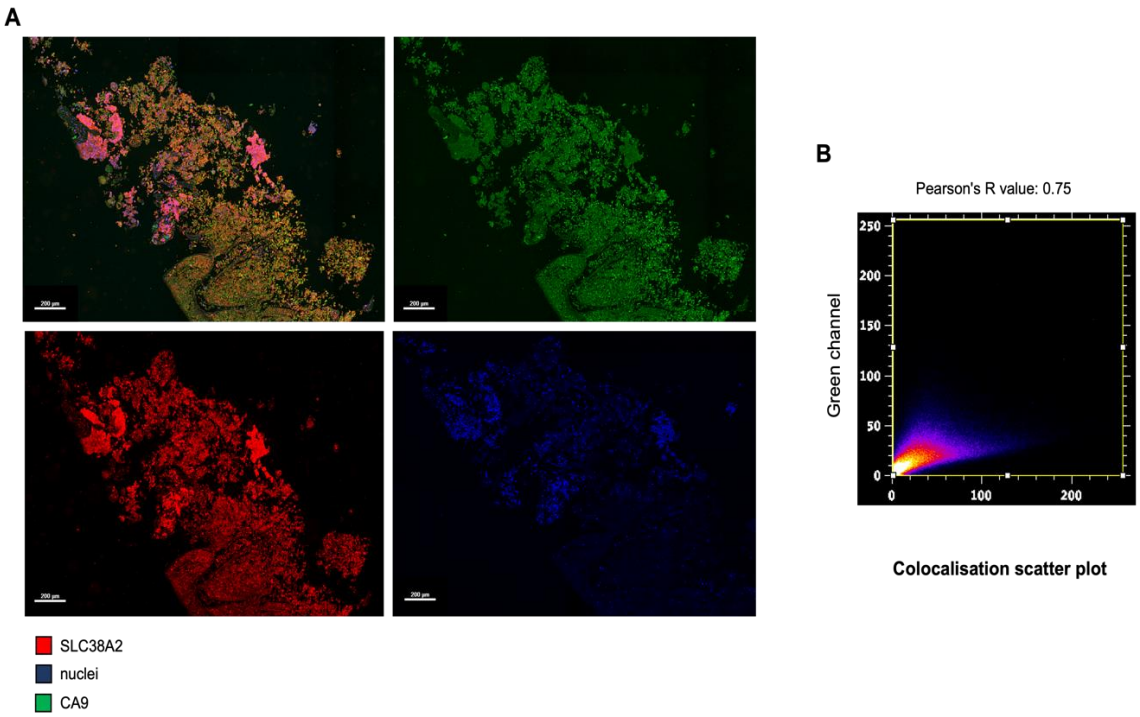

Figure 4.14 SLC38A2 co-localises with the hypoxic marker CA9 in human brain tumour tissue
(A) Immunocytochemistry on human brain tumour tissue stained for SLC38A2 (red), nuclear staining (blue), hypoxic marker CA9 (green). (B) Scatter plot and Pearson's R correlation value measured by ImageJ FIJI on the same tissue.

4.3 Discussion

The proline transporter SLC38A2 is part of the well characterized system A family of transporters. It was shown from previous studies that SLC38A2 can transport proline for osteoclasts differentiation[90], whilst in a study on triple-negative breast cancer SLC38A2 was suggested to transport mainly glutamine[90]. Our results suggest a primary transport for at least 50% of proline in hypoxic conditions (Figure 4.6A) and that the glutamine pool is not altered after knockdown in either normoxia or hypoxia (Figure 4.7B).

We also examined the rate of proline uptake and, contrary to other studies in osteoclasts[90], we have observed a quick turnover of proline (Figure 4.9B). It is therefore possible that the usage of the transporter might be cell and context-specific and might be dependent on additional post-translational modification of the protein. Indeed, SLC38A2 was shown to be highly glycosylated in the triple-negative breast cancer study[148] – condition that we do not observe in our system (Figure 4.6B and Figure 4.7D). It would be interesting to investigate whether the glycosylation residues alter kinetic speed or substrate specificity of the SLC38A2 protein.

A lack of proline has been shown in a clear cell renal cell carcinoma study to result in stalling of translational machinery at proline codons of mRNA encoding proteins highly enriched in proline[63]. We indeed observed decreased growth in hypoxic SLC38A2 KD cells (Figure 4.12B), but as proline levels only drop by about 50% (Figure 4.6A), it suggests that endogenous synthesis remains sufficient for direct physiological needs and protein biosynthesis. We hypothesise that the decreased growth is due to

aspartate being limiting for nucleotide biosynthesis, as it has been rerouted to provide nitrogen to sustain endogenous synthesis of proline through the less redox-expensive urea cycle route, rather than a limitation in proline availability *per se*. Indeed, the increased growth after proline supplementation is evident only in redox compromised cells, such as IDH-mutant gliomas, which are forced to generate more cytosolic $NADP^+$, and therefore pushing the cell towards a more oxidized status. This status might impair the glutamine to proline route that requires more NAD(P)H compared to the urea cycle route that requires aspartate and glutamate for, respectively, urea cycle and OAT function. Redox compromised cells might therefore become proline auxotroph to conduct efficient proline-dependent protein synthesis, otherwise subtracting aspartate from nucleotide biosynthesis to sustain endogenous proline production.

Interestingly, our $^{13}C_5$-proline uptake studies highlight that this amino acid is not used as a fuel for the TCA cycle, suggesting that PRODH is not active in our system to conduct the proline cycling with PYCR enzymes (Figure 4.10A-C). This hypothesised shuttle could be an alternative way of shuttling reducing equivalents between the cytosol and the mitochondria[56]. Overall, we can conclude that exogenous proline mainly contributes to protein synthesis in our system.

Interestingly, expression of SLC38A2 co-localises with the hypoxic marker CA9 (Figure 4.14A-B). This finding is consistent with the triple-negative breast cancer study showing a similar pattern on primary human samples[148].

To date only one inhibitor was shown to block the activity of system A, known as MeAIB, but no specific inhibitor has been developed for SLC38A2. Interestingly, a recent study showed that MeAIB-based positron emission tomography can distinguish between low and high-grade gliomas[149]. In the future, further effort would be required to develop a more specific inhibitor for SLC38A2.

CHAPTER 5:

Discussion

Significance and aims of the investigation

Cancer cells rewire their metabolism to fulfill biomass production, energy generation and redox homeostasis. Hypoxia always pushes cancer cells to adjust their metabolism to survive under harsh environments and selects for the most resistant cancer clones. These tumours are more prone to metastasise and invade nearby tissues and are a frequent cause of relapse after surgery or radiotherapy. It is therefore important to uncover metabolic dependencies under hypoxia that might offer a therapeutic opportunity for cancer patients.

In our study we uncovered metabolic pathways that might help tumours to survive and proliferate under hypoxic conditions. Proline metabolism, in particular, is one of the metabolic sub-networks that my and other evidence shows that it is important to allow the tumours to create an additional layer of redox flexibility that can allow survival under hostile microenvironments. Indeed, the cytosolic proline-producing enzyme PYCRL described in chapter 2, appears to be an additional route to regenerate NAD^+, harnessed by cancers for survival under hypoxia. Other salvage NAD^+ pathways, such as lipid desaturation can be engaged to fulfill the tumours' needs, but they might not be sufficient for all cell types, may be dependent on the genetic and metabolic budget of a specific cancer type, as shown in chapter 3. In addition, as explored in chapter 4, the microenvironment can also provide carbon sources that can be exploited by tumours to save energy for other endogenous pathways. Overall, through this investigation, we propose that the cytosolic proline-producing enzyme PYCRL and the proline transporter SLC38A2 can be considered as potential therapeutic targets that

can be targetable in, respectively, cancer stem cells or in redox-compromised cells, such as IDH-mutant brain tumours.

Cytosolic proline biosynthesis is an additional route to maintain cancer redox plasticity

Previous studies from our and other labs, have shown the importance of proline biosynthesis as a redox shunt in hypoxic conditions, respectively in triple-negative breast cancer and in fibroblasts[73,74]. We extended this finding in a double-PYCR1 and 2 KO system and demonstrated that PYCRL was able to maintain the same levels of proline biosynthesis as the non-targeting control (Figure 2.6A and C-D). Nevertheless, PYCRL could not compensate for the mitochondrial redox defect generated by the lack of PYCR1 and 2, as could be hypothesized to occur from previously published studies from ourselves and others and the decreased cell confluency observed here (Figure 2.6E)[73,74]. This condition occurs because the mitochondrial enzymes involved in proline biosynthesis, PYCR1,2 and ALDH18A1 can use the reducing equivalents available in the mitochondria to protect cancer cells from reductive stress. The latter occurs when the redox balance of NADH and/or NADPH exceeds the capacity of cancer cells to regenerate the oxidized reducing equivalent counterpart. Given that it is not clear from the literature if in hypoxia the total redox equivalents are in a reduced state, we measured by LC-MS the total redox ratio as the sum of reduced NADH and NADPH divided by their oxidized forms NAD^+ and $NADP^+$ and we found that in all glioblastoma cell lines hypoxia influenced redox towards increased oxidation (Figure 4.2). It is important to note that this ratio does not consider $FADH_2$ levels that could be measured and quantified by two-photon microscopy[150]. In addition, our measurement

only considers the amount of free reducing equivalents and not the amount of those bound as co-factors to enzymes. It might be the case that regional availability of reducing equivalents dictates the enzymatic preference towards NADH or NADPH and that hypoxia influences different areas of the cell modulating redox pools in different ways.

Even if PYCRL has been shown to have higher affinity for $NADP^+$ this condition was only observed in a study that used supraphysiological concentrations of its substrate P5C[58]. Indeed, when the P5C was lowered in the same study, the co-factor preference for PYCRL was less evident. In the same way, depending on PYCRL exact cytoplasmic localization, if the NADH pool is more accessible than NADPH, this will likely dictate PYCRL preference for co-factor usage. Indeed, when we measured PYCRL co-factor usage using 4D-glucose as means of labelling the NADH pool, we showed that deuterated NADH incorporated deuterons into proline (Figure 2.5G). This finding proposes PYCRL as an additional route of regenerating NAD^+ in the cytosol of normoxic and hypoxic glioblastoma stem cells.

PYCRL, contrary to what was described in the literature, can use glutamine carbons in addition to ornithine to produce proline. This substrate promiscuity can also be attributable to other PYCRs, even if further experiments need to be performed to validate this hypothesis. The fact that PYCRs can use ornithine as alternative carbons to produce proline can bypass ALDH18A1 dependence on NADK2 for reducing equivalents, allowing cancer cells to effectively produce proline endogenously without depleting the mitochondrial ATP and NADPH pools.

The fact that PYCRL can maintain endogenous proline biosynthesis despite the lack of PYCR1 and 2 implies that its substrate P5C must be shuttled out from the mitochondria. To date, a P5C transporter has yet to be identified, mainly because the molecule of P5C is very reactive and unstable in standard LC-MS or GC-MS extraction conditions. Nevertheless, identifying the mitochondrial P5C transporter would further validate the importance of PYCRL in supplying proline when mitochondrial PYCRs are impaired.

To explore the possibility that PYCRL might shuttle reducing equivalents through PRODH and therefore regenerating mitochondrial NAD^+ through the hypothesized proline shuttle, we used proline deuterated twice in position 2 and once in position 5. If the proline shuttle was active, m+3 proline would have been converted into m+2 by PRODH or reversal of the activity of any of the PYCRs. Nevertheless, we do not observe any change in m+3 proline (Figure 2.7B), nor was $^{13}C_5$-proline incorporated into different metabolites observed in the U87 glioblastoma cell line (Figure 4.10A-C), suggesting that PRODH is not active in our system. It would be therefore interesting to uncover under which conditions PRODH might be active and if the proline cycling occurs *in vivo*.

Interestingly, metabolomics analysis of PYCRL KD cells showed a marked increase in the levels of phosphoethanolamine. This is a reactive metabolite previously characterized in cells that are glutamine deprived[151]. Indeed, lack of PYCRL shows a “pseudostarvation” phenotype, as not only TCA cycle flux from glutamine is low, but also glutathione production is impaired (Figure 2.10A-E and figure 3.9B). Further

experiments are required to better define the role of phosphoethanolamine in PYCRL-deficient cells.

Overall, we have identified PYCRL as a metabolic vulnerability in hypoxic cancer glioblastoma stem cells. To date, only a limited number of compounds have been shown to inhibit mitochondrial proline biosynthesis, and in particular PYCR1, such as deshydroproline or N-formyl l-proline (NFLP)[152]. Nevertheless, the specificity of these inhibitors to block the activity of PYCR isoforms is not yet well-defined and no specific inhibitor against PYCRL has been developed as of yet. We hope that our findings might encourage the development of more specific inhibitors to target the PYCR isoform that plays the major role in a specific tumour type. This inhibitor would also be able to uncover PYCRs tissue-specific roles *in vivo*.

Cytosolic and mitochondrial redox pools are interconnected and confer metabolic flexibility under hypoxic conditions

There is a preference towards the maintenance of a more reductive environment for NAD^+/NADH in the mitochondria, with a ratio reportedly around 7-8, whereas the cytosol tents to be more oxidative, where the NAD^+/NADH ratio fluctuates around 60 to 700[44]. Any alteration in the normal NAD^+ homeostasis can be buffered by indirect pathways, such as the malate-aspartate shuttle or the glycerol-3-phosphate shuttle, or more directly through the newly discovered NAD^+ transporter SLC25A51[45,46]. In our system, the glycerol-3-phosphate shuttle appears impaired after knockdown of PYCRL, as illustrated by glycerol-3-phosphate accumulation (Figure 2.12C). On the other hand, the malate-aspartate shuttle could play a major role in buffering

cytoplasmic NADH accumulation after loss of PYCRL. Indeed, treatment with the pan-transaminase inhibitor AOA inhibits the overall malate-aspartate shuttle activity, increasing the cell dependence on cytoplasmic lactate production for NAD^+ regeneration (Figure 2.12A-B). This implies that the cytoplasmic and mitochondrial NAD^+/NADH pools are interconnected and that the mitochondria *in primis* try to compensate for any cytoplasmic redox defect.

In addition, the NAD^+/NADH and $NADP^+$/NADPH pools can influence each other between compartments. For instance, NADPH-dependent lipid synthesis is partly dictated by the availability of the mitochondrial acetyl-CoA pool. In turn, the acetyl-CoA pool is influenced by mitochondrial NAD^+ availability which will promote or decrease TCA cycle turning. In addition, reactions within the same lipid synthesis pathway can be both NADPH, or NADH-dependent, such as lipid desaturation. Therefore, intra and inter-related NADH or NADPH reactions, as well as co-factor regional availability, will dictate the overall redox status of a cell. Our system – PYCRL knockdown - provides an example of where decreased TCA cycle turning is coupled with reduced cytosolic lipid biosynthesis (Figure 3.1C-D and 3.7B). In the future, it will become even more important to disentangle in which context some enzymes will prefer to use NADH or NADPH to resolve regional redox availability and uncover new cancer-specific compartment interconnections between the two redox pools. An example is MTHFD2 was shown can use NADH - imported into the mitochondria by the malate-aspartate shuttle - instead of NADPH, after the loss of UQCR11 in ovarian cancer[135].

Interestingly, new evidence has shown that cancer cells exiting from pluripotency engage in a non-canonical TCA cycle, a citrate-malate shuttle that regenerates

cytoplasmic NAD^+ while minimising mitochondrial NADH production[153]. Indeed, contrary to the malate-aspartate shuttle, this pathway does not increase the levels of cytoplasmic aspartate but augments the levels of cytosolic citrate. In addition, the model addresses a discrepancy in pancreatic cancer cells cultured *in vitro* which rely more on the enzyme ACLY, whereas *in vivo* rely more on the enzyme ACO2 to increase cytosolic citrate. Further experiments will be required to see if this model is also active in our PYCRL-deficient system and if the malate-aspartate shuttle labelled with 4D-glucose behaves canonically or non-canonically in glioblastoma stem cells *in vivo*.

SLC38A2 can fulfill proline requirements in redox compromised cancer cells

Previous findings from our lab have shown that PYCR1 is important in IDH1-mutant cells as a way of normalizing mitochondrial redox equivalents through regeneration of mitochondrial NAD^+ and uncoupling of the mitochondrial electron transport chain[126]. In our study, we show that IDH-mutant cells further exposed to hypoxic conditions, struggle to engage the canonical glutamine to proline endogenous biosynthesis and, instead, prefer to import exogenous proline. This strategy allows hypoxic IDH-mutant tumours in a highly oxidised status to spare aspartate and reduced redox equivalents. Indeed, SLC38A2 KD cells become more dependent on exogenous aspartate for cell proliferation (Figure 4.13A).

Reduced SLC38A2 expression led to decreased levels of a number of aspartate, purine nucleotide precursors and reduced proliferation. While we showed that aspartate supplementation allows the siSLC38A2 cells to replenish some of their

metabolite pools, the extent to which this rescues nucleotide biosynthesis in the SLC38A2 KD system has yet to be determined, but is a key observation to make. An alternative hypothesis could be that SLC38A2 KD causes drop in proline that results in ribosome stalling in proline rich proteins and that enzymes involved in the nucleotide biosynthesis are highly enriched in this amino acid. This hypothesis is less likely to be true though, as the proline decreases by about 50% in SLC38A2 KD (Figure 4.6A). Therefore, it is likely that proline availability in SLC38A2 KD cells is still sufficient to fulfill the proteinogenic needs of the tumour. Nevertheless, a detailed investigation of the links between proline availability and nucleotide biosynthesis is required as they are not yet clear.

Recent evidence has shown that in a NADK2 KO system, cells become proline auxotrophic[104,105]. Indeed, NADK2 KO cells cannot effectively engage in endogenous proline synthesis due to the lack of NADK2-derived mitochondrial $NADP^+$. In hypoxic SLC38A2 KD IDH-mutant cells we have shown that the redox defect can also affect the cytosolic compartment – more cytosolic $NADP^+$ regeneration through mutant IDH1 - and cells appear to need proline to support their growth. We indeed observe the same nucleotide deficiency as in NADK2 KO cells (Figure 4.11A), nevertheless we do not observe the same dramatic drop in proline levels (more than 50%)[105]. It is therefore important to highlight that different tumour types might have different redox budget allocated for the endogenous proline biosynthesis pathway. This redox budget, in turn, is dictated by the redox plasticity of a cancer cell in a tissue-specific and stage-dependent manner.

The remaining 50% of the intracellular proline produced in the absence of SLC38A2 could be the result of endogenous biosynthesis, but also the contribution of other transporters, such as SLC38A1 which can also import proline. The redundancy in amino acid transport is also well-defined in other contexts such the mitochondrial glutathione importers SLC25A39 and SLC25A40[154]. In our system, we are confident that SLC38A2 is the major driver of proline import in hypoxic conditions, as the drastic drop in labelled proline and total proline pool was observed in other glioblastoma cell lines (Figure 4.8 A and C). Amino acid transport is also promiscuous, indeed SLC38A2 has been shown to import glutamine and alanine in other contexts[155,156]. Despite this, our data suggest that in hypoxic glioblastoma SLC38A2 transports mainly proline and not glutamine (Figure 4.7B), whereas alanine is absent in the conditions we investigated this. It still needs to be determined if the same substrate preference is retained in plasma-like medium or in an *in vivo* context. Indeed, we have also shown that proline transport is context specific. For instance, breast normal fibroblasts and cancer-associated fibroblasts proline transport is different from triple-negative breast cancer cells, as highlighted from the differential protein expression of SLC6A20 and SLC36A4 in those cell types (Figure 4.5). Therefore, targeting cancer specific amino acid transport would open new treatment opportunities for patients in the future.

To date, only a small fraction of inhibitors can cross the blood-tumour brain barrier (BTB). In particular, many compounds cannot cross in intact BTB regions or remain stagnant in the more permeable areas[145]. The challenge of an inhibitor that can effectively cross the BTB and only kill brain tumour cells is very much alive. For

SLC38A2, only one non-selective inhibitor called MeAIB exists, but unfortunately suffers from the lack of selectivity, as it can potentially target all transporters of the SLC38 family[147]. In addition, MeAIB cannot cross the BTB and studies have been conducted in mice with the usage of microdialysis[157]. Further attention must therefore be drawn into the development of effective inhibitors after *in vitro* and *in vivo* validation of a genetically manipulated target.

PYCRL project cell lines	**Findings**
A172 glioblastoma stem-like cells HCC1806 breast cancer stem-like cells HEK293 NCH421k glioblastoma stem cells	Chapter 2: all these cell lines confirm that PYCRL promotes cell proliferation and survival in hypoxic regions (A172, HCC1806, NCH421k cell lines) and that this enzyme is sufficient to maintain intracellular proline levels when PYCR1 and 2 are absent (HEK293 cell line). Chapter 3: Lipid biosynthesis is also impaired in A172 PYCRL KD and lipid desaturation cannot regenerate enough NAD+ for proliferation.
SLC38A2 project cell lines	**Findings**
U87 glioblastoma cell line HOG IDH-wild type (oligodendroglioma) HOG IDH-mutant (oligodendroglioma) T98G glioblastoma cell line	Chapter 4: U87 glioblastoma cells and HOG IDH-mutant show increased total oxidation of redox couples when exposed to hypoxia. Lack of available reduced redox co-factors required for endogenous proline biosynthesis promotes proline import to support cancer proliferation in these cell lines.

Table 1. General overview of the cell lines used and major findings.

CHAPTER 6:

Materials and methods

Materials and methods

Cell culture

A172 (Chapter 2), T98G, U87 glioblastoma, HOG IDH-wt and IDH-mut oligodendroglioma (Chapter 4), HCC1806 triple-negative breast cancer (Chapter 2) cell lines were cultured in Dulbecco's Modified Eagle's Medium (DMEM) high glucose 4,5 g/L (Sigma-Aldrich, D5796), supplemented with 10% foetal bovine serum (FBS), 200 μM of proline and ornithine (Sigma-Aldrich).

NCH421K cells (Chapter 2) were a kind gift from Christel Harold-Mende and were cultured in DMEM-HAM F12 supplemented with 100 ml BIT-100 (Provitro), 5 ml 10X PEN-STREP (10 000UI/ml), 50μl of stock 10kU/heparin. In addition, the DMEM-HAM F12 was supplemented with 20ng/ml of FGF-2 and 20ng/ml EGF and used within 2 weeks. For GC-MS experiments NCH421K cells 10X PEN-STREP was not added to the mix.

Breast-derived normal fibroblasts or cancer associated fibroblasts (Chapter 4) were cultured in DMEM supplemented with 10% FBS, 5 ng/ml of FGF-2 and insulin 5 μg/ml.

Cells were grown in standard conditions in a 37°C humidified incubator, 5% CO_2 and regularly tested for mycoplasma contamination using PCR Mycoplasma Test kit I/C (PromoKine, PK-CA91-1048). All cells resulted negative.

For hypoxia experiments, cells were cultured in the hypoxic chamber (Whitley H35 Hypoxystation) at 37°C, at 1% or 0,3% O_2, 5% CO_2, 94.7% N_2, 62% humidity.

Cell treatments

Cells were seeded onto a 24-well plate to reach 70% confluency. 2 mM of acetate (Chapter 2), or 1 mM of BSO (Chapter 2) or 500 μM of aspartate (Chapter 1), or 200 μM of proline were added to the media and cells were fixed according to SRB viability assay protocol after 48h in normoxia or hypoxia.

For TGF-β treatments (Chapter 2), cells were plated at a density of $1x10^5$ in a 6-well plate and allowed to attach overnight. 15 ng/ml of Human TGF-β1 (PeproTech) were added for 8 hours in DMEM flux media for GC-MS experiments or DMEM with phenol red for Western Blot assay. For Western Blot experiments involving inhibition of TGF-β1 signaling, cells were pre-treated for 24 hours with the inhibitor LY-109761 (1 μM) and then 15 ng/ml of TGF-β1 was added to each well for 8 hours. Cells were then lysed in 1x Laemmli for Western Blot analysis.

Transfection with siRNA or shRNA

In chapter 2 for siRNA, cells were seeded onto a 6-well plate and allowed to attached overnight. The following day cells were treated according to manifacturer's protocol with a non-targeting siRNA (siNT) or siPYCRL (Horizon discovery ON-TARGETplus human siRNA D-001810-10 and L-014246-00-0005) at a concentration of 25 nM/well with DharmaFECT1 transfection reagent (Horizon discovery T-2001-03). After 48h, cells were harvested for experiments.

In the same way as for siPYCRL, in chapter 3 A172 cells were transfected with siNNT (Horizon discovery ON-TARGETplus human siRNA L-009809-00-0005) at a concentration of 25 nM/well in a 6-well plate. U87 in chapter 2 were transfected with

siSLC38A2 (Horizon discovery ON-TARGETplus human siRNA L-007559-01-0005) at a concentration of 100 nM/well in a 6-well plate.

For shRNA, A172 (in chapter 2) or U87 (in chapter 3) cells were seeded at a density of $3{,}3x10^3$ onto a 96-well plate and transfected after 24 hours with 5 μl of lentiviral inducible shRNA, non-targeting or shPYCRL (TransOMIC, TLHVU2300-65263) or shSLC38A2 (TransOMIC, TLHVU2330-54407). After puromycin selection, cells were FACS sorted and induced with 5 μg/ml of doxycycline.

Spheroidal growth

In chapter 2, A172 glioblastoma cells were seeded at a confluency of $7x10^4$ cells/well onto 96-well low attachment plates and grown for 5 days with or without addition of 200 μM of proline. NCH421k (chapter 2) were seeded at a confluency of $5x10^5$ cells/well onto a 12-well plate and grown for 48h with or without proline supplementation (200 μM). Spheroidal volume was assessed by ImageJ software and images were acquired by EVOS FL microscope (Thermo Fischer) at 4x magnification.

Western Blot

In all chapters, cells in a 6-well plate were washed with 1X PBS and lysed in 200 µl of 1x Laemmli buffer (Sigma-Aldrich, S3401-1VL). 30 µl of each sample was loaded on polyacrylamide gels for sodium dodecyl-sulphate polyacrylamide gel electrophoresis (SDS-PAGE). After the run, the polyacrilamyde gel was transferred onto a nitrocellulose membrane and then blocked for 1 hour in PBS-Tween containing 5% Bovine serum albumin (BSA). After the blocking step, membranes were incubated at 4°C overnight with the primary antibody of interest: anti-β-actin (Sigma A4700,

monoclonal mouse, 1:4000 in 1% BSA), anti-PYCRL (mouse monoclonal MA5-25335, 1:500 in 1% BSA), anti-PYCR1 and 2 (Proteintech, respectively 13108-1-AP and 17146-AP, 1:1000 in 1% BSA), anti-HIF1α (BD Biosciences, monoclonal mouse 6109590, 1:500 in 1% BSA), anti-SLC38A2 (MBL, BMP081, 1:500 in 5% BSA), anti-SLC38A1 (Abcam, ab134268 1:2000 in 1% BSA), anti-SLC1A4 (Proteintech, 13067-2-AP 1:500 in 1% BSA), anti-SLC6A20 (Thermo Fisher, PA5-68332, 1:500 in 1% BSA), anti-SLC36A1 (Abcam, ab189441, 1:500 in 1% BSA), anti-SLC36A4 (Proteintech, 24066-1-AP), anti-Vinculin (Abcam, ab91459, 1:1000 in 1% BSA). After incubation with the specific secondary antibody, blots were developed using the chemiluminescence detection kit EZ-ECL (BI, 20-500-120) and acquired with BIO RAD ChemiDoc XRS+ imaging system.

Sulforhodamine B assay

In all chapters, cells were fixed in 20% (v/v) ice-cold trichloroacetic acid solution (TCA) (Sigma- Aldrich, T0699), at ¼ of the volume of the media used. After a 30-minute storage at 4°C, intracellular proteins were stained at room temperature using 0.4% (w/v) sulforhodamine B (SRB) (Sigma-Aldrich, 230162) dissolved in 1% acetic acid. The samples were then washed with 1% acetic acid and left to dry. Afterward, the SRB was dissolved in 50 mM Tris/HCl pH 8.8 and 100 µL/well of the solution was pipetted in a 96-well plate for quantification by absorbance at 510 nm with the plate reader FLUOstar Omega (BMG LabTech). Final absorbance was quantified by the average of technical replicates normalized on day 1.

Gas Chromatography - Mass Spectrometry (GC-MS)

In all chapters, 1 x10^5 cells/well were seeded onto a 6-well plate and left to attach overnight in the incubator. After washing, 2 ml of DMEM flux (Sigma-Aldrich, D5030) was added to the cells. This media contains the tracer of interest: 200 µM 13C(5)-Ornithine or 2 mM 13C(5)-Glutamine or 10 mM 13C(6)- or 4D-Glucose or 200 µM of 13C(5)- or 3D-Proline. All cells were kept in flux media for 48 h. Cells were then washed twice with saline and the plate was extracted with 500 µL of dry-ice cold methanol (Fisher Scientific), 200 µL of ice-cold distilled water with D6-glutaric acid standard and 500 µL of chloroform (Fisher Scientific). The upper phase was transferred into a clean safe lock tube and dried in a speedvac (45°C for 2-3h). Afterward, 40 µl of 2% methoxyamine HCl in pyridine (MOX; Sigma- Aldrich, Dorset, UK) were added to each sample and shaked at 60°C for 1h at 500 rpm. The same procedure was performed after addition of 60 µl of MTBSTFA (Sigma- Aldrich, Dorset, UK). Lastly, 100 µl/sample were transferred to glass vials and loaded onto the GC-MS. The gas chromatograph, Agilent 7890B equipped with a polydimethylsiloxane column connected to a mass spectrometer (MS) (Agilent Technologies UK Limited, Stockport, UK) was used for analysis of the derivatized polar metabolites. After acquisition of the raw data, Mass Isotopomer Distribution (MID, integration and normalization for natural abundance) and Ion counts (peak area) were calculated using an in-house MATLAB script created by Juan Fernandez-Garcia (Sarah-Maria Fendt's Lab). Peak areas were then normalized on the internal standard and protein amount.

For lipids (chapter 3), cells were extracted in 500 µL of pre-chilled at -20°C methanol, 200 µL of ice-cold distilled water and 500 µL of dry ice-cold dichloromethane with C:17 Heptadecanoic acid as internal standard. The dichloromethane layer was collected

and dried in a nitrogen evaporator. Then, samples were saponified with addition of 100 µL potassium hydroxide (200mg/ml) and heated for 4 hours at 60°C. After the heating step, samples were acidified with 1M HCl and 500 µL toluene were added, followed by centrifugation for 10 minutes at 4000 rpm. The upper layer was then collected in a new tube and dried down in a nitrogen evaporator. Samples were then derivatized and analysed as for polar metabolites. Data were acquired as for polar metabolites (in-house MATLAB script)

Metabolomics by LC-MS

Cells were plated to be 80% confluent in a 6-well plate at the time of the extraction. shNT, shPYCRL (chapter 2) or shSLC38A2 (chapter 4) were induced with 5 μg/ml of doxycycline. After 48h of incubation, the samples were then extracted in 250 μl of 80:20 methanol:water supplemented with 1 μg/ml of internal standard D6-glutaric acid. After this step, cells were dried in a vacuum centrifuge at room temperature. The samples were then reconstituted in 100 μl of ultrapure water and 50 μl of each derivatization solution (33 mg/ml of 3-NPH 175 mM; 20 mg/ml of EDC 105 mM; 25 μl/ml of Pyridine, 2.5% in MeOH), was added into the samples. After 30 minutes of incubation at 4°C, samples were dried down in a vacuum centrifuge at room temperature. After this step, the samples were reconstituted in 12.5 μl of methanol and diluited in 37.5 μl of HPLC water. The samples were then injected into a triple quadrupole mass spectrometer (Waters Xevo TQ-S) and the data were analysed using the software Skyline. Pathway enrichment analysis was conducted using Metaboanalyst 2.0. The samples were normalised on total protein.

Redox measurements by LC-MS

For NAD^+:NADH and $NADP^+$:NADPH measurements in chapter 2, $1x10^5$ cells were seeded onto a 6-well plate and shNT or shPYCRL #1 were induced with doxycycline for 48 hours and treated with hypoxia for 24 hours. Experiments were conducted as previously described by Wenyun Lu *et al.* 2018 (DOI: 10.1089/ars.2017.7014). Briefly, cells were harvested in a pre-chilled solution of methanol:acetonitrile:water (40:40:20) and 0.5% formic acid. The cell lysate was then moved into an Eppendorf on ice for 5 minutes. After this step, 15% of ammonium bicarbonate at pH 9 was added to quench the samples that were then kept on dry ice for 15 minutes. Samples were then centrifuged at 21000g for 10 minutes and the supernatant was collected for LC-MS analysis. The samples were then run and analysed as for the metabolomics measurements.

Ubiquinone measurements by LC-MS

Briefly, the cells were plated as for the redox measurements in chapter 2. The extraction method was performed according to the protocol published from Burger et al,[158]. After extraction, the cells were injected into a triple quadrupole mass spectrometer Waters Xevo TQ-S) and the data were analysed and normalised as for the metabolomics measurements.

Glucose and lactate measurements

In chapter 2, cells were plated onto a 24-well plate at a confluency of $2,5x10^4$ in DMEM flux supplemented with 10 mM of glucose, 2mM of glutamine, 200μM of proline and ornithine, and 10% of dialysed FBS. After 48h of incubation either in normoxia or

hypoxia, glucose and lactate in the media were measured using a Nova Biomedical Stat Profile Prime CCS Analyzer. The result obtain was then normalised on protein amount.

GSSG:GSH and total GSH measurements

In chapter 3, cells were plated onto a 6-well plate to be 80% confluent. The cells were then transfected with siNT or siPYCRL (25nM). After 24h, cells were washed with PBS, detached and moved onto a 96-well plate with white bottom at a confluency of $3x10^4$ cells/well. In addition, cells were incubated either at 21%O_2 or moved into the hypoxic chamber. At the 48h time-point, the cells were treated according to the manifacturer's protocol (Promega). Luminescence was measured with plate reader (BMG PHERAstar). For total GSH, samples were normalised on total protein.

Immunofluorescence on tissue

In chapter 4, primary brain tumour tissue was obtained from the Queen Elisabeth Hospital. The tissue was then washed with Histoclear 3 times and deparaffinized with decreasing EtOH concentrations. Antigen retrieval was carried out by boiling the TMA slide at 95°C for 20 minutes in citrate buffer. After blocking for 1 hour at room temperature in PBS + 0.1% Triton X-100 + 2% BSA (Blocking solution) anti-CA9 1:250 (Abcam, ab15086) and anti-PYCRL 1:250 (Thermo Fisher, MA5-25335) were applied on the slide overnight at 4°C. The next day, the TMA was washed with PBS-T and 0.1% BSA (Washing buffer) and incubated for 2 hours with secondary antibodies 1:500 Alexa fluor 568 (Thermo Fisher, A-11004) and Alexa fluor 488 (Thermo Fisher, A-11008), and Hoescht 33342 dye (1:1000, Thermo Fischer). Images were acquired with the slide scanner Zeiss Axioscan and analysed with ZEN software. The co-localisation

plot and Person's R correlation value were generated using the ImageJ-FIJI plugin Coloc2.

Immunohistochemistry

In chapter 2, $7x10^4$ cells of A172 cell line were cultured in low-attachment 96-well plates to allow quick formation of spheroids. After 48 hours, spheroids were treated with 100 μM of pimonidazole overnight. Then, spheroids were fixed in 10% formalin at pH 7 overnight and washed twice with PBS and transferred into a 70% ethanol solution. The solution containing the spheroids is gently dispensed onto the centre of a sheet of biopsy paper (CellPath, UK). The biopsy paper is then folder over twice to seal the spheroids in. The folded biopsy paper is placed into the appropriate processing cassette and the sample undergoes a standard histology processing schedule. After processing the biopsy paper is removed from the cassette and carefully opened up. The paper is placed on a hot plate to melt the wax and then the visible spheroids are gently removed from the paper into an embedding mold with molten wax. The spheroids are allowed to sink to the bottom of the wax and then the cassette is placed onto of the mold. The embedding mold is placed onto the cold plate of the embedding centre to allow a wax block to be produced. 4 μm sections are then cut from the block and stained for H&E and designated IHC stains: cleaved-Caspase 3 (9661, Cell signalling, 1:500), Ki67 (12202 Cell signalling, 1:1000). Images are captured from the stained sections using an Olympus BX53 microscope.

Confocal microscopy

In chapter 3, cells were seeded at a density of $1x10^5$ onto a 6-well plate and cultured for 48h in normoxia or hypoxia 1%. Then, the samples were washed with PBS and

incubated with BODIPY (2 µM) for 15 minutes at 37°C. Afterwards, fixation was carried out with 4% paraformaldehyde for 15 min at RT. Samples were mounted onto glass slides with the addition of a mounting solution with DAPI (Vectashield). Images from BODIPY staining were acquired by the confocal microscope Zeiss LSM780 and visualized with the software ZEN. The settings of the microscope were determined by the control sample and were maintained identical for other conditions. Fluorescence intensity was analyzed with ImageJ.

ATP measurements

In chapter 2, for ATP measurements (CellTiter-Glo, Promega), cells were seeded onto 12-well plates and transfected with siPYCRL or siNT at a concentration of 25 nM. 24h after transfection, cells were moved onto a 96-well plate at a density of $1x10^4$ cells/well. The following day, the assay was conducted as per manufacturer's instructions. ATP luminescent signal was then normalized on protein amount/well. Luminescence was measured with plate reader (BMG PHERAstar).

Oxygen consumption measurements

In chapter 2, for the off-gas measurement device, the day before respiration measurement A172 cells were seeded at a density $8x10^6$ on a gelatin-coated sterile glass disc (Pilkington Microwhite) placed in the bottom of a 100mm dish. Next day, cells were washed with 1xPBS and grown (atmospheric oxygen, CO_2-free at 37 °C) in bicarbonate-free DMEM (Sigma-Aldrich, D5030) supplemented with 25 mM glucose (ThermoFisher, A2494001) and 4 mM glutamine (Sigma-Aldrich, G7513), and buffered with 20 mM HEPES (Sigma-Aldrich, H0887). Before the respiration experiment, 25 µg/ml Carbonic Anhydrase (Sigma-Aldrich, C2624) was added to the medium. Optical

absorption measurements were performed before and after the respiration experiment. Respiration was normalized to cell number based on cyt-c absorbance. Next, the medium was poured off and the disc was placed in the respiration chamber. To prevent the cells from drying out, 0.5 mL medium was pipetted on the disc. Chamber was closed and the system was switched to high throughput mode for 15 seconds to equilibrate the gases in the system. O_2 absorption and CO_2 emission were measured for 25 min or until the signal stabilized in normoxia (~1.7% O_2, 450-500 ppm CO_2, 98.2% N_2). After normoxia, gas flow was switched to hypoxia (~0.3% O_2, 450-500 ppm CO2, 99.7% N_2) for 25 min.

Statistical analysis

The experiments were performed in three biological replicates and in two technical replicates. Error bars indicate mean ± S.E.M. Statistical significance was determined with GraphPad Prism 9, using Mann-Whitney test *p< 0.05; **p< 0.01; ***p< 0.001.

APPENDICES

Publications:

Appendix 1-

Vettore, L.,Westbrook R.L. & Tennant D.A. New aspects of amino acid metabolism in cancer. British journal of cancer 122, 150-156 (2020).

Appendix 2-

Vettore, L.A.,Westbrook R.L. & Tennant D.A. Proline metabolism and redox; maintaining a balance in health and disease. Amino acids (2021)

Bibliography

1. Mukherjee, S. *The emperor of all maladies : a biography of cancer*. (Scribner, 2010).
2. Toporcov, T. N. & Wünsch Filho, V. Epidemiological science and cancer control. *Clinics (Sao Paulo, Brazil)* **73**, e627s (2018).
3. Cairns, R. A., Harris, I. S. & Mak, T. W. Regulation of cancer cell metabolism. *Nature reviews. Cancer* **11**, 85–95 (2011).
4. DeBerardinis, R. J. & Chandel, N. S. Fundamentals of cancer metabolism. *Science Advances* **2**, e1600200 (2022).
5. Elia, I. & Haigis, M. C. Metabolites and the tumour microenvironment: from cellular mechanisms to systemic metabolism. *Nature metabolism* **3**, 21–32 (2021).
6. Warburg, O. Über den Stoffwechsel der Carcinomzelle. *Naturwissenschaften* **12**, 1131–1137 (1924).
7. Cantor, J. R. & Sabatini, D. M. Cancer cell metabolism: one hallmark, many faces. *Cancer discovery* **2**, 881–898 (2012).
8. Lunt, S. Y. & Vander Heiden, M. G. Aerobic Glycolysis: Meeting the Metabolic Requirements of Cell Proliferation. *Annual Review of Cell and Developmental Biology* **27**, 441–464 (2011).
9. Hanahan, D. & Weinberg, R. A. Review Hallmarks of Cancer : The Next Generation. *Cell* **144**, 646–674 (2011).
10. Weinberg, S. E. & Chandel, N. S. Targeting mitochondria metabolism for cancer therapy. *Nature chemical biology* **11**, 9–15 (2015).
11. Vander Heiden, M. G. & DeBerardinis, R. J. Understanding the Intersections

between Metabolism and Cancer Biology. *Cell* **168**, 657–669 (2017).

12. Spinelli, J. B. *et al.* Fumarate is a terminal electron acceptor in the mammalian electron transport chain. *Science* **374**, 1227–1237 (2021).
13. Vazquez, A. *et al.* Cancer metabolism at a glance. *Journal of Cell Science* **129**, 3367 LP – 3373 (2016).
14. Kľučková, K. *et al.* Succinate dehydrogenase deficiency in a chromaffin cell model retains metabolic fitness through the maintenance of mitochondrial NADH oxidoreductase function. *FASEB journal : official publication of the Federation of American Societies for Experimental Biology* **34**, 303–315 (2020).
15. Sciacovelli, M. & Frezza, C. Oncometabolites: Unconventional triggers of oncogenic signalling cascades. *Free radical biology & medicine* **100**, 175–181 (2016).
16. Goncalves, J. *et al.* Loss of SDHB Promotes Dysregulated Iron Homeostasis, Oxidative Stress, and Sensitivity to Ascorbate. *Cancer research* (2021). doi:10.1158/0008-5472.CAN-20-2936
17. Choi, Y.-K. & Park, K.-G. Targeting Glutamine Metabolism for Cancer Treatment. *Biomolecules & therapeutics* **26**, 19–28 (2018).
18. Vučetić, M., Cormerais, Y., Parks, S. K. & Pouysségur, J. The Central Role of Amino Acids in Cancer Redox Homeostasis: Vulnerability Points of the Cancer Redox Code . *Frontiers in Oncology* **7**, (2017).
19. Deberardinis, R. J., Sayed, N., Ditsworth, D. & Thompson, C. B. Brick by brick: metabolism and tumor cell growth. *Current opinion in genetics & development* **18**, 54–61 (2008).

20. Rabinovich, S. *et al.* Diversion of aspartate in ASS1-deficient tumours fosters de novo pyrimidine synthesis. *Nature* **527**, 379–383 (2015).
21. Keshet, R. & Erez, A. Arginine and the metabolic regulation of nitric oxide synthesis in cancer. *Disease Models & Mechanisms* **11**, dmm033332 (2018).
22. Nakanishi, S. & Cleveland, J. L. Targeting the polyamine - hypusine circuit for the prevention and treatment of cancer. *Amino Acids* (2016). doi:10.1007/s00726-016-2275-3
23. Ginguay, A., Cynober, L., Curis, E. & Nicolis, I. Ornithine Aminotransferase, an Important Glutamate-Metabolizing Enzyme at the Crossroads of Multiple Metabolic Pathways. *Biology* **6**, (2017).
24. Snaebjornsson, M. T., Janaki-Raman, S. & Schulze, A. Greasing the Wheels of the Cancer Machine: The Role of Lipid Metabolism in Cancer. *Cell Metabolism* **31**, 62–76 (2020).
25. Koundouros, N. & Poulogiannis, G. Reprogramming of fatty acid metabolism in cancer. *British Journal of Cancer* **122**, 4–22 (2020).
26. Vriens, K. *et al.* Evidence for an alternative fatty acid desaturation pathway increasing cancer plasticity. *Nature* **566**, 403–406 (2019).
27. Plötz, T., Hartmann, M., Lenzen, S. & Elsner, M. The role of lipid droplet formation in the protection of unsaturated fatty acids against palmitic acid induced lipotoxicity to rat insulin-producing cells. *Nutrition & metabolism* **13**, 16 (2016).
28. Carracedo, A., Cantley, L. C. & Pandolfi, P. P. Cancer metabolism: fatty acid oxidation in the limelight. *Nature reviews. Cancer* **13**, 227–232 (2013).

29. Eales, K. L., Hollinshead, K. E. R. & Tennant, D. A. Hypoxia and metabolic adaptation of cancer cells. *Oncogenesis* **5**, e190 (2016).

30. Sonveaux, P. *et al.* Targeting lactate-fueled respiration selectively kills hypoxic tumor cells in mice. **118**, (2008).

31. Petrova, V., Annicchiarico-petruzzelli, M., Melino, G. & Amelio, I. The hypoxic tumour microenvironment. *Oncogenesis* (2018). doi:10.1038/s41389-017-0011-9

32. Durán, R. V *et al.* HIF-independent role of prolyl hydroxylases in the cellular response to amino acids. *Oncogene* **32**, 4549–4556 (2013).

33. McMahon, S., Charbonneau, M., Grandmont, S., Richard, D. E. & Dubois, C. M. Transforming growth factor beta1 induces hypoxia-inducible factor-1 stabilization through selective inhibition of PHD2 expression. *The Journal of biological chemistry* **281**, 24171–24181 (2006).

34. Sikes, K. J. *et al.* TGF-b1 or hypoxia enhance glucose metabolism and lactate production via HIF1A signaling in tendon cells. *Connective tissue research* **59**, 458–471 (2018).

35. Brown, A. J. & Galea, A. M. CHOLESTEROL AS AN EVOLUTIONARY RESPONSE TO LIVING WITH OXYGEN. *Evolution* **64**, 2179–2183 (2010).

36. DeBose-Boyd, R. A. Feedback regulation of cholesterol synthesis: sterol-accelerated ubiquitination and degradation of HMG CoA reductase. *Cell Research* **18**, 609–621 (2008).

37. Kamphorst, J. J. *et al.* Hypoxic and Ras-transformed cells support growth by scavenging unsaturated fatty acids from lysophospholipids. *Proceedings of the National Academy of Sciences* **110**, 8882–8887 (2013).

38. Hac-Wydro, K. & Wydro, P. The influence of fatty acids on model cholesterol/phospholipid membranes. *Chemistry and physics of lipids* **150**, 66–81 (2007).

39. Mei, S. *et al.* Differential roles of unsaturated and saturated fatty acids on autophagy and apoptosis in hepatocytes. *The Journal of pharmacology and experimental therapeutics* **339**, 487–498 (2011).

40. Huang, D. *et al.* HIF-1-mediated suppression of acyl-CoA dehydrogenases and fatty acid oxidation is critical for cancer progression. *Cell reports* **8**, 1930–1942 (2014).

41. Lee, P., Chandel, N. S. & Simon, M. C. Cellular adaptation to hypoxia through hypoxia inducible factors and beyond. *Nature Reviews Molecular Cell Biology* **21**, 268–283 (2020).

42. Katsyuba, E., Romani, M., Hofer, D. & Auwerx, J. NAD+ homeostasis in health and disease. *Nature Metabolism* **2**, 9–31 (2020).

43. Xiao, W., Wang, R.-S., Handy, D. E. & Loscalzo, J. NAD(H) and NADP(H) Redox Couples and Cellular Energy Metabolism. *Antioxidants & redox signaling* **28**, 251–272 (2018).

44. Spinelli, J. B. & Haigis, M. C. The multifaceted contributions of mitochondria to cellular metabolism. *Nature cell biology* **20**, 745–754 (2018).

45. Luongo, T. S. *et al.* SLC25A51 is a mammalian mitochondrial NAD(+) transporter. *Nature* **588**, 174–179 (2020).

46. Kory, N. *et al.* MCART1/SLC25A51 is required for mitochondrial NAD transport. *Science Advances* **6**, eabe5310 (2022).

47. Hagedorn, C. H. & Phang, J. M. Transfer of reducing equivalents into

mitochondria by the interconversions of proline and delta 1-pyrroline-5-carboxylate. *Archives of biochemistry and biophysics* **225**, 95–101 (1983).

48. Ray, P. D., Huang, B.-W. & Tsuji, Y. Reactive oxygen species (ROS) homeostasis and redox regulation in cellular signaling. *Cellular signalling* **24**, 981–990 (2012).

49. Birben, E., Sahiner, U. M., Sackesen, C., Erzurum, S. & Kalayci, O. Oxidative stress and antioxidant defense. *The World Allergy Organization journal* **5**, 9–19 (2012).

50. Ursini, F., Maiorino, M. & Forman, H. J. Redox homeostasis: The Golden Mean of healthy living. *Redox biology* **8**, 205–215 (2016).

51. Rustin, P. Mitochondria, from cell death to proliferation. *Nature genetics* **30**, 352–353 (2002).

52. Gorrini, C., Harris, I. S. & Mak, T. W. Modulation of oxidative stress as an anticancer strategy. *Nature reviews. Drug discovery* **12**, 931–947 (2013).

53. Smith, K. A., Waypa, G. B. & Schumacker, P. T. Redox signaling during hypoxia in mammalian cells. *Redox biology* **13**, 228–234 (2017).

54. Loscalzo, J. Adaptions to Hypoxia and Redox Stress: Essential Concepts Confounded by Misleading Terminology. *Circulation research* **119**, 511–513 (2016).

55. Semenza, G. L. Hypoxia-inducible factors: coupling glucose metabolism and redox regulation with induction of the breast cancer stem cell phenotype. *The EMBO Journal* **36**, 252–259 (2017).

56. Tanner, J. J., Fendt, S.-M. & Becker, D. F. The Proline Cycle As a Potential Cancer Therapy Target. *Biochemistry* **57**, 3433–3444 (2018).

57. Liang, X., Zhang, L., Natarajan, S. K. & Becker, D. F. Proline Mechanisms of Stress Survival. **19**, 998–1011 (2013).

58. De Ingeniis, J. *et al.* Functional specialization in proline biosynthesis of melanoma. *PloS one* **7**, e45190 (2012).

59. Vettore, L., Westbrook, R. L. & Tennant, D. A. New aspects of amino acid metabolism in cancer. *British journal of cancer* **122**, 150–156 (2020).

60. Vettore, L. A., Westbrook, R. L. & Tennant, D. A. Proline metabolism and redox; maintaining a balance in health and disease. *Amino acids* (2021). doi:10.1007/s00726-021-03051-2

61. Nakayama, T. *et al.* Mutations in PYCR2, Encoding Pyrroline-5-Carboxylate Reductase 2, Cause Microcephaly and Hypomyelination. *American journal of human genetics* **96**, 709–719 (2015).

62. Reversade, B. *et al.* Mutations in PYCR1 cause cutis laxa with progeroid features. *Nature genetics* **41**, 1016–1021 (2009).

63. Loayza-Puch, F. *et al.* Tumour-specific proline vulnerability uncovered by differential ribosome codon reading. *Nature* **530**, 490–494 (2016).

64. Zhang, T. *et al.* Increased PYCR1 mRNA predicts poor prognosis in kidney adenocarcinoma: A study based on TCGA database. *Medicine* **100**, e27145 (2021).

65. Ding, Z. *et al.* Metabolic pathway analyses identify proline biosynthesis pathway as a promoter of liver tumorigenesis. *Journal of Hepatology* **72**, 725–735 (2020).

66. Wang, S. *et al.* The upregulation of PYCR2 is associated with aggressive colon cancer progression and a poor prognosis. *Biochemical and biophysical*

research communications **572**, 20–26 (2021).

67. Struys, E. A., Jansen, E. E. W. & Salomons, G. S. Human pyrroline-5-carboxylate reductase (PYCR1) acts on Δ 1 -piperideine-6-carboxylate generating L-pipecolic acid. 1–6 (2014). doi:10.1007/s10545-013-9673-4

68. Patel, S. M., Seravalli, J., Stiers, K. M., Tanner, J. J. & Becker, D. F. Kinetics of human pyrroline-5-carboxylate reductase in L-thioproline metabolism. *Amino acids* **53**, 1863–1874 (2021).

69. Natarajan, S. K. & Becker, D. F. Role of apoptosis-inducing factor, proline dehydrogenase, and NADPH oxidase in apoptosis and oxidative stress. *Cell health and cytoskeleton* **2012**, 11–27 (2012).

70. Elia, I. *et al.* Proline metabolism supports metastasis formation and could be inhibited to selectively target metastasizing cancer cells. *Nature Communications* **8**, 15267 (2017).

71. Ryan, D. G. *et al.* Disruption of the TCA cycle reveals an ATF4-dependent integration of redox and amino acid metabolism. *bioRxiv* 2021.07.27.453996 (2021). doi:10.1101/2021.07.27.453996

72. Hollinshead, K. E. R. *et al.* Oncogenic IDH1 Mutations Promote Enhanced Proline Synthesis through PYCR1 to Support the Maintenance of Mitochondrial Redox Homeostasis. *Cell Reports* **22**, 3107–3114 (2018).

73. Westbrook, R. L. *et al.* Proline synthesis through PYCR1 is required to support cancer cell proliferation and survival in oxygen-limiting conditions. *Cell reports* **38**, 110320 (2022).

74. Schwörer, S. *et al.* Proline biosynthesis is a vent for TGFβ-induced mitochondrial redox stress. *The EMBO Journal* **n/a**, e103334 (2020).

75. Liu, M. *et al.* Inhibiting both proline biosynthesis and lipogenesis synergistically suppresses tumor growth. *The Journal of experimental medicine* **217**, (2020).

76. Stegen, S. *et al.* HIF-1α metabolically controls collagen synthesis and modification in chondrocytes. *Nature* **565**, 511–515 (2019).

77. Xiong, G. *et al.* Collagen prolyl 4-hydroxylase 1 is essential for HIF-1α stabilization and TNBC chemoresistance. *Nature Communications* **9**, 4456 (2018).

78. Du, J., Zhu, S., Lim, R. R. & Chao, J. R. Proline metabolism and transport in retinal health and disease. *Amino acids* 1–18 (2021). doi:10.1007/s00726-021-02981-1

79. Takanaga, H., Tokuda, N., Ohtsuki, S., Hosoya, K.-I. & Terasaki, T. ATA2 is predominantly expressed as system A at the blood-brain barrier and acts as brain-to-blood efflux transport for L-proline. *Molecular pharmacology* **61**, 1289–1296 (2002).

80. Yoneyama, D. *et al.* Involvement of system A in the retina-to-blood transport of l-proline across the inner blood-retinal barrier. *Experimental eye research* **90**, 507–513 (2010).

81. Yam, M. *et al.* Proline mediates metabolic communication between retinal pigment epithelial cells and the retina. *The Journal of biological chemistry* **294**, 10278–10289 (2019).

82. Newton, H. *et al.* Systemic muscle wasting and coordinated tumour response drive tumourigenesis. *Nature Communications* **11**, 4653 (2020).

83. Shafqat, S. *et al.* Human brain-specific L-proline transporter: molecular cloning, functional expression, and chromosomal localization of the gene in human and

mouse genomes. *Molecular pharmacology* **48**, 219–229 (1995).

84. Sagné, C. *et al.* Identification and characterization of a lysosomal transporter for small neutral amino acids. *Proceedings of the National Academy of Sciences* **98**, 7206–7211 (2001).

85. Meyer, J. Proline transport in rat liver mitochondria. *Archives of Biochemistry and Biophysics* **178**, 387–395 (1977).

86. Di Martino, C., Pizzuto, R., Pallotta, M. L., De Santis, A. & Passarella, S. Mitochondrial transport in proline catabolism in plants: the existence of two separate translocators in mitochondria isolated from durum wheat seedlings. *Planta* **223**, 1123–1133 (2006).

87. Miller, G. *et al.* Unraveling Δ1-Pyrroline-5-Carboxylate-Proline Cycle in Plants by Uncoupled Expression of Proline Oxidation Enzymes*. *Journal of Biological Chemistry* **284**, 26482–26492 (2009).

88. Pallotta, M. L. L-Proline uptake in Saccharomyces cerevisiae mitochondria can contribute to bioenergetics during nutrient stress as alternative mitochondrial fuel. *World journal of microbiology & biotechnology* **30**, 19–31 (2014).

89. Tan, B. S. N., Lonic, A., Morris, M. B., Rathjen, P. D. & Rathjen, J. The amino acid transporter SNAT2 mediates L-proline-induced differentiation of ES cells. *American journal of physiology. Cell physiology* **300**, C1270-9 (2011).

90. Shen, L. *et al.* SLC38A2 provides proline to fulfill unique synthetic demands arising during osteoblast differentiation and bone formation. *eLife* **11**, e76963 (2022).

91. Zulkifli, M. *et al.* Yeast homologs of human MCUR1 regulate mitochondrial proline metabolism. *Nature Communications* **11**, 4866 (2020).

92. Hatanaka, T., Hatanaka, Y., Tsuchida, J.-I., Ganapathy, V. & Setou, M. Amino acid transporter ATA2 is stored at the trans-Golgi network and released by insulin stimulus in adipocytes. *The Journal of biological chemistry* **281**, 39273–39284 (2006).

93. Hyde, R., Hajduch, E., Powell, D. J., Taylor, P. M. & Hundal, H. S. Ceramide down-regulates System A amino acid transport and protein synthesis in rat skeletal muscle cells. *FASEB journal : official publication of the Federation of American Societies for Experimental Biology* **19**, 461–463 (2005).

94. Menchini, R. J. & Chaudhry, F. A. Multifaceted regulation of the system A transporter Slc38a2 suggests nanoscale regulation of amino acid metabolism and cellular signaling. *Neuropharmacology* **161**, 107789 (2019).

95. Yoshida, A. *et al.* SLC36A1-mTORC1 signaling drives acquired resistance to CDK4/6 inhibitors. *Science advances* **5**, eaax6352 (2019).

96. Wu, G. *et al.* Proline and hydroxyproline metabolism: implications for animal and human nutrition. *Amino acids* **40**, 1053–1063 (2011).

97. Schmidt, J. A. *et al.* Plasma concentrations and intakes of amino acids in male meat-eaters, fish-eaters, vegetarians and vegans: a cross-sectional analysis in the EPIC-Oxford cohort. *European journal of clinical nutrition* **70**, 306–312 (2016).

98. Liu, Z., Jeppesen, P. B., Gregersen, S., Bach Larsen, L. & Hermansen, K. Chronic Exposure to Proline Causes Aminoacidotoxicity and Impaired Beta-Cell Function: Studies In Vitro. *The review of diabetic studies : RDS* **13**, 66–78 (2016).

99. Mitsubuchi, H., Nakamura, K., Matsumoto, S. & Endo, F. Inborn Errors of

Proline Metabolism. *The Journal of Nutrition* **138**, 2016S-2020S (2008).

100. Chao, J. R. *et al.* Human retinal pigment epithelial cells prefer proline as a nutrient and transport metabolic intermediates to the retinal side. *The Journal of biological chemistry* **292**, 12895–12905 (2017).
101. Madsen, D. H. *et al.* M2-like macrophages are responsible for collagen degradation through a mannose receptor-mediated pathway. *The Journal of cell biology* **202**, 951–966 (2013).
102. Kay, E. J. *et al.* Cancer-associated fibroblasts require proline synthesis by PYCR1 for the deposition of pro-tumorigenic extracellular matrix. *Nature Metabolism* **4**, 693–710 (2022).
103. Olivares, O. *et al.* Collagen-derived proline promotes pancreatic ductal adenocarcinoma cell survival under nutrient limited conditions. *Nature Communications* **8**, 16031 (2017).
104. Zhu, J. *et al.* Mitochondrial NADP(H) generation is essential for proline biosynthesis. *Science* eabd5491 (2021). doi:10.1126/science.abd5491
105. Tran, D. H. *et al.* Mitochondrial NADP(+) is essential for proline biosynthesis during cell growth. *Nature metabolism* **3**, 571–585 (2021).
106. Pomerantz, D. J. *et al.* Clinical heterogeneity of mitochondrial NAD kinase deficiency caused by a NADK2 start loss variant. *American journal of medical genetics. Part A* **176**, 692–698 (2018).
107. Wynn, T. A. Cellular and molecular mechanisms of fibrosis. *The Journal of pathology* **214**, 199–210 (2008).
108. McAnulty, R. J. Fibroblasts and myofibroblasts: their source, function and role in disease. *The international journal of biochemistry & cell biology* **39**, 666–671

(2007).

109. Clish, C. B. Metabolomics: an emerging but powerful tool for precision medicine. *Cold Spring Harbor molecular case studies* **1**, a000588 (2015).
110. DeBerardinis, R. J. & Keshari, K. R. Metabolic analysis as a driver for discovery, diagnosis, and therapy. *Cell* **185**, 2678–2689 (2022).
111. Figueroa, M. E. *et al.* Leukemic IDH1 and IDH2 mutations result in a hypermethylation phenotype, disrupt TET2 function, and impair hematopoietic differentiation. *Cancer cell* **18**, 553–567 (2010).
112. Rohle, D. *et al.* An inhibitor of mutant IDH1 delays growth and promotes differentiation of glioma cells. *Science (New York, N.Y.)* **340**, 626–630 (2013).
113. Wang, F. *et al.* Targeted inhibition of mutant IDH2 in leukemia cells induces cellular differentiation. *Science (New York, N.Y.)* **340**, 622–626 (2013).
114. Choi, C. *et al.* Prospective Longitudinal Analysis of 2-Hydroxyglutarate Magnetic Resonance Spectroscopy Identifies Broad Clinical Utility for the Management of Patients With IDH-Mutant Glioma. *Journal of clinical oncology : official journal of the American Society of Clinical Oncology* **34**, 4030–4039 (2016).
115. Sánchez-Guijo, A., Hartmann, M. F. & Wudy, S. A. Introduction to Gas Chromatography-Mass Spectrometry BT - Hormone Assays in Biological Fluids. in (ed. Wheeler, M. J.) 27–44 (Humana Press, 2013). doi:10.1007/978-1-62703-616-0_3
116. Wolfe, Robert R., C. D. L. Isotope tracers in metabolic research: Principle and practice of kinetic analysis. *Wiley* (2004).
117. Pitt, J. J. Principles and applications of liquid chromatography-mass

spectrometry in clinical biochemistry. *The Clinical biochemist. Reviews* **30**, 19–34 (2009).

118. Williamson, L. N. & Bartlett, M. G. Quantitative liquid chromatography/time-of-flight mass spectrometry. *Biomedical chromatography : BMC* **21**, 567–576 (2007).
119. Hu, Q. *et al.* The Orbitrap: a new mass spectrometer. *Journal of Mass Spectrometry* **40**, 430–443 (2005).
120. Buescher, J. M. *et al.* A roadmap for interpreting 13C metabolite labeling patterns from cells. *Current Opinion in Biotechnology* **34**, 189–201 (2015).
121. Jang, C., Chen, L. & Rabinowitz, J. D. Metabolomics and Isotope Tracing. *Cell* **173**, 822–837 (2018).
122. Dai, Z. & Locasale, J. W. Understanding metabolism with flux analysis: From theory to application. *Metabolic engineering* **43**, 94–102 (2017).
123. Midani, F. S., Wynn, M. L. & Schnell, S. The importance of accurately correcting for the natural abundance of stable isotopes. *Analytical biochemistry* **520**, 27–43 (2017).
124. Dong, W., Rawat, E. S., Stephanopoulos, G. & Abu-Remaileh, M. Isotope tracing in health and disease. *Current Opinion in Biotechnology* **76**, 102739 (2022).
125. Kim, I.-Y., Park, S., Jang, J. & Wolfe, R. R. Quantifications of Lipid Kinetics In Vivo Using Stable Isotope Tracer Methodology. *J Lipid Atheroscler* **9**, 110–123 (2020).
126. Hollinshead, K. E. R. *et al.* Oncogenic IDH1 Mutations Promote Enhanced Proline Synthesis through PYCR1 to Support the Maintenance of Mitochondrial

Redox Homeostasis. *Cell reports* **22**, 3107–3114 (2018).

127. Lewis, C. A. *et al.* Tracing compartmentalized NADPH metabolism in the cytosol and mitochondria of mammalian cells. *Molecular cell* **55**, 253–263 (2014).
128. Sullivan, L. B. *et al.* Supporting Aspartate Biosynthesis Is an Essential Function of Respiration in Proliferating Cells. *Cell* **162**, 552–563 (2015).
129. Luengo, A. *et al.* Increased demand for NAD(+) relative to ATP drives aerobic glycolysis. *Molecular cell* **81**, 691-707.e6 (2021).
130. Eriksson, L. S., Broberg, S., Björkman, O. & Wahren, J. Ammonia metabolism during exercise in man. *Clinical physiology (Oxford, England)* **5**, 325–336 (1985).
131. Van Eijk, H. M. H., DeJong, C. H. C., Deutz, N. E. P. & Soeters, P. B. Influence of storage conditions on normal plasma amino-acid concentrations. *Clinical Nutrition* **13**, 374–380 (1994).
132. Sahu, N. *et al.* Proline Starvation Induces Unresolved ER Stress and Hinders mTORC1-Dependent Tumorigenesis. *Cell metabolism* **24**, 753–761 (2016).
133. Spinelli, J. B. *et al.* Metabolic recycling of ammonia via glutamate dehydrogenase supports breast cancer biomass. *Science (New York, N.Y.)* **358**, 941–946 (2017).
134. Kim, W. *et al.* Polyunsaturated Fatty Acid Desaturation Is a Mechanism for Glycolytic NAD+ Recycling. *Cell Metabolism* **29**, 856-870.e7 (2019).
135. Achreja, A. *et al.* Metabolic collateral lethal target identification reveals MTHFD2 paralogue dependency in ovarian cancer. *Nature Metabolism* (2022). doi:10.1038/s42255-022-00636-3

136. Argus, J. P. *et al.* Development and Application of FASA, a Model for Quantifying Fatty Acid Metabolism Using Stable Isotope Labeling. *Cell reports* **25**, 2919-2934.e8 (2018).

137. den Hartigh, L. J., Connolly-Rohrbach, J. E., Fore, S., Huser, T. R. & Rutledge, J. C. Fatty Acids from Very Low-Density Lipoprotein Lipolysis Products Induce Lipid Droplet Accumulation in Human Monocytes. *The Journal of Immunology* **184**, 3927 LP – 3936 (2010).

138. Olzmann, J. A. & Carvalho, P. Dynamics and functions of lipid droplets. *Nature Reviews Molecular Cell Biology* **20**, 137–155 (2019).

139. Hörl, G. *et al.* Sequential synthesis and methylation of phosphatidylethanolamine promote lipid droplet biosynthesis and stability in tissue culture and in vivo. *The Journal of biological chemistry* **286**, 17338–17350 (2011).

140. Bi, J. *et al.* Altered cellular metabolism in gliomas — an emerging landscape of actionable co-dependency targets. *Nature Reviews Cancer* **20**, 57–70 (2020).

141. Patriarca, E. J. *et al.* The Multifaceted Roles of Proline in Cell Behavior . *Frontiers in Cell and Developmental Biology* **9**, 2236 (2021).

142. Baxter, C. F., Baldwin, R. A., Pomara, N. & Brinkman, S. D. Proline in the cerebrospinal fluid of normal subjects and Alzheimer's-disease patients, as determined with a new double-labeling assay technique. *Biochemical medicine* **32**, 189–198 (1984).

143. Dolgodilina, E. *et al.* Brain interstitial fluid glutamine homeostasis is controlled by blood-brain barrier SLC7A5/LAT1 amino acid transporter. *Journal of cerebral blood flow and metabolism : official journal of the International Society*

of Cerebral Blood Flow and Metabolism **36**, 1929–1941 (2016).

144. Daykin, C. A., Bro, R. & Wulfert, F. Data handling for interactive metabolomics: tools for studying the dynamics of metabolome-macromolecule interactions. *Metabolomics* **8**, 52–63 (2012).

145. Arvanitis, C. D., Ferraro, G. B. & Jain, R. K. The blood–brain barrier and blood–tumour barrier in brain tumours and metastases. *Nature Reviews Cancer* **20**, 26–41 (2020).

146. Zafra, F., Aragón, C. & Giménez, C. Characteristics and regulation of proline transport in cultured glioblastoma cells. *The Biochemical journal* **302 (Pt 3)**, 675–680 (1994).

147. Gauthier-Coles, G. *et al.* Quantitative modelling of amino acid transport and homeostasis in mammalian cells. *Nature Communications* **12**, 5282 (2021).

148. Morotti, M. *et al.* Increased expression of glutamine transporter SNAT2/SLC38A2 promotes glutamine dependence and oxidative stress resistance, and is associated with worse prognosis in triple-negative breast cancer. *British Journal of Cancer* **124**, 494–505 (2021).

149. Nishii, R. *et al.* Differential Diagnosis between Low-Grade and High-Grade Astrocytoma Using System A Amino Acid Transport PET Imaging with C-11-MeAIB: A Comparison Study with C-11-Methionine PET Imaging. *Contrast media & molecular imaging* **2018**, 1292746 (2018).

150. Skala, M. C. *et al.* In vivo multiphoton microscopy of NADH and FAD redox states, fluorescence lifetimes, and cellular morphology in precancerous epithelia. *Proceedings of the National Academy of Sciences of the United States of America* **104**, 19494–19499 (2007).

151. Osawa, T. *et al.* Phosphoethanolamine Accumulation Protects Cancer Cells under Glutamine Starvation through Downregulation of PCYT2. *Cell reports* **29**, 89-103.e7 (2019).

152. Christensen, E. M. *et al.* In crystallo screening for proline analog inhibitors of the proline cycle enzyme PYCR1. *The Journal of biological chemistry* **295**, 18316–18327 (2020).

153. Arnold, P. K. *et al.* A non-canonical tricarboxylic acid cycle underlies cellular identity. *Nature* **603**, 477–481 (2022).

154. Wang, Y. *et al.* SLC25A39 is necessary for mitochondrial glutathione import in mammalian cells. *Nature* **599**, 136–140 (2021).

155. Morotti, M. *et al.* Hypoxia-induced switch in SNAT2/SLC38A2 regulation generates endocrine resistance in breast cancer. *Proceedings of the National Academy of Sciences of the United States of America* **116**, 12452–12461 (2019).

156. Parker, S. J. *et al.* Selective alanine transporter utilization creates a targetable metabolic niche in pancreatic cancer. *Cancer Discovery* CD-19-0959 (2020). doi:10.1158/2159-8290.CD-19-0959

157. Kanamori, K. & Ross, B. D. Quantitative determination of extracellular glutamine concentration in rat brain, and its elevation in vivo by system A transport inhibitor, alpha-(methylamino)isobutyrate. *Journal of neurochemistry* **90**, 203–210 (2004).

158. Burger, N. *et al.* A sensitive mass spectrometric assay for mitochondrial CoQ pool redox state in vivo. *Free radical biology & medicine* **147**, 37–47 (2020).